ELECTROLYTES FOR REDOX FLOW BATTERY SYSTEMS

By

Portia Modiba

Dissertation presented
for the degree of

Doctor of Philosophy
Chemistry

at the University of Stellenbosch
Department of Chemistry and Polymer Science

March 2010

Republic of South Africa

Promoter: **Professor Andrew M. Crouch**

Declaration

I, the undersigned, hereby declare that this research work contained in this thesis is the results of my own original work and investigation, which has not been accepted in candidature for any degree and is not being submitted previously in its entirety in any university for a degree.

Portia Modiba

We hereby certify that this statement is correct

Professor AM Crouch

Supervisor

University of Stellenbosch
Department of Chemistry and Polymer Science
Stellenbosch
South Africa
December 2009

Acknowledgements

I sincerely thank Professor Andrew Crouch for his guidance and supervision during the course of this project. I respectfully thank Dr. Mmangaka Matoetoe for her invaluable assistance, which is most appreciated

I would like to thank Professor Emmanuel Iwuoha, Dr Joseph Owino and Dr Omotayo Arotiba for making EIS experiments possible.

I would particularly like to thank Dr. Vernon Somerset, Dr Nagaraju Valepula and Dr. Michael Klink for their support, assistance and fruitful discussions throughout my PhD Study.

Big thanks to thank Dr. Lebogang Katata and Dr Astrid Buica with their CE expertise.

I also acknowledge the financial support of the National Research Foundation (NRF) South Africa and the Tertiary Education Support Program (TESP) of Electricity Supply Commission (ESKOM), South Africa.

I would like to thank all my fellow colleagues and staff of the University of Stellenbosch and University of the Western Cape.

Many thanks to my Bishop Baloyi and His wife, all my Pastors and their wife's, friends, brothers and sisters in Chris specially Lindiwe Qave, Johanna Masebe, Jacks Masebe and Phuti Mogase, for their constant encouragement and prayers.

Above all, thanks to my mom Florence Modiba, my daughter Marcia Nthabiseng Modiba, my husband Mlungisi Nkanunu, my sister Lerato Modiba, and my family (Modiba, Nkanunu, Ndlovu, Masebe and Tsomele) for their love, patience, support and their prayers.

Finally, I thank GOD LORD ALMIGHT who makes everything possible

Patience is an important tool in life.
Immediate achievement do not stays long, but the best things in life that last long require years of hard work, hope, faith and waiting.

by the late Johanna Makosha Modiba and Rachael Ndlovu, construed by Dr Portia Modiba

If you stay calm, you are wise, but if you have hot temper, you only show how stupid you are.
Proverbs: 14:29(GNB)

Everything is possible thought Christ the Lord GOD Almighty

Outline of thesis

LIST OF FIGURES

Chapter 2

Chapter 3

Chapter 4

Chapter 5

Chapter 6

Chapter 7

Chapter 8

Chapter 10

LIST OF TABLES

Chapter 2

Chapter 4

Chapter 5

Chapter 6

Chapter 7

Chapter 8

LIST OF ABBREVIATIONS:

In alphabetical order:

- A Amps
- AE Auxiliary electrode
- BAS BioAnalytical Systems
- BR Britton-Robinson buffer
- CE Capillary electrophoresis
- CVs Cyclic voltammograms
- DMF 2,4-dimethylphenyl formamide
- DMPF 2,4-dimethylphenyl formamidine
- DMSO Dimethyl sulphoxide
- DPV Differential pulse voltammetry
- EIS Electrochemical impedance spectroscopy
- ECD Electron capture detector
- ECECE Electrochemical, Chemical
- FB Flow Battery
- GC Gas chromatography
- GCE Glassy carbon electrode
- HMDE Hanging mercury drop electrode
- HPLC High performance liquid chromatography
- I Current
- pa Anodic current
- pc Cathodic current
- LLE Liquid-liquid extraction
- LOD Limit of detection
- MPC metallophthalocyanine
- MS Mass spectrometer
- MV/s Millivolts per second
- NPD Nitrogen-phosphorous detector
- O Oxidation
- OD Optical density
- PPM Parts per million
- R Reduction
- RDE Rotating disc electrode
- RE Reference electrode
- RB Redox Battery
- RFB Redox Flow Battery
- RPM Revolutions per minute
- SCE Saturated calomel electrode
- SD Standard deviation
- SHE Standard hydrogen electrode
- SPE Screen printed electrode
- SPME Solid-phase micro-extraction
- Spp. Species
- TMB Tetramethylbenzidine
- UV Ultra violet
- V Volts
- WE Working electrode

SYMBOLS

- a Pre-factor in the power law
- A Surface area (cm^2)
- B Power in the power law relationship
- $_0c$ Initial concentration of a diffusing species ($mol \cdot cm^{-3}$)
- $_Rc$ Final concentration of a diffusing species ($mol \cdot cm^{-3}$)
- $_sc$ Current concentration of a diffusing species at the surface of an electrode($mol \cdot cm^{-3}$)
- C Capacitance (F)
- C_0 Initial bulk concentration of the electroactive species ($mol \cdot cm^{-3}$)
- $_{Li}C$ Maximum concentration of intercalated lithium in an intercalant ($mol \cdot cm^{-3}$)
- D Diffusion coefficient ($cm \cdot s^{-1}$)
- e Charge on an electron (C)
- E Electrochemical potential (V)
- E_f Final potential in a potential sweep (V)
- E_i Initial potential in a potential sweep (V)
- E_F Fermi energy (eV)
- E_g Band gap energy in semiconductors (eV)
- E_{OC} Open circuit potential (V)
- E_P Potential at which a peak is formed in voltammetry (V)
- $E_{P/2}$ Potential at half the peak height (current) (V)
- E_S Steady state potential (V)
- ΔE_τ Change in potential between the start and the end of a galvanostatic step.
- $_jf$ Probability that the jth electron energy state in a substance is occupied.
- F Faraday's constant ($96485\ C \cdot mol^{-1}$)
- h Planck's constant ($6.626 \times 10^{-34}\ Js$)
- i Current (A)
- i_P Peak current in a voltammetry experiment (A)
- $i_{,pa}$ Peak anodic current in a voltammetry experiment (A)
- $i_{pc,}$ Peak cathodic current in a voltammetry experiment (A)
- $t_{(t)}$ Total current as a function of time (A)
- k Boltzmann's constant ($1.381 \times 10^{-23}\ J \cdot K^{-1}$)
- m Mass of active material (g)
- m_e Effective mass of an electron
- m_h Effective mass of a hole
- m_0 Mass of an electron
- n Number of electrons transferred in an electrochemical process (mol)
- n_a Number of electrons transferred in the rate limiting step of a multistep electrochemical process (mol)
- N Number of moles of intercalated (mol)
- q_c Coulombic charge passed for a specific reaction during the cathodic sweep in a voltammogram (C)
- Q Coulombic charge passed during a potentiostatic step (C)
- r Particle radius or diffusion length (cm)
- R Gas constant ($8.314\ J \cdot mol^{-1} \cdot K^{-1}$)
- t Time (s)
- T Temperature (K)

- V Volume of a thin film electrode (cm^3)
- ${}_m V$ Molar volume ($cm^3 \cdot mol^{-1}$)
- ${}_A z$ Charge on an ion
- α Transfer coefficient (dimensionless)
- Γ^*_{Li} Maximum surface concentration of intercalated lithium in a adsorbed film model ($mol \cdot cm^{-2}$)
- Γ^*_{Li+} Surface concentration of adsorbed Li_+ ions
- ε Dielectric constant
- ${}_j\varepsilon$ Energy of the *j*th electron energy state (eV)
- ν Scan rate in a voltammetry experiment ($V \cdot s^{-1}$)
- τ Time taken during a galvanostatic step during a galvanostatic intermittent titration experiment (s)

Abstract

Electrochemical behaviour of Ce, Fe, Cr,V and Mn in the presence of DTPA, EDTA, EDDS, NTA ligands were investigated by using cyclic voltammetry, a rotating disc electrode and electrochemical impedance spectroscopy for use in redox flow battery (RFB) systems. RFB is currently used for energy storage, the vanadium, which is used in most of the RFB's, however suffers from species crossover and sluggish reactions, which limit the lifetime of the battery. These various ligands and metal complexes mentioned above where all examined to identify the suitable and favoured electrolyte that can be used for a RFB system.

Kinetic parameters such as potential, limiting current, transfer coefficient, diffusion coefficients, and rate constants were studied. RDE experiments confirmed that the parameters measured by CV are similar under hydrodynamic conditions and can be used to determine the kinetic parameters of the redox couples. The use of DTPA as a ligand for complexation of Ce(IV) gave more favourable results compared to other ligand with various metal complexes used in this study [1-3]. The results of kinetic studies of Ce(IV)–DTPA complex shows promise as an electrolyte for a redox flow battery.

The separation of V(IV)/(V), Fe (III)/(IV),Cr(III)/(IV),Mn (III)/(IV) and Ce(III)/(IV) with various ligands (EDTA, EDDS, NTA and DTPA) were also investigated using capillary electrophoresis. To understand the speciation of these metal complexes as used in this study and particularly the vanadium, for the reason that it has a complicated (V) oxidation state. The charge/discharge performance of all electrolytes used in this work was determined and a high voltage achieved when Ce-DTPA was used, and it is compared to that of the vanadium electrolyte currently in use. This was evaluated with systems studied previously. Therefore, Ce-DTPA will be a suitable electrolyte for redox flow battery systems.

Chapter 1

Introduction

1.1 Background

Worldwide the demand for electrical energy is continuously increasing. It is well know that the entire world is now suffering from the worst energy crisis. Although over the last two decades growth in energy consumption has been slower than was anticipated in the late 1970s, recent economic growth and improved distribution of electricity to households have resulted in significant increases in electricity demand.

In South Africa the demand for electricity between 1980 and 2004 increased by about 50% and, from 2004 until recently it was underestimated (more energy was required than could be produced). It is predicted that there will be more than a 60 % increase in energy usage as a result of increase consumption by 2030 to fuel economic development [1]. Energy demand is expected to grow significantly by 5.7% annually, driven particularly by important forward changes in the living conditions of the millions of people who currently live at or below the poverty line.

Growth in demand is not the only reason to consider alternative energy supply options. Currently, in South Africa, the energy supply is primarily coal. However, supplies will not last more than 20 years if used at the current rates. Coal has many other uses, and it needs to be preserved for future utilization. Coal and other fossil fuels, including oil, produce carbon dioxide when burned to produce energy. Furthermore is now widely accepted that climate change, partially caused by human-generated carbon dioxide, represents an extremely serious environmental threat to the whole world.

Today researchers have the potential to increase the flexibility of power systems and improve on the response to a sudden demand of energy. Presently the world is facing new challenges in electricity, since much has been ignored for the past decays. The need to meet growing energy demand will require innovation, such as energy generation and storage. Over the past years several energy storage technologies have been investigated and developed. Some technologies have reached the marcher level but only a few have become commercially available. Pumped hydro facilities have been successfully used to store electricity for many decades, but suitable locations present problems. Redox flow batteries (RFB) are also capable

of accumulating electrical energy. The flow batteries are very good for power and energy on a large scale because they are environmentally friendly, have a long life and high reliability require low maintenance, and are simple efficient. More research work and development has already been done and now researchers are progresing to improve the electrochemistry of the RFBs and reduce its high manufacturing cost. The focus of this dissertation is on the evaluation of various electrolytes that can be suitable for RFB application and also the battery performance and offer a good efficiency to conceivable replace vanadium that is presently used, but presents its own problems.

1.2 Aim and Objectives

The critical questions to be addressed in this dissertation are: how can one improve on the problems currently associated with RFBs, namely: cross contamination, strong activity, reversibility of the redox processes, stability of electrolytes, solubility of electrolytes, and electrochemical activity. The current industry standard in RFBs is the vanadium redox flow batteries (VRFB).

1.2.1 Aim

This thesis addresses issues of the reversibility, stability, cross contamination, strong activity, and solubility of electrolytes. Electrochemical techniques such as CV and EIS were utilized to investigate fundamental kinetics and thermodynamics of selected redox couples of Fe, Cr, Mn and Ce and complexes there of with aminocarboxylic acids

1.2.2 Specific objectives

- Investigate the electrochemical behaviour of redox couples (cerium (Ce), chromium (Cr), iron (Fe), manganese (Mn), and vanadium (V) for redox flow batteries.
- Study the kinetics and thermodynamics of complexes of various aminocarboxylates ethylenediamine disuccinate (EDDS), ethylenediaminetetra acetic acid (EDTA), nitrilotriacetic acid (NTA) and diethylenetriaminepenta acetic acid (DTPA) with metals (Ce, Cr, Fe, Mn, and V) by electrochemical techniques.
- Determine the performance of potential redox couples for use in RFB systems.
- Speciation of metal complexes, (Ce-EDTA, Ce-DTPA, Cr-EDTA, Cr-DTPA, Fe-EDTA, Fe-DTPA, Mn-EDTA, Mn-DTPA, V-EDTA, and V-DTPA).

1.3 Methodology and Approach

The electrochemical behaviour of the redox couples used in this study will be examined using cyclic voltammetry (CV), a rotating disc electrode (RDE), and electrochemical impedance spectroscopy (EIS) for redox flow battery systems. CV has become an important and commonly used electroanalytical technique in many areas of chemistry [2]. It is usually used for the study of redox processes, for understanding reaction intermediates, and for determining the stability of reaction products. This technique is based on varying the applied potential at a working electrode in both forward and reverse directions.

The RDE is similar to CV technique in that the working electrode potential is swept back and forth across the formal potential of analyte. It varies in the working electrode; it rotates at a very high speed. This rotational motion sets up a well defined flow of solution towards the surface of the rotating disk electrode. The flow pattern is similar to a current that literally sucks the solution towards the electrode [2]. RDE was used in this study to verify the CV results. EIS was used to evaluate a suitable electrolyte for redox couple systems.

EIS has great advantages: it can not only provide detailed kinetic information, but can also be used to monitor changes in battery properties under different usage or storage conditions. Due to its great advantages it is now widely applied to the study of batteries and fuel cells [3]. It is a very sensitive technique and offers a wealth of information about battery systems, such as an analysis of the state of charge, study of reaction mechanisms, and change of active surface area during operation separator evaluation, separation and comparison of electrode kinetics on each electrode, investigation of the kinetics at each electrode. EIS can give accurate, error-free kinetic and mechanistic information using a variety of techniques and output formats [4, 5].The performance of a test battery will be evaluated with constant- current charge-discharge experiments and open-circuit voltage measurements with a battery system.

Capillary electrophoresis (CE) is an attractive approach for the separation of metal species because of its high efficiency and rapid separation [5, 6]. In this investigation the separation of V (IV)/(V), Fe(III)/(IV), Cr(III)/(IV), Mn (III)/(IV), and Ce(III)/(IV) with various ligands e.g. EDTA, EDDS, NTA and DTPA were studied using CE. A major problem associated with CE is the separation of cations of similar mobility, even though the complexation of cations with ligands to form anionic complexes can be used to modify cation mobility [7].

1.4 Layout of thesis

Chapter 1

Overview of this project

Chapter 2

Literature review of the advance electrolyte for redox flow batteries application technology, the development of theories involved, and the landmark of the redox flow batteries are presented.

Chapter 3

Description of all electrochemical techniques used during this project. Which are CV, RDE, EIS, CE and electrochemical charge/discharge battery performance test.

Chapter 4

Electrochemical evaluation of different electrode (carbon, platinum and gold electrode) materials for studying RFB electrolytes.

Chapter 5

Electrochemical study of cerium (IV) in the presence of ethylenediaminetetraacetic acid (EDTA) and diethylenetriaminepentaacetate (DTPA) ligands. (Published as a paper, Modiba P, Crouch A.M, J. Appl. Electrochem 38 (2008)1293.

Chapter 6

Electrochemical impedance study of Ce(IV) with aminopolycarboxylate ligands for redox flow batteries applications, (resubmitted as a paper, Modiba P, Matoetoe M, Crouch A.M, J. Electrochimica Acta (2009).

Chapter 7

Electrochemical properties of metals (Cr, Fe, Mn, and V) for RFB applications, (submitted to J. Electrochimica Acta (2009) Modiba P, Matoetoe M, Crouch A.M.

Chapter 8

Testing and measuring the performance of redox couples for potential system for flow batteries, (published as a paper, Modiba P, Crouch A.M, Proceedings of the 43rd Power Source Conference, Philadelphia, New York, 7-10 July 2008.

Chapter 9

Conclusions and future recommendation.

Chapter 10

Addendum

Reference:

[1] Basis: available on line at http://www.environmentalinvest.com. (Accessed on 17 December 2009)

[2] Bard A.J, Faulkner L.R. Electrochemical Methods, Fundamentals and Applications, Wiley Interscience, New York, Publications 2nd edition (2001).

[3] Theory: A Primer, available online at www.gamry.com App_Notes/EIS_Primer.htm. (Accessed on 15 January 2010)

[4] Macdonald D.D, Urquidi-Macdonald M, J. Electrochem. Soc. 132 (1985) 2316.

[5] Gohr H.M, Mirnik M, Shiller C.A, J. Electroanal. Chem. 180 (1984) 273.

[6] Allongue P, Cachet H.B, J. Electrochem. Soc. 132 (1985) 45.

[7] Course Notes: available on line http://www.cp.umist.ac.uk/lecturenotes/echem.

Chapter 2

Literature Overview

2.1 Electrolytes

Electrolytes play a significant role in electrochemical procedures. Their fundamental function is independent of the greatly expanded chemistries and applications of the procedure. Electrolytes in batteries, electrolytic cells, capacitors, and fuel cells provide the medium for the transfer of charges, which are in the form of ions, between a pair of electrodes. The vast majority of electrolytes are electrolytic solution types that consist of salts, also called electrolyte solutes, dissolved in solvents, either aqueous or non-aqueous, and are in a liquid state in the service-temperature range.

According to the literature, an electrolyte is any substance containing free ions that behaves as an electrically conductive medium [1]. Because they generally consist of ions in solution, electrolytes are also known as ionic solutions, but molten electrolytes and solid electrolytes are also possible. An electrolyte is also a chemical compound that, when its complexes or is dissolved in certain solvents (normally water) will conduct an electric current. All electrolytes in the fused state or in solution give rise to ions that conduct the electric current [1]. We can also simply define an electrolyte as a liquid substance that acts as a medium to conduct electricity.

One speaks of an electrolyte in a number of different contexts; the most common are health and fitness, and various electronics and automotive disciplines. An electrolyte is full of ions, which are atoms that have some sort of net electric charge, either positive or negative. A dilute electrolyte has a relatively small number of ions for its volume, while a concentrated electrolyte has a larger amount of ions. In basic fuel cells, such as those used in automotive technology, an electrolyte acts as the liquid that allows ions to travel between the cathode and anode to keep the power-generating process underway, while keeping the reactive oxygen and hydrogen apart. In the type of fuel cell known as a proton exchange membrane cell, the electrolyte specifically moves protons (positively charged hydrogen ions) to the cathode from the anode, where they are produced, with the result being the production of water and electricity [1].

There are several promising materials such as yttria-stabilized zirconia (YSZ), doped cerium oxide, and doped bismuth oxide. Of these, the first two are the most promising. Bismuth oxide based materials have a high oxygen ion conductivity and lower operating temperature (lower than 800 C), but do not offer sufficient crystalline stability at high temperature to be widely useful [2]. YSZ has emerged as the most suitable electrolyte material. Yttria serves the dual purpose of stabilizing zirconia into the cubic structure at high temperatures and also providing oxygen vacancies at the rate of one vacancy per mole of dopant [2].

Batteries also employ an electrolyte of some sort, both to conduct electricity between the battery plates and to store energy on the plates themselves [3]. The electrolyte used in a battery depends on the batteries type and purpose. Most car batteries, for example, use an electrolyte, which contains sulphuric acid, which is why they require careful handling. Alkaline batteries use an alkaline solution as their electrolyte. Lithium batteries use a special organic electrolyte, which freezes, at much lower temperatures than the more traditional water-based electrolytes. Redox flow batteries also use electrolyte on both side tanks, namely the cathode and anode [3]. Electrolyte is especially important in the redox flow batteries.

2.1.1 Principles of electrolyte

Electrolytes commonly exist as solutions of acids, bases, or salts. Furthermore, some gases may act as electrolytes under conditions of high temperature or low pressure. Electrolyte solutions can also result from the dissolution of some biological polymers(e.g. DNA, polypeptides) and synthetic polymers (e.g. polystyrene sulfonate), termed polyelectrolytes, which contain multiple charged molecules [1].

Electrolyte solutions are normally formed when a salt is placed into a solvent such as water and the individual components dissociate due to the thermodynamic interactions between solvent and solute molecules, in a process called solvation. For example, when table salt (NaCl) is placed in water, the salt (a solid) dissolves into its component elements, according to the dissociation reaction

$$NaCl_{(s)} \leftrightarrow Na^{+}_{(aq)} + Cl^{-}_{(aq)}.$$

It is also possible for substances to react with water when they are added to it, producing ions, for example, carbon dioxide gas dissolves in water to produce a solution, which contains hydronium, carbonate, and hydrogen carbonate ions [1].

Note that molten salts can be electrolytes as well. For instance, when sodium chloride is molten, the liquid conducts electricity. An electrolyte in a solution may be described as concentrated if it has a high concentration of ions, or dilute if it has a low concentration. If a high proportion of the solute dissociates to form free ions, the electrolyte is strong; if most of the solute does not dissociate, the electrolyte is weak. The properties of electrolytes may be exploited using electrolysis to extract constituent elements and compounds contained within the solution [1].

2.1.2 Electrochemistry of electrolytes

It is well known from the literature [4-5] when electrodes are placed in an electrolyte and a voltage is applied, the electrolyte will conduct electricity. Lone electrons normally cannot pass through the electrolyte, instead, a chemical reaction occurs at the cathode consuming electrons from the cathode, and another reaction occurs at the anode producing electrons to be taken up by the anode. As a result, a negative charge cloud develops in the electrolyte around the cathode, and a positive charge develops around the anode. The ions in the electrolyte move to neutralize these charges so that the reactions can continue and the electrons can keep flowing [4-5].

For example, in a solution of ordinary salt (sodium chloride, NaCl) in water, the cathode reaction will be:

$$2H_2O + 2e^- \rightarrow 2OH^- + H_2 \qquad (2.1)$$

(hydrogen gas will bubble up)

and the anode reaction will be

$$2H_2O \rightarrow O_2 + 4H^+ + 4e^- \qquad (2.2)$$

(oxygen gas will be liberated)

The positively charged sodium ions (Na^+) will react in the direction of the cathode, neutralizing the negative charge of (OH^-) there, and the negatively charged chlorine ions (Cl^-)

will react towards the anode neutralizing the positive charge of (H^+) there. Without the ions from the electrolyte, the charges around the electrodes would delay the electron flow, diffusion of H^+ and OH^- through water to the other electrode takes longer than movement of the much more prevalent salt ions [5].

In other systems, the electrode reactions can involve the metals of the electrodes as well as the ions of the electrolyte. Electrolytic conductors are used in electronic devices where the chemical reaction at a metal/electrolyte interface yields useful effects [1, 3-6]

- In batteries, two metals with different electron affinities are used as electrodes; electrons flow from one electrode to the other outside of the battery, while inside the battery the circuit is closed by the electrolyte's ions. Here the electrode reactions convert chemical energy to electrical energy.
- In some fuel cells, a solid electrolyte or proton conductor connects the plates electrically while keeping the hydrogen and oxygen fuel gases separated.
- In electroplating tanks, the electrolyte simultaneously deposits metal onto the object to be plated, and electrically connects object in the circuit.
- In operation gauges, two thin columns of mercury are separated by a small electrolyte-filled gap, and, as charge is passed through the device, the metal dissolves on one side and plates out on the other, causing the visible gap to slowly move along.
- In electrolytic capacitors the chemical effect is used to produce an extremely thin 'dielectric' or insulating coating, while the electrolyte layer behaves as one capacitor plate.
- In some hygrometers the humidity of air is sensed by measuring the conductivity of a nearly dry electrolyte.
- Hot, softened glass is an electrolytic conductor, and some glass manufacturers keep the glass molten by passing a large current through it [1, 3-6].

2.2 Metal complexes

Metal complexes consist of a central metal atom or ion surrounded by several atoms, ions or molecules, called ligands. Ligands are ions or molecules that can be independentely attached to the central metal atom or ion. Examples of ligands are halide ions, carbon monoxide, ammonia and cyanide ions, etc. In describing complexes, the ligands directly attached to the metal (usually as Lewis bases, donating electrons to the metal) are counted to determine the

coordination number of the complex. Ions that are directly coordinated to the metal are written within the brackets of the formula, and are referred to as inner sphere. Ions that serve as counter ions in order to produce a neutral salt, and are not coordinated to the metal called the outer sphere, and written outside of the brackets in the formula [7-9].

2.2.1 Bonding of metal complexes

2.2.1.1 The crystal field theory

There are two widely used approaches for explaining the bonding and stability of transition metal complexes. In the crystal field theory [10], the electronic field created by the ligand electron pairs surrounding the central metal is viewed as point negative charges that repel and interact with the *d* orbitals of the metal ion. This theory explains the splitting of the *d* orbitals to remove their degeneracy, and the number of unpaired electrons in transition metal complexes, their color, spectra, and magnetic properties.

The magnitude of the splitting is determined experimentally from spectra of transition metal complexes. As the size of the gap changes, so does the color of the complex, as most of the t_{2g} to e_g transitions occur in the visible range. Analysis of the absorption spectra of a variety of transition metal complexes has resulted in the spectrochemical series, a list that orders the ligands from the weakest ligand fields to the strongest [10-11].

$I^-<Br^-<S^{2-}<Cl^-<NO_3{}^1<N_3^-<F^-<OH^-<C_2O_4^{2-}<H_2O<NCS^-<CH_3CN$
$<pyridine<NH_3<en<bipy<phen<NO_2^-<PPh_3<CN^-<CO$

Generally, the halogens are considered relatively weak ligands, water is somewhat intermediate in strength, ammonia is considerably stronger, and the strong p bonding ligands of cyanide and carbon monoxide are quite strong [10-11].

2.2.1.2 The ligand field theory

An alterative approach to understanding the bonding of transition metal complexes is the ligand field theory. Crystal field theory is a simple model that explains the spectra, thermochemical, and magnetic data of many complexes. Its main flaw is that it treats the ligands as point charges or dipoles, and fails to consider the orbitals of the ligands. Ligand

Field Theory applies molecular orbital theory and symmetry concerns to transition metal complexes. In octahedral symmetry, group theory can be used to determine the shapes and orientation of the orbitals on the metal and the ligands.

According to the literature [10-12], the ligand field theory enables the 3*d*, 4*s*, and 4*p* orbitals on the metal to overlap with orbitals on the ligand to form the octahedral covalent bond skeleton that holds the complex together. Simultaneously, this model generates a set of five orbitals in the center of the diagram that are split into t_{2g} and e_g subshells, as predicted by the crystal field theory. As a result, we do not have to worry about "inner-shell" versus "outer-shell" metal complexes. In effect, the 3*d* orbitals can be used in two different ways. They can be used to form the covalent bond skeleton and then used again to form the orbitals that hold the electrons that are originally in the 3*d* orbitals of the transition metal [10-12].

2.3 Batteries

A battery is an electric cell, a device that produces electricity from a chemical reaction. It converts energy stored in the chemical bonds of a material into electrical energy passing through oxidation/reduction (redox) reactions. Redox reactions are chemical reactions in which an electron is either required or produced by the chemical reaction. It consists of two or more cells connected in series or parallel, but the term is generally used for a single cell. A cell consists of a negative electrode; an electrolyte, which conducts ions; a separator, an ion conductor; and a positive electrode. The electrolyte may be aqueous or non aqueous in liquid, paste, or solid form. If the cell is connected to an external load, or device to be powered, the negative electrode supplies a current of electrons that flow through the load and are accepted by the positive electrode. When the external load is removed, the reaction comes to an end [13].

The key components that determine many of the basic properties of the battery are the materials used for the electrode and electrolyte for both the oxidation and reduction reactions. The electrode is the physical location where the core of the redox reaction (the transfer of electron) takes place. In many battery systems, including lead acid and alkaline batteries, the electrode is not only where the electron transfer takes places, but is also a component in the chemical reaction that either uses or produces the electron. However, in other battery systems (most commonly fuel cells) the electrode material is itself inert and is only the site for the electron transfer from one reactant to another. For a discharging

battery, the electrode at which the oxidation reaction occurs is called the anode and by definition, it has a positive voltage, while the electrode at which the reduction reaction occurs is the cathode and it has a negative voltage. While in recharging the anode has by definition a negative charge and the cathode a positive charge.

The electrode alone is not sufficient for a redox reaction to take place, since a redox reaction involves the interaction of more than a single component. The other chemical components of the reaction are contained in the electrolyte. For many practical battery systems, the electrolyte is an aqueous solution. One reasons for having an aqueous solution is the oxidized or reduced form of the electrode exists in an aqueous solution. Further, it is important that the chemical species in the electrolyte be mobile in order that they can move to the site on the electrode where the chemical reaction takes places, and also such that ion species can travel from one electrode to the other [14].

2.3.1 Types of batteries

Batteries are classified into two broad categories: primary and secondary batteries. In a primary battery, the chemical energy is converted to electrical energy in a one way process. Although there are those kinds of batteries, which are irreversibly transforming chemical energy to electrical energy, when the initial supply of reactants, is exhausted, energy cannot be readily restored to the battery by electrical means. Therefore, the process is not reversible and electrical energy cannot be converted to chemical energy. This means that a primary battery cannot be recharged; it will only convert its chemicals into electricity once, and then must be discarded. Some types of primary batteries are for instance, telegraph circuits, which are restored to operation by replacing the components of the battery consumed by the chemical reaction, and alkaline consumer batteries, which are in flashlights [13-15]. ***Figure 2.1*** shows all types of battery systems.

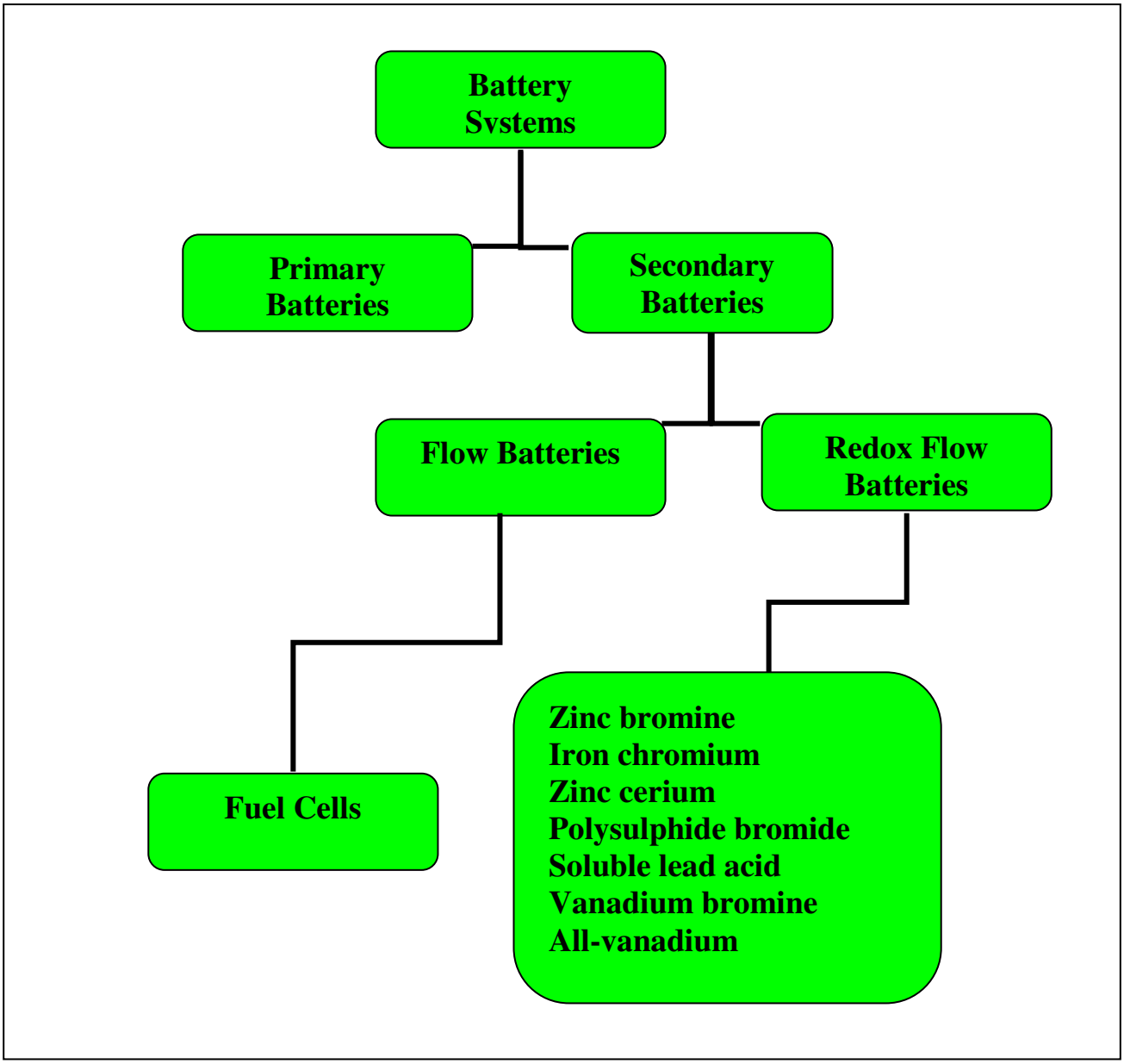

Figure 2.1: Flow chart of all types of battery systems

In a secondary battery, the conversion process between electrical and chemical energy is reversible: chemical energy is converted to electrical energy, and electrical energy can be converted to chemical energy, and batteries can be recharged. Specifically batteries can have their chemical reactions reversed by supplying electrical energy to the cell, restoring their original composition. A secondary battery has electrodes that can be reconstituted by passing electricity back through it; therefore it is also called a storage or rechargeable battery, it can be reused many times. For photovoltaic systems, all batteries used must be rechargeable or secondary batteries. Common examples of secondary batteries are lead acid batteries (including those used in cars) and lithium-ion batteries used in higher power consumer

electronic equipment such as computer laptops, camcorders, mobile telephones, and some digital cameras [14-16].

One of the first space batteries was the silver zinc battery, which dominated the industry in the 1960's. This is a premium system with very high specific power and energy, but is quite expensive due to the use of silver. They are still used in selected applications, such as launch vehicles and torpedoes. Mars Pathfinder also used a silver zinc battery, but it was designed to be rechargeable. They have a relatively short cycle life, and are not used for multi-year missions. This type of battery is commonly used in the commercial market as hearing aid batteries [15].

2.3.2 Redox Chemistry

Batteries generate electricity and store chemical energy by a redox (reduction/oxidation) reaction, as described above (***Section 2.2***). Galvanic cells, fuel cells and flow cells are all based on a redox reaction. Flow batteries (FB) are the second category of electrochemical storage systems. They are large energy storage devices that have a wide range of potential applications in a distributed generation network. The NASA group started to work on redox flow batteries (RFB) in 1979, when they developed and demonstrated the RFB system with the plan to increase stationary energy storage applications [17].

2.3.3 Oxidation and reduction

A reaction in which both oxidation and reduction is occurring is called a redox reaction. Redox reactions are very common; as one substance loses electrons the other substance accepts them. Oxidation requires an oxidant. Oxygen is an oxidant, but not the only one. Despite the name, an oxidation reaction does not necessarily need to involve oxygen. In fact, even fire can be fed by an oxidant other than oxygen: fluorine fires are often unquenchable, as fluorine is an even stronger oxidant (it has a higher electronegativity) than oxygen [18-19]. A redox reaction is a transformation of matter at the atomic level by electron transfer from one species to another. A molecule is oxidized when it loses electrons. It is reduced when it gains electrons.

An oxidizing agent (called an oxidant) where electrons are taken from another substance and becomes reduced.

$$oxidant + electron = product$$

A reducing agent (called a reductant) gives electrons to another substance and is oxidized in the process.

$$Reductant = Product + electron$$

In the RFB, the redox reaction is separated in two simultaneous steps occurring on both sides of the membrane. During the discharge, electrons are removed from the anolyte and transferred through the external circuit to the catholyte. The redox reaction in this case is:

Oxidation $Ce^{3+} = Ce^{4+} + electron$

Reduction $Ce^{4+} + electron = Ce^{3+}$

$$Ce^{3+} + Ce^{4+} \longrightarrow Ce^{4+} + Ce^{3+}$$

The oxidant Ce^{4+} takes an electron from the reductant Ce^{3+}, as the reaction proceeds from left to right, Ce^{4+} is reduced and Ce^{3+} is oxidized.

The flow of electrons is reversed during the charge, the reduction now takes place in the anolyte and the oxidation in the catholyte. The redox reaction in this case is

Reduction $Ce^{4+} + electron = Ce^{3+}$

Oxidation $Ce^{3+} = Ce^{4+} + electron$

$$Ce^{4+} + Ce^{3+} \longrightarrow Ce^{3+} + Ce^{4+}$$

Because there is no net change in charge during a redox reaction, the number of electrons in excess in the oxidation reaction must equal the number consumed by the reduction reaction [18].

2.3.4 Flow batteries

Flow batteries are often called redox flow batteries. The name redox flow battery is based on the redox reaction between the two electrolytes in the system. Redox as already mentioned above in ***Section 2.2.4*** stands for reduction/oxidation reaction. These reactions include all chemical processes in which atoms have their oxidation number changed. A flow battery is a form of battery in which electrolyte containing one or more dissolved electroactive species flows through a power cell and, the reactor in which chemical energy is converted to electricity. Its stores electrolyte externally, generally in tanks, and is usually pumped through the cell of the reactor.

A flow battery is a type of battery that is designed to be very flexible. It can be designed for high power applications as well for high capacity electrical energy storage. There are several types of electrical energy storage, like conventional batteries and flywheels that do not show flexibility and have some limitations to their applications. Flywheels are mostly used for short durations of less than 5 minutes and high power storage greater than 500 kW, while batteries are used for lower power less than 500 kW and long durations of more than 1 hour. Flow batteries are used for large-scale projects that require high-capacity storage and also high power storage, for instance for grid-connected electricity storage at wind farms. There are many types of flow batteries using aqueous electrolytes. These include the early developed iron chromium cell, as well as polysulfide bromine, zinc bromine and all-vanadium redox flow cells. All flow cells have a same design but use different electrolytes in the positive and negative half cells. Each cell varies in terms of an open circuit potential, coulombic efficiency, energy efficiency and cycle life, but cells share similar challenges such as electrolyte management and membrane failure [17, 20].

In a flow battery the battery is charged and discharged by a reversible chemical reaction between the two liquid electrolytes of the battery. These electrolytes are not stored in the power cell of the battery as in a conventional battery, but in separated storage tanks. During operation these electrolytes are pumped through the electrochemical reactor in which a chemical redox reaction takes place and electricity is produced. Due to this storage of the electrolytes outside the reactor, the specifications of the battery are flexible; the power and the energy content of the system can be specified separately. It is very easy to increase the amount of electrolytes or to replace the electrolytes. Moreover, the design of the power cell can be optimized for the power rating needed, as this is independent of the amount of

electrolyte used. The development of flow batteries has reached the stage of demonstration projects. Small-scale products are already available on a commercial basis, while for the larger-scale projects demonstrations have been started. These demonstration projects prove the technology and show that it can be applied on a large scale. The costs of the technology will decrease as soon as the technology becomes available as a commercial product. Based on current feasibility studies, the life cycle costs will be lower than those of the alternatives, based on the capital costs and the expected life time. Flow batteries can be very attractive for future applications, especially for large-scale applications, like peak power support at wind farms or distribution level balancing [17, 20-23].

2.3.5 Redox flow battery

A redox flow battery (RFB) is an electrochemical system that allows energy to be stored in two solutions containing different redox couples, with electrochemical potentials sufficiently separated from each other to provide an electromotive force to drive the oxidation/reduction reactions needed to charge and discharge the cell [23]. RFBs are stationary storage batteries that operate by continually pumping two electrolytes past a pair of high-surface-area electrodes that are separated by an ionically conductive spacer. Energy is stored and harvested via the oxidation/reduction reactions of redox-active solutes in the two electrolytes. The capacity of the redox flow battery system is increased by simply increasing the concentration of the electrolytes or the volume of the electrolyte reservoirs, while the storage capacity of conventional secondary batteries depends on the size of the electrodes. It is an indication of the potential of redox flow battery technology that three alternative systems have recently been commercialised: an all-vanadium system, a polysulphide–bromine system and zinc–cerium system.

The redox flow cell concept was proposed first by NASA [17], as mentioned previously in this ***Section 2.2.3***. RFBs become more interesting in the 1970's, especially where the NASA group became active in different projects. RFBs containing the Fe–Ti couple, where $FeCl_3$ was used as the oxidising agent and $TiCl_2$ as the reducing agent, both couples where in an alkaline electrolyte [24]. Then Ti^{2+} was replaced by Cr^{2+}, leading to better performances.

During the years in 1980's, much work was carried out by NASA on the Fe–Cr system, as well as on the zinc/alkaline/sodium ferricyanide ($Na_3Fe(CN)_6$,H_2O) couple [25]. Bartolozzi [20] has summarised the redox principle, the main reports on RFBs, and also the historical

background of RFB. He mentions that redox flow batteries differ from conventional batteries because the active materials are concentrated solutions of redox-active solutes and not solid-state materials. RFB is one type of an advanced rechargeable battery. One of the most attractive features is the possibility of an independent scaling of electric energy storage.

A RFB is a new type battery, which is composed of stacks, electrolytes, pumps, tanks (see ***Figure 2.2***). In the system, RFB is stored with electric energy through the oxidization of the positive electrolyte (M^{4+} / M^{5+}) and the reduction of the negative electrolyte (M^{3+} / M^{2+}).The energy is discharged through the reverse reactions. The volume of the electrodes in the battery changes with the charge and discharge and this phenomenon causes the electrode to powder or to drop out [26-27].

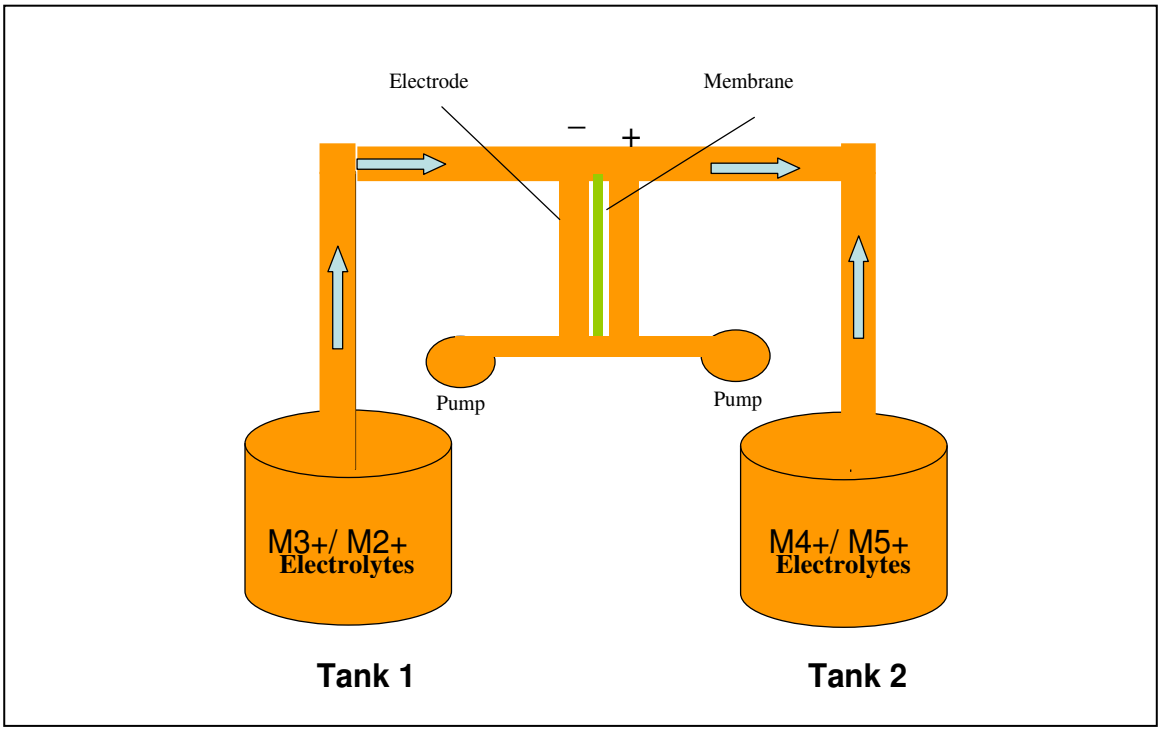

Figure 2.2: Basic construction of a redox flow battery.

Recently much attention has been focused on the all-vanadium RFB [26-28] particularly because it's various advantages. There is no decrease in capacity caused by the cross mixing of the positive electrolyte and negative electrolyte, meaning that there will be no energy efficiency loss during the process. The effect of cross-contamination of an all-vanadium RFB does not need catalysts for both electrode reactions, and the evolution of hydrogen gas will not be observed, which needs rebalancing power and additional equipment. Even though these qualities exist for all-vanadium redox flow systems, the open-circuit voltage for each single

cell after full charging is about 1.4 V, which is relatively low. Many researchers were concerned with investigating different ways to make RFBs the best, safest and most suitable and high energy storage system [27-35].

2.4 Types of flow batteries

2.4.1 Zinc bromine redox system

The zinc bromine battery (ZBB) is a hybrid flow battery because one of its electrodes participates in the reaction. This technology is currently being developed primarily for stationary energy storage applications, but also for electric vehicle applications. The system offers a good specific energy (65-84 Wh/kg) and can withstand 2000 cycles [36].

The concept of a battery based on a zinc bromine originated as long ago as the 1880s, but due to technical difficulties halted development was until the mid 1970s [37]. ZBBs have attracted great interest as a rechargeable power source because of their good energy density, high cell voltage, high degree of reversibility, and the availability of low cost materials. As in other redox flow cells, the aqueous electrolyte solutions containing reactive species are stored in external tanks and circulated through each cell in the stack. Each cell contains two electrodes at which reversible electrochemical reactions occur. The electrolyte is zinc bromide salt dissolved in water; during the charge, zinc is plated on the negative electrode, thus limiting the capacity of the battery. At the positive electrode, bromine is produced and forms a bromine complex that sinks to the bottom of the positive electrolyte tank. During the discharge, zinc is redissolved to form zinc ions and bromide ions are formed at the positive electrode. A third pump is required to re-circulate the bromine complex. The ZBB efficiency is around 60 –75 %. Over the years, some multi-kWh ZBB have been built and tested [38-39].

2.4.2 The iron–chromium redox system

The NASA group [40-44] first studied the iron–chromium redox system. The positive reactant is an aqueous solution of ferric–ferrous redox couple while the negative reactant is a solution of the chromous–chromic couple, both acidified with hydrochloric acid. In this redox flow cell the flow rate of each reactant is always higher than the stoichiometric flow requirement,

which would result in total reactant utilization in a single pass through the cell. In each cell, an anionic and cationic ion exchange membrane separates the two flowing reactant solutions.

In principle, the membrane prevents cross diffusion of the iron and chromium ions, permitting free passage of chloride and hydrogen ions for completion of the electrical circuit through the cell. These early cells have been studied by various researchers and groups like NASA [20], and the research group of the University of Alicante in Spain [45-46], Shimada et al. [47] reported on an investigation into the performance of a Fe–Cr redox flow cell. They reported that the coulombic efficiency increased when the structure of the carbon fibbers changed from amorphous to graphite and that 95% coulombic efficiency. In another study by Johnson and Reid [48], the Fe–Cr redox system was evaluated using 1/8 inch carbon felt electrodes.

2.4.3. Zinc–cerium redox system

This system has been developed by Plurion Systems Inc. [49], they have successfully managed to operate a cell at high current densities of 400–500mA cm^{-2}. Their cell voltage of the Zn–Ce system during charge was approximately 2.5V and droped to below 2V on the discharge cycle. Another Zn–Ce system, patented in 2004 [50], was used with a cell containing carbon plastic anodes and platinized titanium mesh cathodes of 100 cm^2 geometrical area separated by a non-specified type of Nafion membrane.

Lopez-Atalaya et al. [51] describe the performance of a Fe–Cr redox flow battery, which operates in bipolar mode. They studied the optimization of electrolyte composition, temperature, and membrane type, and obtained the following results: Coulombic efficiency of 97%, and an energy efficiency of 73% for an electrolyte composition of 2.3 M HCl + 1.25 M $FeCl_2$ + 1.25 M $CrCl_3$, using a Nafion 117 membrane, and working at the temperature of 44 °C with a current density of 40 mA/cm^2. They also obtained a maximum discharge power density of 73 mW/cm^2.

2.4.4 Polysulphide bromide battery

A polysulphide bromide battery (PSB) is a FB using sodium bromide and sodium polysulphide as salt solution electrolytes. Sodium ions pass through the membrane to maintain the electroneutrality of the cell. Although this technology is maintained to be environmentally friendly by Price et al. [52], there is concern that toxic bromine vapour might

be released in the event of an accident. Some multi-kilowatts batteries have been built. Innogy has built a 100 kW stack with a 1 m^2 electrode area, with a net efficiency of about 75%. The construction of two large (12, 15 MW, and 120 MWh) storage plants in the UK and US has ceased due to engineering difficulties and financial constraints. Ever since then active PSB development has been neglected [53].

2.4.5 Soluble lead-acid battery

This is a flow battery based on the electrode reactions of lead(II) in methanesulfonic acid. This system differs from the traditional lead-acid battery as Pb(II) is highly soluble in the aqueous acid electrolyte. It also differs from the reported redox flow batteries because it only requires a single electrolyte, i.e., no separator or membrane is necessary, which significantly reduces the cost and design complexity of the batteries [54]. The electrode reactions involve the conversion of the soluble species into a solid phase during charging and dissolution at the discharging cycles. Dissolution and deposition of lead should be fast and no overpotential should be required, however, if overpotentials occur hydrogen evolution might take place and reduce the storage capacity. These cells have been studied in several electrolytes: perchloric acid, hydrochloric acid, hexafluorosilicic acid, tetrafluoroboric acid and most recently, methanesulfonic acid [54-58].

2.4.6 Vanadium–bromine redox system

The vanadium–bromide redox flow system was considered long time ago and most researchers have recently shown interest. The energy density is related to the concentration of the redox ions in solution, the cell potential and the number of electrons transferred during the discharge per mol of active redox ions. All –vanadium redox flow cells have a maximum vanadium concentration in the region of 2 mol dm^{-3}, which limits energy density and represents the solubility limit of V(II) and V(III) ions in sulfuric acid at temperatures between 5 and 40 $^{\circ}C$, at which the V(V) ions are still stable [59-60]. A variation of the vanadium–bromide cell is the vanadium–polyhalide cell in which the polyhalide presents higher oxidation potential and exists as a result of the interaction between halogen molecules and halide ions such as Br_2Cl^- or Cl_2Br^- equivalent to the species I^{3-} of Br^{3-}. Vandium RFB system has been tested in a small laboratory scale redox flow cell with two glassy carbon

sheet current collectors and graphite felt electrodes, separated by a Nafion® 112 membrane, and VCl^{2}/VCl^{3} electrolyte on the negative side and Br^{-}/$ClBr^{2-}$ on the positive [60].

2.4.7 All–vanadium redox flow battery (VRFB)

Maria Skyllas-Kazacos and coworkers [61-62] first developed the VRFB at the University of New South Wales, Australia. It employs vanadium redox couples in both half-cells, by this means, eliminating the problem of cross–contamination by diffusion of ions across the membrane. The VRFB exploits the ability of vanadium to exist in four different oxidation states, and utilizes this property to make a battery that has just one electroactive element instead of two. These flow batteries are excellent candidates for large stationary storage applications. A VRFB consists of an assembly of power cells, each of which contains two half-cells that are separated by an ion–permeable membrane. In the half-cells, the electrochemical reactions take place on inert carbon felt electrodes from which the current is collected. The balance of components required for the VRFB consists of pipes and pumps so that the electrolyte can flow from the tanks to the stack. The electrolyte is a solution of vanadium mixed with dilute sulphuric acid; and has the same acidity as a conventional lead–acid battery. Unlike lead–acid systems, the VRB electrolyte has an indefinite life span and is reusable [62-65].

According to Skyllas-Kazacos and co-workers [59-60, 65-73] the VRFB is not damaged by fluctuating power demand or by repeated total discharge or charge rates as high as the maximum discharge rates [66-69]. VRFB can also be charged to ensure that gassing is eliminated during the high charge rates associated with rapid charging cycles. Furthermore, VRB cells can be overcharged and overdischarged, within the limits of the capacity of the electrolytes, and can be cycled from any state of charge or discharge, without permanent damage to the cells or electrolytes. There is however the problem that the strong activity of a certain type of vanadium ion, V(V), degrades the ion exchange membrane. Vanadium batteries are being studied in detail by the research group of Skyllas-Kazacos at the University of New South Wales (Australia) and by various industrial organizations [59-75].

Table: 2.1.Advantages and disadvantages of battery energy storage systems compared to redox flow system [3]

Battery energy storage system	**Advantages**	**Disadvantages**	**Redox flow system**
Conventional systems	Well-known technology	Frequent maintenance	Flooded lead-acid battery
	Low maintenance	Heavy	Valve-regulated lead-acid (VRLA)
	Small size	High construction cost	
		Expensive technology	
		Short life span	
		Not portable	
Developmental systems	Transportability	Thermal management	Sodium –sulfur battery
	High energy (charging) efficiency	Difficult maintenance	Zinc –bromine redox flow cell
	Flexible operation		
Redox flow cells	Low cost	Latest technology	Bromine –polysulphide redox flow cell
	Modularity		Vanadium redox flow cell
	Transportability		Iron –chromium redox flow cell
	Flexible operation		Zinc –cerium redox flow cell
	High efficiency		
	Large scale		

The advantages and disadvantages of conventional developmental and redox flow battery systems are listed and compared in ***Table 2.1*** [3]. There are some systems with fewer

advantages than disadvantaged and some systems with more advantages and fewer disadvantaged. In the cases of the ones with more disadvantages, researchers have recommended further studies. Particularly developing new redox flow systems that will be safe, suitable, reliable, have higher energy storage, and be relatively low cost.

2.5 The performance of RFBs

The purpose of a battery is to store energy and release it at the appropriate time and in a controlled manner. VRB stores energy by employing vanadium redox couples: $V2^{+}/V3^{+}$ in the negative and $V4^{+}/V5^{+}$ in the positive half-cells. These are stored in mild sulphuric acid solutions (electrolytes). During the charge/discharge cycles, H^{+} ions are exchanged between the two electrolyte tanks through the hydrogen-ion permeable polymer membrane. During that process the voltage of the cell is measured and recorded. The cell coulombic efficiency (CE) is defined as the discharge capacity divided by the charge capacity. The energy efficiency (EE) is defined as the discharge energy divided by the charge energy. Then the voltage efficiency (VE) is calculated from VE = EE/CE. The cell voltage of vanadium RFB is about 1.4 to 1.6 V. The net efficiency of this battery can be as high as 85%. The power and energy ratings of VRB are independent of each other, as with other flow batteries [76].

The charge/discharge current of a battery is measured in terms of the C-rate. Most portable batteries are rated at 1C. This means that a 1000 mAh battery would provide 1000 mA for one hour if discharged at 1C rate. The same battery discharged at 0.5C would provide 500 mA for two hours. At 2C, the 1000 mAh battery would deliver 2000 mA for 30 minutes. 1C is often referred to as a one-hour discharge; a 0.5C would be a two-hour, and a 0.1C a ten hour discharge [77].

The capacity of a battery is commonly measured with a battery analyzer. If the analyzer's capacity read out is displayed in terms of percentage of the nominal rating, 100% is shown if a 1000 mAh battery can provide this current for one hour. If the battery only lasts for 30 minutes before cut-off, 50% is indicated. A new battery sometimes provides more than 100% capacity.

When discharging a battery with a battery analyzer that allows the setting of different discharge C-rates, a higher capacity reading is observed if the battery is discharged at a lower C-rate and vice versa. By discharging the 1000 mAh battery at 2C, or 2000 mA, the analyzer is scaled to derive the full capacity in 30 minutes. Theoretically, the capacity reading should

be the same as with a slower discharge, since the identical amount of energy is dispensed, only over a shorter time. Due to internal energy losses and a voltage drop that causes the battery to reach the low-end voltage cut-off sooner, the capacity reading may be reduced to 95%. Discharging the same battery at 0.5C, or 500mA over two hours may increase the capacity reading to about 105%. The discrepancy in capacity readings with different C-rates is related to the internal resistance of the battery [78-79].

One battery that does not perform well at a 1C discharge rate is the portable sealed lead-acid battery. To obtain a reasonably good capacity reading, manufacturers commonly rate these batteries at 0.05C or 20-hour discharge. Even at this slow discharge rate, a 100% capacity is difficult to attain. To compensate for different readings at various discharge currents, manufacturers offer a capacity offset. Applying the offset to correct the capacity readout does not improve battery performance; it simply adjusts the battery capacity if is discharged at a higher or lower C-rate than specified [80-81]. ***Table 2.1*** summarizes the development of RFB between 1973 and 2009.

Table 2.2: Summary history of RFB

YEAR	AUTHORS	DEVELOPMENT
1973	NASA Group	RFB
1976	Thaller	(Fe^{2+}/Fe^{3+}) &(Cr^{2+}/Cr^{3+}) as electrolytes
1979	Roy & Kaplan (USA)	Analysed the performance capacity for RFB
1980	De Nora (Italy)	(Cr^{2+}/Cr^{3+}) in Fe/Cr RFB
1981	NASA	Investigated factors affecting the performance of Fe-RFB
1983	Nozaki	(Fe^{2+}/Fe^{3+}) & (Cr^{2+}/Cr^{3+})
1984	Nozaki	Fe-Cr electrolytes
1985	Maria Skyllas	Investigated V^{5+}/V^{4+} system for RFB
1986	Gahn from NASA	Investigated new all-VRFB
1987	Keneko	Investigated new electode for Cr-Fe RFB
1988	Maria Skyllas & Rychnik Shimizu, Hamamoto Hatta (Japan) Maria Skyllas & Rychnik	New Characterization of all-VRFB Describe new method for RFB, using UV Rad. New electrode operation in RFB Evaluated membranes for All-VRFB
1997	Mitsubishi	Demonstrates numbers of prototype load leveling VRBS
2001	Federation group Federation group & Vantek	Developed & utilized RFB in South Africa Installation of VRB in Cape Town Stellenbosch universities & largest VRB outside Japan
2002	Bae C. H, Roberts	Cr-EDTA RFB
2006	Yamamura and Shiokawa from Japan	Determine the energy efficiency of neptunium redox battery and compare it with VRFB
2008	Research group from Chinese Academy of Sciences	Investigated the VRFB for energy storage in China
2009	Rahman and Maria Skyllas	Investigated a positive half-cell electrolyte for VRFB

2.6 References:

[1] Robinson R.A, Stokes R.H, Electrolyte Solutions: the measurement and interpretation of conductance, chemical potential and diffusion in solutions of simple electrolytes, London Butterworths Scientific, 2nd edition (1955).

[2] Moon J-W, Hwang H-J, Awano M, Maeda K, Materials Letters 57 (2003) 1428

[3] http://www.vanadiumbattery.com/page4.html.

[4] Zanello P, Inorganic Electrochemistry Theory, Practice and Application, The Royal Society of Chemistry, Cambridge, (2003).

[5] Bard A.J, Faulkner L.R. Electrochemical Methods, Fundamentals and Applications, Wiley Interscience Publications, 2nd edition, New York (2001).

[6] Plambeck J.A, Electroanalytical chemistry: basic principles and applications, Wiley Interscience, (1982).

[7] Schwarzenbach Gerold, Flaschka Hermann, Complexometric titrations London: Methuen (1957).

[8] Schwarzenbach Gerold, Flaschka Hermann, Complexometric titrations, 2nd English edition translated and rev. in collaboration with the authors by H.M.N.H. Irving, London: Methuen (1969).

[9] Skoog D.A, West D.M, Holler F.J, Fundamentals of Analytical Chemistry, Saunders College Publishing, New York 7th edition (1997).

[10] Cotton F A, J. Chem. Ed. 41 (1964) 466.

[11] Mahan Herbert Bruce, University Chemistry, Reading, Mass, Addison-Wesley (1965).

[12] Huheey.E. James, Inorganic Chemistry: Principles of Structure and Reactivity, 3rd edition Harper & Row, New York (1983).

[13] Baxter Richard, Energy Storage: a nontechnical guide, Tulsa, Okla, PennWell (2006).

[14] Nuñez Magdalena, Electrochemical studies of batteries, New York, Nova Science Publishers (2005).

[15] http://www.exide.com/history/history4.html

[16] http://www.buchmann.ca

[17] National Aeronautics and Space Administration, Redox Flow Cell Development and Demonstration Project, NASA TM-79067, U.S. Dept. of Energy (1979).

[18] Latimer W.M, The Oxidation States of the Elements and Their Potentials in Aqueous Solutions, Prentice-Hall, Englewood Cliffs, New Jersey (1952).

[19] Monk P M S, Fundamental of Electroanalytical Chemistry, Wiley Interscience, England (2001).

[20] Bartolozzi M, Development of redox flow batteries. A historical bibliography, J. Power Sources 27 (1989) 219.

[21] Modiba P, Crouch A.M, J. Appl. Electrochem. 38 (2008)1293.

[22] Modiba P, Crouch A.M, Proceedings of the 43rd Power Source Conference (2008).

[23] Modiba P, Matoetoe M, Crouch A.M, submitted to Electrochim. Acta (2009).

[24] Liu C.C, Galasco R.T, Savinell R.F, J. Electrochem. Soc.129 (1982) 2502.

[25] Reid MA, Thaller LH (1980) NASA Tech Membr No. 809289:1471.

[26] Fabjan C, Garche J, Harrer B, Jörissen L, Kolbeck C, Philippi F, Tomazic G, Wagner F, Electrochim. Acta, 47 (2001) 825.

[27] Tsuda I, Nozaki K, Sakuta K, Kurokawa K, Solar Energy Materials and Solar Cells 47 (1997) 101.

[28] Skyllas-Kazacos M, Rahman F, J. Power Sources 189 (2009)1212.

[29] Shah A.A, Watt-Smith M J, Walsh F.C, Electrochim. Acta 53 (2008) 8087.

[30] Xi J, Wu Z, Qiu X, Chen L, J. Power Sources 166 (2007)531.

[31] Chakrabarti M.H, Dryfe R.A.W, Roberts E.P.L, Electrochim. Acta 52 (2007) 2189.

[32] Oriji G, Katayama Y, Miura T, Electrochim. Acta 52 (2004) 3091.

[33] Sun B, Skyllas-Kazacos M, Electrochim. Acta 37 (1992) 1253.

[34] Paulenova A, Creager S.E, Navratil J.D, Wei Y, J. Power Sources 109 (2002) 431.

[35] Bae C.H, Roberts E.P.L, Dryfe R.A.W, Electrochim. Acta 48 (2002) 279.

[36] Evans T.I, White R.E, J. Electrochem. Soc. 134 (1987) 866.

[37] Evans T.I, White R.E, J Electrochem. Soc. 134 (1989) 2725.

[38] Simpson G.D, White R.E, J. Electrochem. Soc. 136 (1989) 2137.

[39] Simpson G.D, White R.E, J. Electrochem. Soc. 137 (1990) 1843.

[40] Hodgdon R.B, Waite W.A, S.S. Alexander, Anion permselective membrane, NASA CR-174725, DOE/NASA/0264-1 (1984).

[41] Hagedorn N.H, Thaller L.H, Design flexibility of redox flow systems NASA TM-82854, DOE/NASA/12726-16 (1982).

[42] Thaller L.H, Electrically rechargeable redox flow cells, NASA TM-X-71540, 1974.

[43] Thaller L.H, Redox flow cell energy storage systems, NASA TM-79143, DOE/NASA/1002-79/3 (1979).

[44] Hagedorn N.H, NASA redox storage system development project, NASA TM-83677, DOE/NASA/12726-24 (1984).

[45] Codina G, Perez J.R, Lopez-Atalaya M, Vazquez J.L, Aldaz A, J. Power Sources 48 (1994) 293.

[46] Yang C.Y, J. Appl. Electrochem. 12 (1982) 425.

[47] Shimada M., Tsuzuki Y, Iizuka Y, Inoue M, Chem. Ind. 3 (1988) 80.

[48] Johnson D.A, Reid M.A, J. Electrochem. Soc. 132 (1985) 1058.

[49] http://plurionsystems.com/tech_flow_v_conventional.html

[50] Clarke R.L, Dougherty B.J, Harrison S, J.P. Millington, Patent number: WO 2004/095602 A2, 4 November (2004).

[51] Lopez-Atalaya M, Codina G, Perez J. R, Vazquez J. L, Aldaz and A, J. Power Sources 39 (1992)147-154

[52] Price A, Bartey S, Male S, Cooley G., Power Engineering Journal 13 (1999) 122-129

[53] Divya K.C, Ostergaard J, Electric Power Systems Research 79 (2009) 511.

[54] McDonald G.D, Weissman E.Y, Roemer T.S, J. Electrochem. Soc. 119(1972) 660.

[55] Hazza A, Pletcher D, Wills R, Phys. Chem. Chem. Phys. 6 (2004) 1773.

[56] Qian P, Zhang H, Chen J, Wen Y, Luo Q, Liu Z, You D, Yi B, J Power Sources (2008) 175:613.

[56] Hazza A, Pletcher D, Wills R, J. Power Sources 149 (2005) 103.

[57] Pletcher D, Wills R, Phys. Chem. 6 (2004) 1779.

[58] Pletcher D, Wills R, J. Power Sources 149 (2005) 96.

[59] Skyllas-Kazacos M, Limantari Y, J. Appl. Electrochem. 34 (2004) 681.

[60] Skyllas-Kazacos M, J. Power Sources 124 (2003) 299.

[61] Mohammadi T, Skyllas-Kazacos M, J. Power Sources 63 (1996).

[62] Skylla-Kazacos M, Menictas C, Kazacos M, J. Electrchem. Soc. 143 (1996) L86.

[63] Skyllas-Kazacos M, Rychick M, Robins R, All-vanadium redox battery, US Patent 4,786,567 (November 1988).

[64] Sum E, Skyllas-Kazacos M, J. Power Sources 15 (1985) 179.

[65] Sum E, Rychcik M, Skyllas-Kazacos M, J. Power Sources 16 (1985) 85.

[66] Zhong S, Kazacos M, Burford R.P, Skyllas-Kazacos M, J. Power Sources 36 (1991) 29.

[67] Skyllas-Kazacos M, Kasherman D, Hong D.R, Kazacos M, J. Power Sources 35 (1991) 399.

[68] Kazacos M, Skyllas-Kazacos M, J. Electrochem. Soc. 136 (1989) 2759.

[69] Haddadi-Asl V, Kazacos M, Skyllas-Kazacos M, J. Appl. Electrochem. 25 (1995) 29.

[70] Mohammadi T, Skyllas-Kazacos M, J. Appl. Electrochem. 27 (1997) 153.

[71] Mohammadi T, Chieng S.C, Skyllas-Kazacos M, J. Membr. Sci. 133 (1997) 151.

[72] Zhong S, Padeste C, Kazacos M, Skyllas-Kazacos M, J. Power Sources 45 (1993) 29.

[73] Skyllas-Kazacos M, Grossmith F, J. Electrochem. Soc. 134 (1987) 2950.

[74] Menictas C, Cheng M, Skyllas-Kazacos M, J. Power Sources 45 (1993) 43.

[75] Chieng S.C, Kazacos M, Skyllas-Kazacos M, J. Power Sources 39 (1992) 11.

[76] Peng Q, Zhang H, Chen J, Wen Y, Luo Q, Liu Dongjiang Y, Yiu B, J. Power Sources 175 (2008) 613.

[77] http://www.cea.fr/english_portal

[78] www.electricitystorage.org/tech/technologies

[79] Richard Baxter, Energy storage: a nontechnical guide, Tulsa, Okla, PennWell (2006).

[80] Mpho Diko, An investigation into the use of the vanadium redox flow energy storage system for peak-saving and load-leveling, MSc Thesis in Engineering Science, University of Stellenbosch (2003).

[81] Ronald M. Dell, David A. Rand, Clean energy, Cambridge Royal Society of Chemistry (2004).

Chapter 3

Analytical Techniques for Electrolyte Determination

Physical electrochemistry addresses the broad area of fundamental electrochemistry. This includes theoretical and experimental aspects of the kinetics and thermodynamics of heterogeneous electron transfer at electrode–electrolyte interfaces, and the application of spectroscopic and other techniques to the study of the electrochemical interface and processes. In this chapter the analytical techniques that were used for electrolyte determination, cyclic voltammetry (CV), rotating disc electrode (RDE), electrochemical impedance spectroscopy (EIS), change discharge performance determination and capillary electrophoresis (CE), are described.

3.1 Cyclic voltammetry

CV is one of the most widely used techniques for the characterization of redox systems. CV involves linearly scanning the potential of a stationary working electrode, using a triangular potential waveform at a certain speed. Depending on the information sought, single or multiple cycles can be used. During the potential sweep, the potentiostat measures the current resulting from the applied potential. The resulting plot of current vs. potential is termed a cyclic voltammogram [1-3]. CV is also a very useful technique to study redox reactions in aqueous solutions, surface deposition and adsorption [4-6]. CV can also be used for kinetic studies of aqueous solutions and solids by monitoring surface deposition and adsorption

CV can be used in combination with simulation software to calculate rates of homogeneous and heterogeneous reactions. Such studies typically involve varying the scan rate under conditions and examining how the peak currents and peak potentials change in response to differences. Current responses are measured by imposing a cyclic potential sweep on an electrode. Analysis of the current response provides information about the thermodynamics and kinetics of electron transfer at the electrode–electrolyte interface, as well as the kinetics and mechanisms of solution chemical reactions initiated by the heterogeneous electron transfer [1-4].

The primary events in most CV experiments are electrode-mediated oxidation and reduction processes of electroactive species in solution. In order to react, the electroactive species have to diffuse from the bulk solution to the electrode–solution interface. The three modes of mass transfer responsible for transporting the electroactive species from bulk solution to the interface are migration, diffusion, and convection [1, 3]. Migration refers to the movement of an electroactive species under the influence of an electric field. Diffusion is the movement of an electroactive species under the influence of a gradient of chemical potential such as a concentration gradient. Convection is a mode of transport during which the electroactive species is moved by the influence of density gradients, laminar flow, turbulent flow, and agitation.

An electrode mediated reaction involves three main steps [1-2]: mass transfer of a reactant to the electrode, heterogeneous electron transfer involving non-adsorbing species, and mass transfer of the product to the bulk solution. However, in most cases scientists deal with more complex reactions involving hydrolysis steps, a series of electron transfers and protonations, branching mechanisms, parallel paths, or surface adsorption reactions.

Figure 3.1: A typical combination of CV and RDE instrument.

A potentiostat is one of the most widely used instruments in electrochemical studies and it makes possible the performance of techniques such as CV. The potentiostat–galvanostat (voltammetric analyzer model BAS 100B/W provided with the software version 2.3, 2001,

Bioanalytical Systems, Inc. Indiana) was available to perform the CV experiments in this study and is illustrated in ***Figure 3.1.*** A potentiostat system sets the control parameters of the experiment. Its purpose is to impose on an electrode (the working electrode) a cyclic linear potential sweep and to output the resulting current-potential curve. The sweep potential is described in general by its initial (E_i), switching (E_s), final (E_f) potentials, and scan rate (v, in V/s) [1, 3-4].

The potential as a function of time is:

$$E = E_i + vt \text{ (forward sweep)}$$

$$E = E_s - vt \text{ (reverse sweep)}$$

More complicated sweeps are possible, such as in the case where a third delimiting potential is required and $E_i \neq E_f$. In addition, multiple consecutive cycles are sometimes used, but in some instances these are not more instructive than a single cycle. The term linear sweep voltammetry (LSV) is used for a half cycle (½CV). In the present study, two potential values were selected for each cycle: E_i and E_f were made equal, and differed from *Es*. Although the option of a single cycle was used in some instances, consecutive subsequent cycles were recorded when necessary [1, 3].

The electrochemical reaction of interest takes place at the working electrode (WE). Electrical current at the WE, due to electron transfer is termed faradaic current. The potentiostat operates with a three–electrode system in an analytical cell. The three–electrode systems function is to maintain the potential of the working electrode at a desired level with respect to a fixed reference electrode. This goal is achieved by passing the necessary current between the working electrode and a third electrode, called the counter or auxiliary electrode (AE). The counter electrode is driven by the potentiostatic circuit to balance the faradaic process at the working electrode with an electron transfer of opposite direction (e.g. if oxidation takes place at the WE, reduction takes place at the AE). The process at the AE is not of interest in this study, and in most experiments the small currents observed mean that the electrolytic products at the AE have no influence on the processes at the WE. The reference electrode is designed in such a way that its composition remains constant over time and then its potential is fixed. Therefore, any changes in the cell are ascribed to processes occurring at the working electrode. The faradaic current at the WE is transduced to a potential output at a selected sensitivity, expressed in amperes per volt, and recorded in a digital or analog form. The CV response is plotted as current versus potential [1-4].

In order to understand the basics of a CV experiment it is important to consider what happens before and after the working electrode is connected to the potentiostat and placed in contact with a solution containing an electroactive species. Before connection to the potentiostat and immersion into the solution, electrons in the electrode occupy a continuous range of free energies, according to the conduction band model [1-2]. The electron that is easiest to remove is at the top of the conduction band. This energy is termed the *Fermi level energy*. The free energy change associated with the removal of an electron from the electrode is equal and opposite to the Fermi level free energy. The Fermi level is also called the electrochemical potential of the electron in the conducting material [2-3].

In thermodynamics, the electrochemical potential is defined as the change in free energy per unit species (temperature and pressure) kept constant. When the three electrodes are connected to the potentiostat it is possible to control the potential of the working electrode with respect to the reference, which is equivalent to controlling the energy of the electrons within the working electrode. When the working electrode potential is driven toward negative values by applying negative potentials, the energy of the electrons is increased as the potential becomes more negative. When the applied negative potential is sufficient in magnitude and the electrodes are placed in the solution, the electrons will reach a level that is high enough to transfer into vacant electronic states on electroactive species in the solution. Consequently, electrons flow from the working electrode to electroactive species in solution and a reduction current is obtained. In this case, electroactive species in solution are reduced at the electrode–electrolyte interface. In an analogous manner, when the energy of the electron is lowered by imposing a sufficiently positive potential, the electrons flow from electroactive species in solution to the working electrode and an oxidation current is obtained. In this case, electroactive species in solution are oxidized at the electrode–electrolyte interface [1-4].

The magnitude of the potential difference at the interface applies an effect in the relative energies between the electrode and electrolyte. The potential difference controls the direction and the rate of the electron transfer processes. The measured current i due to the number of electrons that cross the interface, is related to the extent of the chemical reaction, and therefore to the amount of reactant consumed and product generated. The measured current can be plotted as a function of potential to obtain the corresponding cyclic voltammogram [1-2, 4].

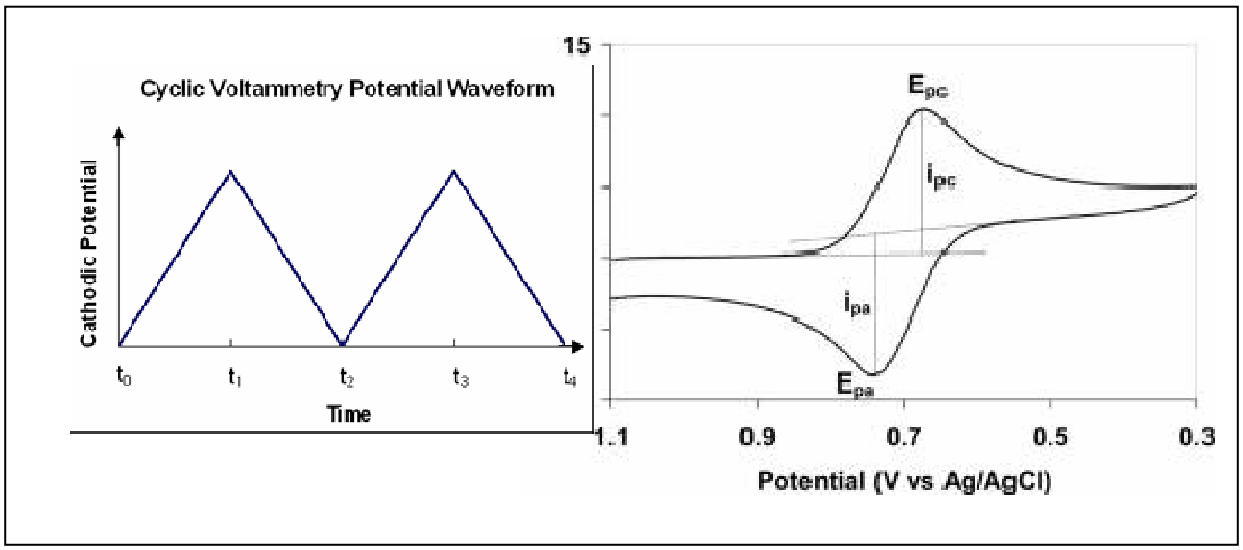

Figure 3.2: *(a)* Cyclic potential sweep and *(b)* a resulting cyclic [1-2].

Figure 3.2 shows an example of *(a)* a cyclic potential sweep and *(b)* a resulting cyclic voltammogram. The potential changes linearly toward negative values and then the potential is reverted linearly in the opposite direction toward positive values. While scanning in the negative direction, at a sufficiently negative potential, a reduction peak that appears corresponds to the reduction of an electroactive species in solution. This peak is often called the reduction peak or cathodic peak and its area is proportional to the amount of electrons crossing the interface. Similarly, the oxidation peak or anodic peak is obtained at a sufficiently positive potential and the peak area is proportional to the amount of electrons that cross the interface [1-2,4].

Although ***Figure 3.2(a)*** presents a cyclic potential sweep where the initial scanning direction is positive and at time t_s reverts to the positive direction, this is not necessarily true for all experiments. Experiments can be designed in such a way that the initial scanning direction is positive and at time t_s reverts to the negative direction. A variety of voltammogram shapes that differ from that shown in ***Figure 3.2(b)*** can be obtained. In some instances, the cathodic peak is obtained but the anodic peak is absent, implying that the electroactive species in solution can be reduced but oxidation processes are inhibited. Conversely, when the anodic peak is observed but no cathodic peak is present, the oxidation of the electroactive species occurs but reduction is inhibited.

The cyclic voltammogram is a complicated time-dependent function of a several number of physical and chemical parameters, which can be explored in more detail by coupling it with time resolved RDE and EIS technology. Applications such as mechanism, number electrons involved in the reaction, sensitivity, are not applicable for routine quantitative analysis.

3.2 Rotating disc electrode

A RDE is a hydrodynamic working electrode used in a three electrode system [1]. The electrode actually rotates during experiments, inducing a flux of analyte to the electrode. These working electrodes are used in electrochemical studies when investigating reaction mechanisms related to redox chemistry among other chemical phenomena. The more complex rotating ring-disk electrode can be used as a rotating disk electrode if the ring is left inactive during experiments [5-6].

CV couple to the use of RDE, it can be used to investigate the kinetics of charge transfer at the electrode–electrolyte interface in the way that the working electrode potential is swept back and forth across the formal potential of the analyte. RDE varies in the working electrode where it is rotated at a very high speed. This rotational motion sets up a well defined flow of solution towards the surface of the RDE. The flow pattern is similar to a current that literally sucks the solution and the analyte towards the electrode [1, 7-9].

The RDE is usually used for laboratory studies due to its ability to control hydrodynamic conditions. RDE is the most popular among the electrodes used for electrochemical experiments under controlled mass transfer. The first person to develop the method to obtain well defined diffusion conditions was Levich [1-2]. The major advantages of RDE are the direct current and mass transport controlled current, double-layer charging effects and the steady-state background current, are advantages that CV does not have.

A RDE consists of a disk of the electrode material embedded in a rod of insulating material, typically made of Teflon with epoxy resin. The rod is directly attached to a motor directly by means of a chuck or by a flexible rotating shaft, and rotates at a certain angular velocity ω (s^{-1}), where $\omega = 2\pi f$ (f is the frequency in rad /s). The electrical connection is made by a brush contact. The motion of the electroactive species is due to the rotation of the electrode [1, 7-9].

Analyte is transported to the electrode surface by a combination of two types of transport. First, the current flow in the bulk solution continuously brings fresh analyte to the outer edge of the stagnant layer. Then, the analyte moves across the stagnant layer via simple molecular diffusion. The thinner the stagnant layer is the faster the analyte can diffuse across it, to reach the electrode surface. Faster electrode rotation makes the stagnant layer thinner. Thus, faster rotation rates permit the analyte to diffuse to the electrode faster, resulting in a higher current being measured at the electrode [1-2, 4]. Experimental results are generally plotted as a graph of current versus potential, and a typical rotated disk voltammogram. The voltammogram exhibits a sigmoidal shaped wave, and the height of the wave, which provides the analytical signal.

It is important to note that the layer of solution immediately adjacent to the surface of the electrode behaves as if it were stuck to the electrode. While the bulk of the solution is being stirred vigorously by the rotating electrode, the thin layer of solution manages to cling to the surface of the electrode, and appears to be motionless from the perspective of the rotating electrode. This layer is called the stagnant layer in order to distinguish it from the remaining bulk of the solution [3].

The Levich equation predicts the current observed at a RDE. This equation takes into account both the rate of diffusion across the stagnant layer and the complex solution flow pattern. In particular, the Levich equation gives the height of the sigmoidal wave observed in rotated disk voltammetry as illustrated in ***Figure 3.3***. The sigmoid wave height is often called the Levich current, i_L, and it is directly proportional to the analyte concentration, C. The Levich equation is written as [1, 9]:

$$i_L = (0.620)\, n\, F\, A\, D^{2/3}\, w^{1/2}\, v^{-1/6}\, C \qquad (3.1)$$

where i_L is the Levich current, n is the number of electrons, F is the Faraday constant, A is the electrode area (cm^2), D is the diffusion coefficient (cm^2/s), w is the rotation rate (radians/s), C is the concentration of solution (mol cm^{-3}) and v is the kinematic viscosity (cm^2/s) is the ratio of the solution's viscosity to its density. For pure water, v = 0.0100 cm^2/sec, and for the background solution (1.0 M KNO_3), v = 0.00916 cm^2/sec. The rotation rates may have to be converted from units of rate per minute (rpm) to radians per second (rps) using the relationship: $w = 2\pi f / 60$ [1, 3, 9].

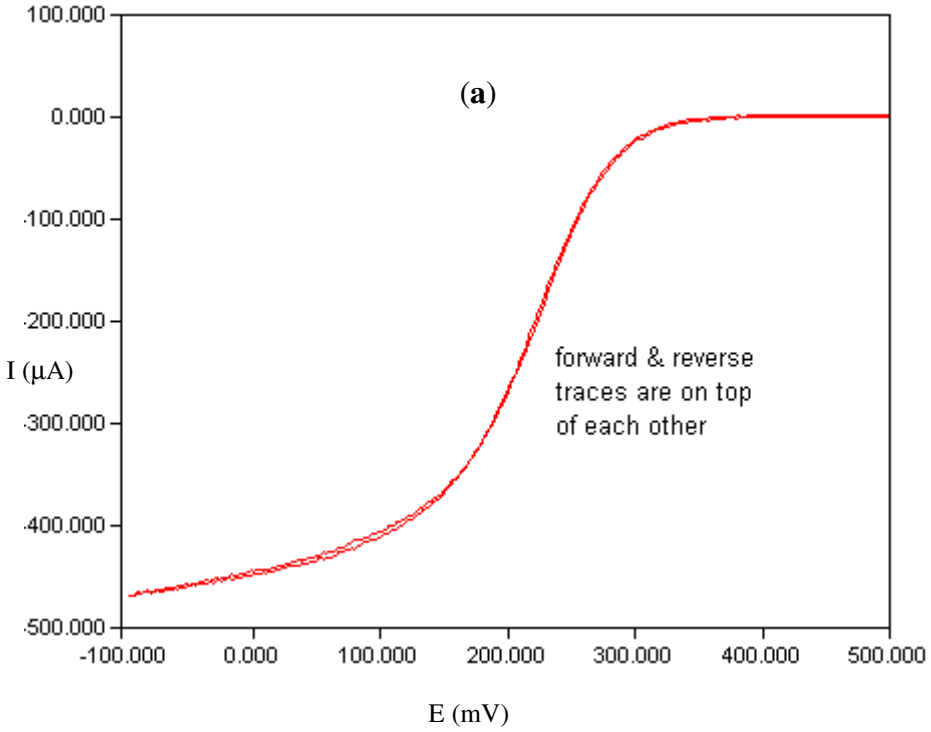

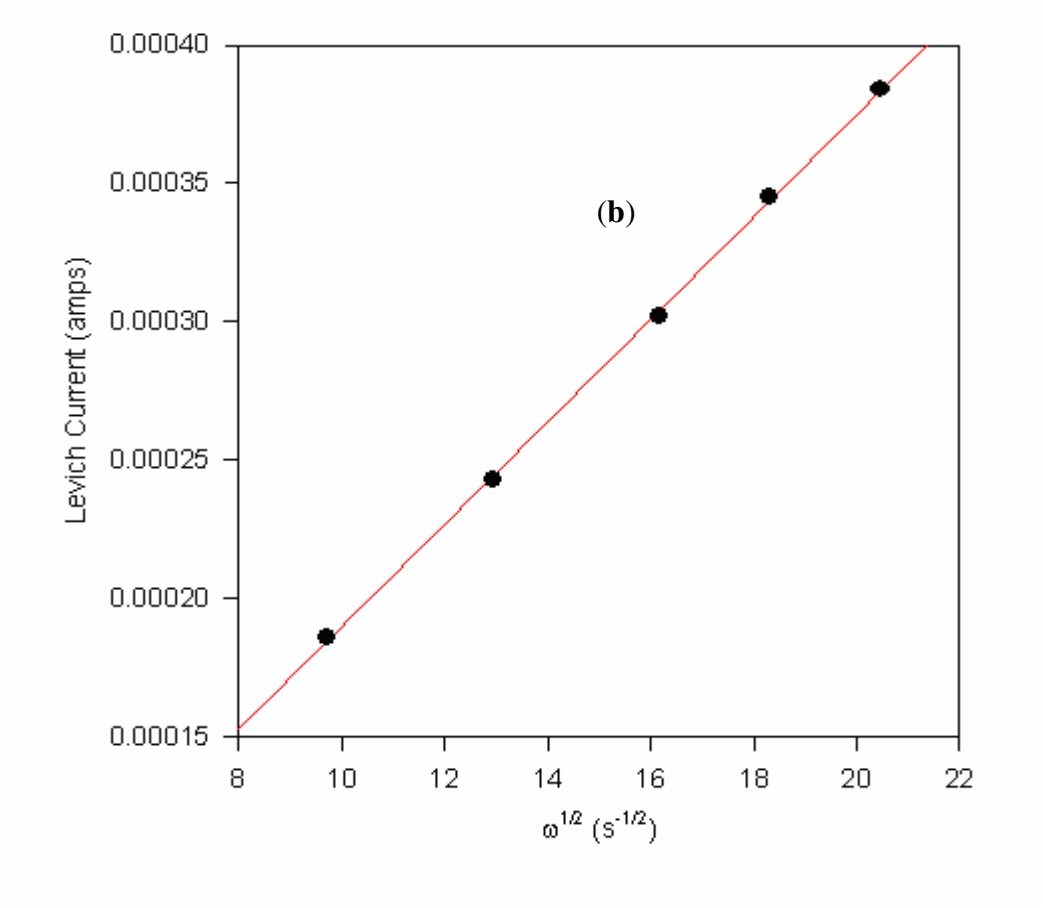

3.3: Hydrodynamic voltammogram (a) for reverse and forward reaction at the rotation rate of 1000 rpm (b) Plot of Levich current vs. square root of rotation rate [1-2].

In the voltammograms for a rotated disk, the limiting current is measured and plotted against the square root of the rotation rate, producing a Levich plot. The experimental rotation rate, *f* is measured in rpm and must be converted to the angular rotation rate, *w*, so that it has units of rps. The linear relationship between the Levich current and the square root of the rotation rate is obvious from the Levich plot. In ***Figure 3.3*** a linear least squares fit of the data produces an equation for the best straight line passing through the data [9]. ***Figure 3.3***(a) shows a hydrodynamic voltammogram for reverse and forward reaction for the solution of the convective-diffusion equation and the steady-state limiting current density. It can be written as in ***equation (3.1),*** where jl_{im} is the limiting current density (A / cm^2), *n is* the number of exchanged electrons, *D is* the diffusion coefficient (cm^2/s), *w* is the angular velocity (s^{-1}), *v* the scan rate (V /s) and C is the bulk concentration (mol /cm^3). A plot of i_L vs. $w^{1/2}$ in ***Figure 3.3 (b)*** gives a straight line with slope proportional to $D^{2/3}$. For a quasi-reversible process, the peak potential E_p is a function of scan rate, and where the difference between E_p and the formal potential E^o is related to the standard rate constant. The peak current may also be expressed as in ***Equation (3.2)*** [1, 9].

$$i_p = (0.227)\, n\, F\, A\, C\, k\, exp\,[-(\alpha n F/RT)\,(E-E^o)) \qquad (3.2)$$

where i_p is the peak current (A), n is the number of electrons transferred per mole of analyte, A is the area of the electrode (cm^2), k is the rate constant (cm^2/s), α is the rate coefficient (V/s) and C is the bulk concentration of analyte (mol /cm^3). The dependence on bulk concentration (rather than the concentration at the electrode surface) allows peak current to be used for quantitative measurements.While the Levich equation suffices for many purposes, improved forms based on derivations utilizing more terms in the velocity expression are available [7-8].

In this study the redox kinetics of redox couples will be pursued using RDE to confirm the results from CV. As mentioned in ***Section 3.1.2*** CV and RDE techniques complement each other [9].

3.3 Electrochemical Impedance Spectroscopy

EIS is an experimental method used to characterize electrochemical systems. This technique measures the impedance of a system over a range of frequencies, and therefore the frequency response of the system, including the energy storage and dissipation properties are revealed. Often, data obtained by EIS are expressed graphically in a Bode plot or a Nyquist plot. During the past few decades, EIS has been developed into a powerful and practical tool for studying electrochemistry. More problems in various systems were encountered especially during the 1980's, although there are disadvantages, difficulties and critical issues associated within its application, EIS has become a very important analytical technique, it has broadened the range of corrosion phenomena that can be studied using electrochemical techniques [1, 4].

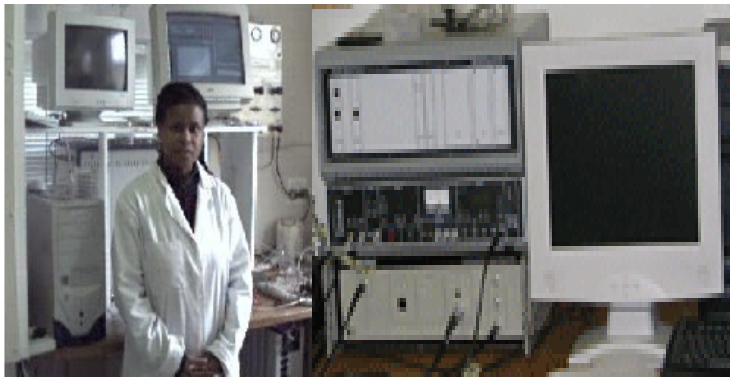

Figure 3.4: A typical EIS instrument.

In EIS the focus is especially on the properties of the polarization layer at a metal to electrolyte or ion conductor interface, and the related chemical reactions. This is just the opposite of dielectric, conductivity, or impedance material spectroscopy, where these effects are known as electrode polarization. ***Figure 3.4*** illustrates a typical EIS instrument.

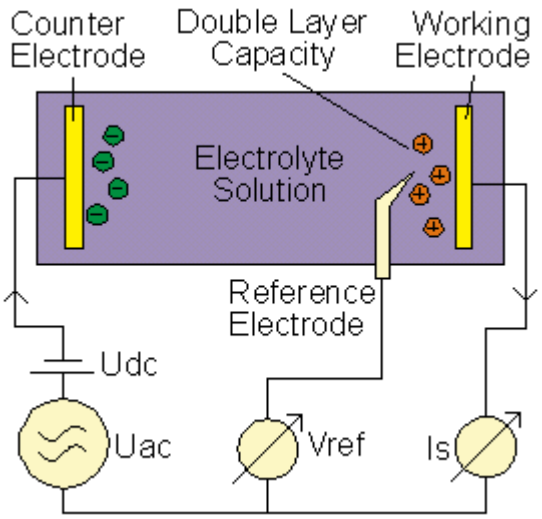

Figure 3.5: Principle of a three–electrode EIS set-up [10].

The two parallel plate electrodes (denoted as the counter and working electrode) and a third voltage reference electrode are placed close to the polarization layer and measures the voltage difference between the polarization double layer capacity and that of the working electrode. In contrast to the case of dielectric, conductivity and impedance material spectroscopy where all electrodes are made of inert metal e.g. gold, stainless steel or platinum, this applies for the electrochemical cell only for the counter electrode feeding current into the electrolyte. The working electrode consists of the metal to be characterized in combination with the electrolyte. The reference electrode is usually an open–tipped glass capillary filled with a standard electrolyte coupled to a standard metal in order to create a defined electrochemical potential to the electrolyte [1, 4]. The principle of an EIS set-up is shown in ***Figure 3.5***.

The total potential drop across the cell is the sum of all contributions of the chemical process like mass transport, chemical and adsorption steps, electron transfer, etc. By measuring the impedance spectrum $V_{Ref}(w)$ /$I_S(w)$ and fitting it with an equivalent circuit model, the several process contributions can be separated from each other. A typical evaluation includes determination of Warburg impedance related to mass transport, electron transfer resistance, electrolyte resistance and double layer capacity. When the working electrodes an electrochemical reaction takes place, it is necessary to keep the DC potential V_{Ref} at a defined value or alternatively apply a constant DC current to the cell. This can be done by using a potentiostat / galvanostat DC circuit as shown in ***Figure 3.6*** [4].

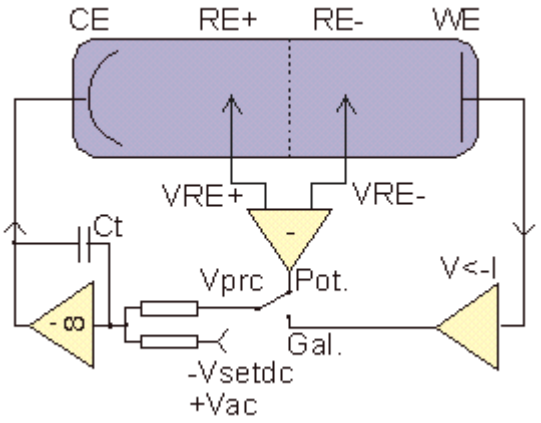

Figure 3.6: Principle of potentiostat / galvanostat circuit with differential reference voltage inputs [10].

The voltage amplifier connected to the CE electrode compares in potentiostat mode the differential voltage $V_{Prc} = V_{RE+} - V_{RE-}$ of both reference electrodes with the intended voltage $V_{set\ DC}$. The amplifier adjusts its output voltage until V_{Prc} and $V_{set\ DC}$ match resulting in a constant and sample impedance independent reference voltage differential which can be adjusted by Vset dc. In galvanostat mode V_{Prc} is created proportional to the measured cell current by a current to voltage converter (V < -I), resulting in constant sample cell current. In both modes, the variable capacitor C_t adjusts the control loop time constant in order to avoid free high frequency oscillations caused by too high an open loop gain [4].

EIS is used in the electrochemical study of corrosion, in areas such as semiconductors, batteries, electrodeposition, electro organic synthesis, and organic coating evaluation [10]. In these areas EIS offers some distinct advantages over DC techniques. Firstly, EIS uses very small excitation potential amplitudes, generally in the range of 5-10 mV peak to peak, which cause only minimal perturbation of the electrochemical test system. Secondly, EIS offers valuable mechanistic information because EIS can provide data on both electrode capacitance and charge transfer kinetics. Last, but not least EIS can be used for electrodes in low conductivity solutions and with organic coatings [4, 10].

EIS has increasingly become the method of choice for achieving a comprehensive understanding of the electrochemical processes. It is a very useful technique for redox flow batteries because it can provide information about the status of the element or redox couple inside the battery cell compartment (for example an electrolyte). EIS is a single technique that is able to identify several different failure modes. This makes it interesting because, even though the instrumentation required for EIS can be expensive, only one involved analytical

system is required. EIS results give a good operating performance data set for developing advanced analytical tools, for delivering immediate information about internal cell behavior and for predicting or identifying failures during operation of cell system [10-12].

In general, impedance analyzers measure the complex impedance $Z^*(\omega) = Z'(\omega) + jZ''(\omega)$ between electrical ports of a system under test and is dependent on frequency $\omega/(2\pi)$. For materials analysis, the $Z^*(\omega)$ spectrum of two or more electrodes with the sample material in between is measured. Depending on the sample material, the requirements to the impedance analyzer are extraordinarily high, thus the result concerning quality and availability strongly depends on its performance. In practice one is generally not so much interested in extreme high accuracy, but to measure both components of $Z^*(\omega)$, permittivity $\varepsilon^*(\omega)$ or conductivity $\sigma^*(\omega)$. Beside the frequency range, the impedance range and the tan (δ) or phase accuracy are the most important performance parameters [4, 10].

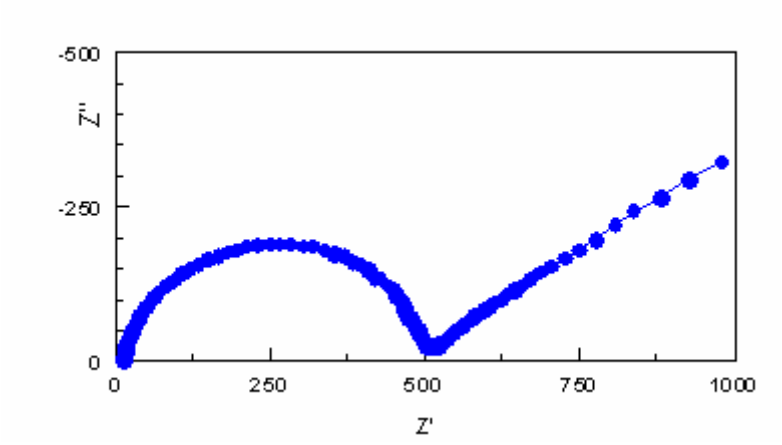

Figure 3.7: Typical Nyquist plot.

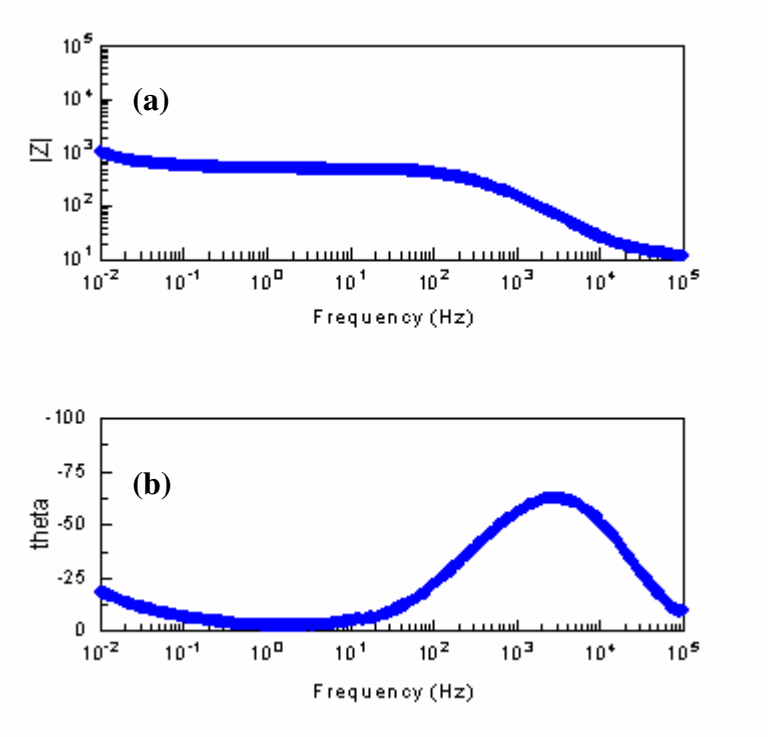

Figure 3.8: (a) Bode-magnitude plot and (b) Bode-phase plot

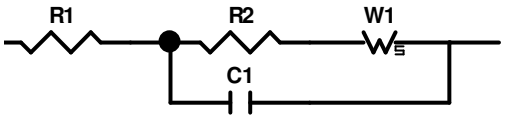

Figure 3.9: Equivalent circuit model used for the impedance data fitting.

EIS is a suitable method for investigating the kinetics of an electrochemical reaction, as the elementary reaction steps that limit the rate of the reaction can, in principle, be separated. EIS is an AC method where a sinusoidal potential, *E*, with varying frequency, *f*, is applied to the electrode:

$$E = AEexp(jwt) \qquad (3.3)$$

where: AE is the amplitude, *j* is the imaginary unit, *w* is the angular frequency (2πf) and t is the time. In the linear current - overvoltage range (small AE in Equation 2.1) the current response, i, as a function of f is also a sin function

$$i = Aiexp(j(wt-\varphi)) \qquad (3.4)$$

where: A*i* is the current amplitude and φ is the phase angle. The impedance, Z, equals

$$Z = E/i = (AE/Ai)exp(j\varphi) \qquad (3.5)$$

The impedance is often plotted in the complex plane, minus the imaginary part along the ordinate axis, and the real part along the axis of Nyquist plot for a mixed control circuit. In ***Figure 3.7,*** a semicircle with a long straight line with a slope of more than 45º from higher to lower frequency region is produced. In addition, a Bode-magnitude plot with Bode–phase plot obtained from equivalent electrical circuit model in ***Figure 3.8***, illustrated by the equivalent circuit shown in ***Figure 3.9***. In this figure, R1 represents the electrolyte resistance, C1 stands for the constant phase element of interface between the electrode and the electrolyte, R2 is the charge transfer resistance, and W is the Warburg diffusion. If C1 is not a perfect capacitor a depressed arc will appear but if is perfect it will be a complete semicircle arc. In the case of a more complex electrode reaction, several elementary processes may limit the reaction rate, and each of these processes may appear in the impedance spectrum as a more or less depressed arc. The arcs may overlap and it can be difficult to separate them in practice. More details about the interpretation of impedance measurements are given in the literature [10, 13].

EIS is able to measure electrochemical cell complex impedance over a wide range of AC frequencies. Typically, several cell elements and cell characteristics contribute to a system EIS spectrum. A partial list of possible elements includes; electrode double layer capacitance, electrode kinetics, diffusion layer, and solution resistance. Unfortunately, the systems impedance at any given frequency usually depends on more than one cell element. This greatly complicates the analysis of EIS spectra. The most common method used to analyze EIS spectra is equivalent circuit modelling [11]. The behaviour of each element is described in terms of “classical” electrical components (resistors, capacitors, inductors) plus a few specialized electrochemical elements (such as Warbug diffusion elements).

3.4 EIS interpretation of measurements

The electrochemical impedance response obtained on composite cathodes generally comprises a high frequency induction tail, L, ascribed to the measurement leads, an ohmic resistance, R_s, mainly originating from the electrolyte (the high frequency intercept adjusted for induction), and a number of more or less overlapping arcs. The data results are always fitted using the computer software EQUIVCRT (Boukamp) or Zplot software (version 2b), in order to determine the magnitude of R_s and the polarization resistance, R_{pol}, and to separate the individual arcs in the impedance spectrum.

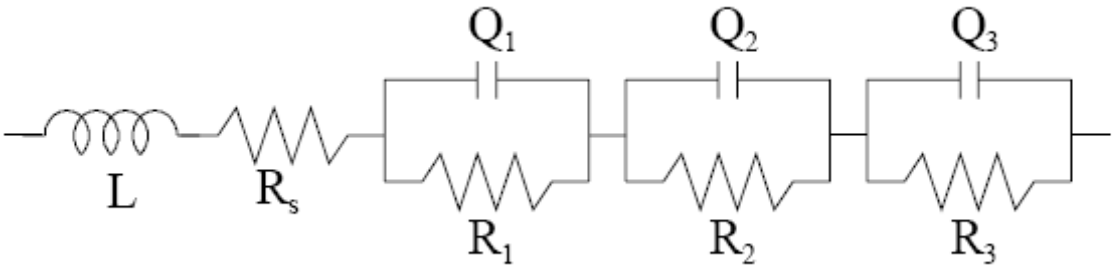

Figure 3.10: The equivalent circuit used for fitting the data. L is an inductance, R_s is the series resistance, R is a resistance, and Q is a constant phase element, $R_{pol} = R_1 + R_2 + R_3$ [10].

In this study the data were fitted to an equivalent circuit of the type $R_s(R_1Q_1)(R_2Q_2)(R_3Q_3)$ see ***Figure 3.10***. R is a resistance, Q is a constant phase element with the admittance $Y' = Y_0 (jw)_n$, where Y_0 is an admittance factor and n is the frequency exponent. RQ is a depressed arc in the impedance spectrum [10-11]. The equivalent circuit has three series connected arcs, which gives the simplest possible description of impedance spectra containing three limiting processes. When fitting the data one or two of the arcs may turn out to be zero. However, this circuit is not adequate to describe the impedance of all composite electrodes. More than three processes may contribute to the impedance response [11]. The circuit is used to determine R_{pol} and the magnitude of the individual arcs present in the impedance spectrum, and the circuit has been found to serve this purpose well.

For the symmetric test cell, the measured polarisation resistance, R_p, reflects the sum of the polarisation resistances of the two electrodes investigated. Therefore, to get the average area-specific polarisation resistance of the two electrodes, R_p, the measured value, R_p, needs to be divided by two and corrected for area. The value of R_p determined in this way is comparable to the polarisation resistance measured using three-electrode cells [10-11].

3.5 Charge–discharge performance

Charging a battery is the act of applying an electric potential across the electrodes or plates of a capacitor, from a diverse source of electrical energy, to increase the amount of useful and available electrical energy stored in the capacitor. It can also be the amount of energy stored in a capacitor that is available for release to usefully supply electrical energy to an electric load. Discharging is the act of removing available electrical energy from storage in a battery, cell or capacitor, via flow of electric current from the battery or capacitor to a load. ***Figure 3.11*** shows the electrochemical cell for charge–discharge performance of a battery electrolyte. The three commonly used performance measures of a flow cell that are obtained from the resultant charge–discharge response are coulombic, voltaic and energy efficiency. Coulombic efficiency, also known as the Amp–hour efficiency, is a ratio of the discharge to charge capacity of the cell. Theoretical capacity or electrical charge (QT) can be calculated from Faraday's Law, therefore in theoretically QT is the product of the cell charging current (I, Amps) and the theoretical discharging time (t_T, seconds) [14].

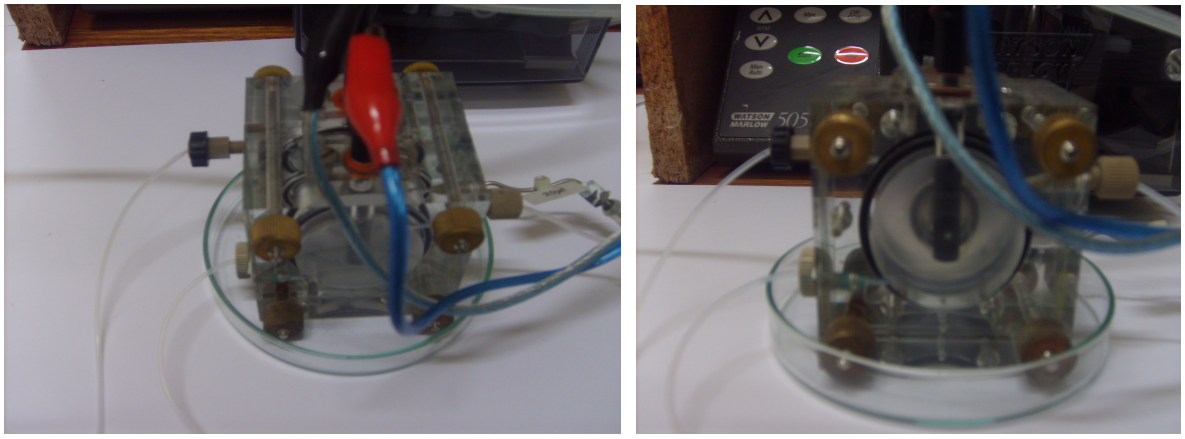

Figure 3.11: Electrochemical cell for charge–discharge performance of battery electrolyte.

Experimentally, the capacity of a cell will be lower than the theoretical value that is calculated as an integral of charge or discharge current (I, Amps or C/s) with time. After the charge and discharge capacity (Ahr) are calculated separately, the coulombic efficiency (%) can be determined. The theoretical available energy (energy T, J) is calculated by multiplying the electrical charge (QT, C) and cell potential (Ecell, V or J/C). Energy is normally recorded in a more common unit, Watt-hours (Wh) which can be converted from Joules (J), using 1Wh = 3600J, while the practical available energy determined experimentally, is an integration of the product of cell potential (V, J/C) and the current (I, C/s) with time. When the

charge–discharge practical energy is obtainable after the calculation, therefore the energy efficiency of the cell can be determined. For an experimental setup with constant charge–discharge current, an energy efficiency calculation would differ slightly from the above description. Since the energy efficiency is also a product of coulombic and voltaic efficiency, the voltaic efficiency can then be determined. Alternately, voltaic efficiency can be approximated as the ratio between discharge and charge voltage at 50%, state of charge (SOC) 50% from the voltage response curve obtained experimentally [14].

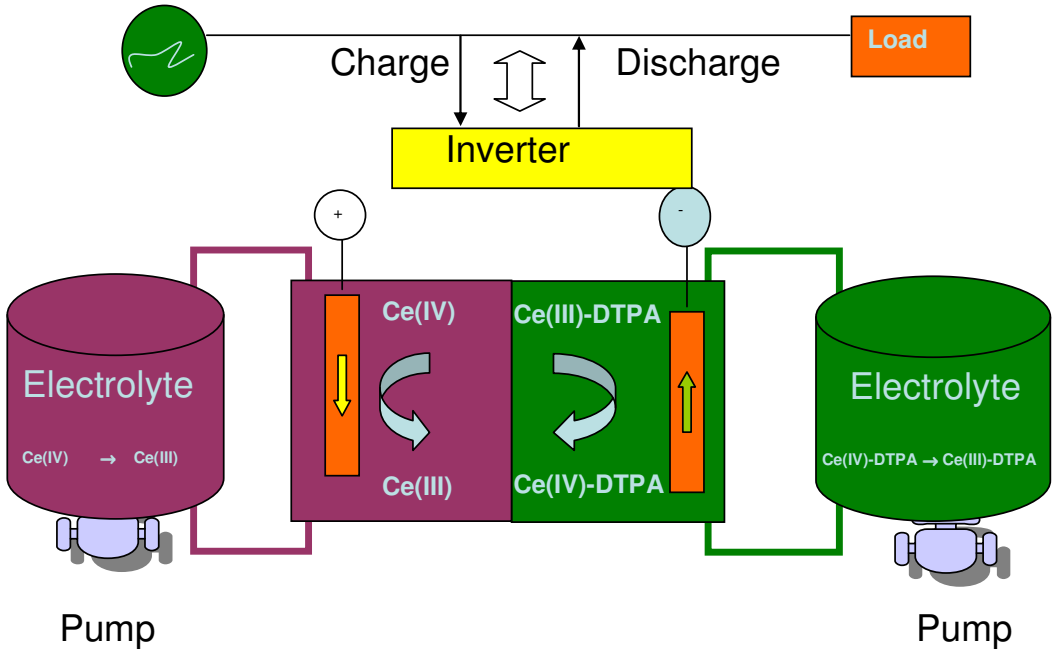

Figure 3.12: A typical charge–discharge diagram [P]

A battery is composed of two electrodes, and a positive cathode and a negative anode, with a porous separator sandwiched between the two. In terms of battery charging, the speed of charge is usually determined by the milliamp hour (mAh) capacity of the battery. If a source is rated at 400 milliamps, charging a 400 mAh battery would take 400/400 = 1 hour (C), while charging a 200 mAh battery would take 200/400 = 0.5 hours (0.5 C). In all reality, however, charging a battery actually requires at least 1.5 C to reload fully. To avoid confusion, the notation for capacitance is an italicized C and the notation for the capacity of a battery is C [15].

[P] Presented Orally by P Modiba at 43rd Power Sources Conference, Philadelphia, New York, 7-10 July 2008.

To test the performance of a flow cell the most common technique is to monitor the cell voltage with time when the cell is charged and discharged at a constant current. A typical charge / discharge response ***(Figure 3.12)*** would have an increasing cell voltage during the charging stage and a gradual decrease when the cell discharges. The electrochemical cell test makes it possible to control the voltage limit and applied current for each charge–discharge cycle and to be able to specify the number of cycles to be repeated. For safety reasons, when measuring voltage range, the current limit has to be set to prevent the occurrence of extreme voltages or currents. For a continuing charge–discharge process, the applied constant current can be changed after a fixed number of cycles. The cell efficiency versus current plot can be obtained without manually restarting the charging process, hence eliminating the stationary time [14].

3.6 Capillary electrophoresis

Electrophoresis is defined as the differential movement of charged ions by attraction or repulsion in an electric field. Tiselius first established CE as a separation technique in 1937 [16]. The separation efficiency in free solution is limited by thermal diffusion and convection. Therefore, electrophoresis has traditionally performed in anti-convective media, such as polyacrylamide or agarose gels. Gels in the slab or tube format that use primarily for the size-dependent separation of biomacromolecules like nucleic acids and proteins. Slab gel electrophoresis is a powerful analytical technique but suffers from some disadvantages including long analysis times, low efficiencies, necessity for staining after the separation and difficulty to automate. Electrophoretic and chromatographic methods are routine separation techniques used to analyze a variety of analytes ranging from small ions to large biomolecules. Although both methods will apply to similar types of analytes, the separation mechanisms are different, resulting in complementary and distinct separation patterns.

Tiselius [16] also developed the moving boundary called “zone electrophoresis” to separate serum proteins in solution. He applied a mixture of proteins in a U-shaped cell containing a buffer solution. The electrodes immersed at each end of the U-tube. Under an applied voltage, the protein samples migrated at different velocities toward the anode or cathode depending on their charges and the movements of boundaries, detected at both ends using Schlieren optics. Due to the significance of Tisselius’s work, he was awarded the Nobel Prize for Chemistry in

1948. The first example of CE in 5 mm narrow tubes was described in 1958 and was cited by Stellen Hjerten in 1967 [17]. To overcome band broadening caused by Joule heating, Hjerten's instrument employed a rotating capillary to diminish the thermal gradient. There have been subsequently attempts to improve CE separation performance by reducing the diameter of the capillary. In 1979, Mikkers et.al [18] reported the use of 200 μm i.d. capillaries in high performance zone electrophoresis with UV and conductimetric detection.

CE is a modern analytical separation technique that is used for a variety of compounds such as amino acids, drugs peptides and various ionic species. It is extremely useful for the analysis of ions, when rapid results are desired. It has become the predominant technique for the analysis of both basic and chiral pharmaceuticals. This technology is making its mark in biotechnology, replacing traditional electrophoresis for the characterization and analysis of macromolecules such as proteins and carbohydrates, and promises to be a valuable tool in tackling the characterization challenges posed by proteome-wide analysis. CE technology has also served to accelerate the accumulation of genome-level knowledge by automating DNA sequencing and genotyping. The "in solution" approach, which is a key feature of this technique, is also ideal for creating environments in which molecular interactions are detected and studied [19-20].

CE is also very well suited for the separation of proteins. It covers a family of related separation techniques that use narrow-bore fused-silica capillaries to separate a complex array of large and small molecules. High electric field strengths are used to separate molecules based on differences in charge, size, and hydrophobicity. Sample introduction is accomplished by immersing the end of the capillary into a sample vial and applying pressure, vacuum or voltage. Depending on the types of capillary and electrolytes used, the technology of CE can be segmented into several separation techniques. Even though CE technology is applied to many different types of research, it has gained its reputation from the study of molecules that have traditionally been difficult to separate. It should be the one to be considered first when dealing with highly polar and charged analytes. The CE separation mechanism is controlled by electrophoretic mobility, which is a function of charge and size of the studied ionic species [19-21]. The capillary electrophoresis technique is clearly illustrated in ***Figure 3.13***.

Figure 3.13: Photograph of a typical CE instrument.

In CE, the only source of band broadening is longitudinal diffusion and therefore narrow peak widths (resolution) can be achieved. Short analysis time, high resolution, low electrolyte and sample consumption are the main advantages of CE compared to other separation techniques like HPLC and GC in particularly high selectivity and lower operating cost, which is the reason CE, was chosen in this study. Separation conditions can be optimized quite effectively by modifying the capillary temperature and separation voltage, and the nature, pH and concentration of the background electrolyte. The main components of a CE system are high voltage power supply, two buffer reservoirs, a capillary and a detector. Basic CE instrumentation can be enhanced with the use of auto samplers, multiple injection devices, multiple detector, sample and capillary temperature control, fraction and computer interfacing. [22] The sample solution is introduced as a small plug at the inlet side of the capillary, with the application of high voltage from 5 to 30 kV across the capillary. Different zones of analyte ions develop, and start to migrate with different velocities toward the outlet side of the capillary. Before reaching the end of the capillary (most commonly), the separated analyte bands (peaks) are registered by absorbance detection directly through the capillary wall yielding an electropherogram.

The foundation to utilize the polyamide coated fused silica capillary used in GC as a standard capillary in CE was the fundamental point in CE development [21]. Numerous properties of fused silica have proved useful in CE e.g, ability to manufacture the capillary with precision, ease of handling, inert surface compared to glass, and excellent UV transparency when the coating is removed. In 1981 Jorgenson and Luckacs [21] published they first used fused silica capillaries of 75 μm, and a length of 80-100 cm pyrex glass capillary and a 30 kV for

separation of derivatized amino acids, peptides and amines. This was a milestone in the development of CE. In 1984, CE applications were extended when Terabe et al [23] introduced micelles as buffer modifiers to separate neutral and charged compounds based on relative affinity for the hydrophobic interior and/or ionic exterior of a micellar pseudo-stationary phase [24]. Nowadays, capillaries with internal diameters ranging from 10 to 100 µm are available and applied in CE [25-27].

3.7 References

[1] Bard A.J, Faulkner L.R. Electrochemical Methods, Fundamentals and Applications, Wiley Interscience, Publications 2nd edition (2001).

[2] Zanello P, Inorganic Electrochemistry Theory, Practice and Application, The Royal Society of Chemistry, Cambridge (2003).

[3 Plambeck J.A, Electroanalytical Chemistry: Basic Principles and Applications, Wiley Interscience Publications (1982).

[4] Brett C. M.A. and Brett A. M O, Electrochemistry: Principles, Methods, and Applications, Oxford University Press Inc., New York (1993).

[5] Polat K, Aksu M.L, Pekel A.T, J. Appl. Electrochem. 32 (2002) 217.

[6] Wartena R, Winnick J, P.H. Pfromm, J. Appl. Electrochem. 32 (2002) 725.

[7] Maciel J.M, Agostinho S.M.L, J. Appl. Electrochem. 30 (2000) 981.

[8] Neville A, Hodgkiess T, Morizot A.P, J. Appl. Electrochem. 29 (1999) 455.

[9] Modiba P, Crouch A.M, J. Appl. Electrochem 38 (2008) 1293.

[10] Theory: A Primer, available online at www.gamry.com App_Notes/EIS_Primer.htm. (Accessed on 15 January 2010)

[11] Baker, Priscilla G. L. Sol-gel Preparation, Characterisation and Electrochemistry of Mixed Metal Tin Oxide Electrodes, PhD Thesis University of Stellenbosch (2004)

[12] Gohr H.M, Mirnik M, Shiller C.A, J. Electroanal. Chem. 180 (1984) 273

[13] Modiba P, Crouch A.M, submitted Electrochim. Acta (2009)

[14] Modiba P, Crouch A.M, Proceedings of the 43rd Power Source Conference (2008).

[15] Skyllas-Kazacos M, Grossmith F, J. Electrochem. Soc. 34 (1987) 2950.

[16] Tiselius A, Trans Faraday Soc. 33 (1937) 524.

[17] Hjerten S, Chromatogr. Rev. 9 (1967) 122.

[18] Mikkers F. E. P, Everaerts, F. M, Verheggen, P. E. M. J. Chromatogr. A 169 (1979) 11.

[19] Jenkins M. A, Guerin, M. D, J. Chromatogr. B 699 (1997) 257.

[20] Hu S, Dovichi N, J. Anal. Chem. 74 (2002) 2833.

[21] Jorgenson J.W, Luckacs K, J. Chromatogr. 218 (1981) 209. Right

[22] Watzig H, Gunter S, Clin chem. Lab Med.41 (2003) 724.

[23] Terabe S, Otsuka K, Ichikawa K, Anal. Chem. 56 (1984) 111.

[24] Terabe S, Otsuka K, Ando T, Anal. Chem. 57 (1985) 834.

[25] Katata Lebogang M, Separation of Readily Biodegradable Aminocarboxylate Complexes By Electrodriven Methods, PhD Thesis University of Stellenbosch (2008).

[26] Khotseng, Lindiwe Eudora, Separation and Speciation of Biodegradable Complexes Using Capillary Zone Electrophoresis, PhD Thesis University of Stellenbosch (2004).

[27] http://www.microsolvtech.com/hplc/cec.

Chapter 4

Study of the Ce (III)/(IV) Redox Couple Using Three Different Working Electrode Systems

The previous chapter (**Chapter 3**) dealt with all the analytical techniques used in the study. In this chapter (**Chapter 4**) the focus is on the electrochemical behaviour of the Ce (IV)/Ce(III) redox couple in a sulphuric acid medium with various working electrodes i.e. carbon (C), gold (Au) and platinum (Pt) electrodes.

This work was undertaken in view of the interest in the study of the electrochemical kinetic parameters of the Ce(III)/Ce(IV) redox couple, using CV and RDE with different electrodes (C, Au and Pt electrodes). When three electrodes (C, Au and Pt) where compared, higher potential was reached when Pt–electrode was used, followed by C and then Au–electrode, making the Pt–electrode the most preferable electrode for the cerium (III/IV) redox flow system. A high rate constant for the cerium (III/IV) system was obtained with Pt and Au electrodes, which make Pt–electrode the ideal electrode material for the cerium (III/IV) redox flow system, C–electrode was found to be the second preferred electrode.

4.1 Introduction

The electrochemical kinetics of the Ce(III)/Ce(IV) couple at high over potential has been attributed almost entirely to the reduction of Ce(IV), usually with H_2SO_4 as the stabilizing electrolyte. Randle and Kuhn [1] investigated the reduction reaction of the Ce(III)/Ce(IV) couple in 0.5 M H_2SO_4 and concluded that the mechanism was simple, with no coupled bond breakage or adsorption steps. The following reaction applied:

$$Ce^{4+}_{aq} + e \leftrightarrow Ce^{3+}_{aq}$$

The reduction of Ce^{4+} at Pt, highly boron-doped conductive diamond electrodes and the oxidation of Ce^{3+} on Au were investigated [2-6]. Kiekens et al. [7] report that the reduction of Ce^{4+} was independent of the electrode material, and that the charge-transfer coefficient (α) and the heterogeneous rate constant (k_c) were similar for different electrodes. For instance, at

Pt and glassy carbon (GC) electrodes the k_c was 3.7 x 10^{-4}cms^{-1}and 4.8 x 10^{-4}cms^{-1} respectively and α was 0.21 & 0.35 respectively. Regarding the oxidation of Ce^{3+}, the different electrodes had different effects on the reaction of $Ce^{3+} \rightarrow Ce^{4+}$+e. These effects are due to electrode material, background reactions, oxygen evolution, and a catalytic effect [8-12].

Of most of the research [13-23], we are interested in the examining of the cerium because of its higher potential. Earlier work on the Ce(IV)/Ce(III) couple was mostly focused on the electro-analysis and the concentration of the Ce(IV)/Ce(III) couple at low concentration in mmol/dm^3. However since the electro-active materials are used in redox flow cells, the concentration should be high, therefore the concentration of Ce(IV) and Ce(III) has to be above 0.1mol dm^{-3}. From the cyclic voltammogram response of a Ce(IV)/Ce(III) couple at an inert working electrode, Liu et al. [8] investigated the reversibility of the couple in a H_2SO_4 solution. In addition, the kinetic parameters of the Ce(IV)/Ce(III) couple and the oxidation efficiency of Ce(III) at various electrodes has been obtained using a rotating disk electrode and rotating ring-disk voltammetry [6,8].

For this study sulphuric acid was chosen as the acid medium mainly because $Ce(SO_4)_2$ is stable in H_2SO_4 solution and a redox reaction seldom takes place. Although the potential of the Ce^{4+}/Ce^{3+} couple is also high in H_2SO_4 solution, Kunz [9] proved that in a $HClO_4$ or HNO_3 solution, the potential of the Ce^{4+}/Ce^{3+} couple is also high, and far above the over potential for oxygen evolution. The Ce^{4+}/Ce^{3+} couple is not stable in $HClO_4$ or HNO_3 solution since ClO_4^- and NO_3^- cannot form stable complexes with Ce^{4+} and Ce^{3+}. (This is also the reason that the potential of this couple is higher than that in H_2SO_4 solution). However, SO_4^{2-} can form a complex with Ce^{4+}, in the form of $CeSO_4^{2+}$, $Ce(SO_4)_2$ and $Ce(SO_4)_3^{2-}$ [6]. Because of the formation of a stable complex, it was generally accepted that the Ce(IV) and Ce(III) would not undergo hydrolysis in H_2SO_4 solution. When hydrochloric acid was used as the acid medium, Ce^{4+} would oxidize Cl^- to Cl_2. Mills and Giddings [10] used the Ru, Ir oxide as the catalyst to accelerate this reaction, which demonstrated that the Ce(IV)/Ce(III) couple was unstable in HCl solution [11].

Liu et al. [8] and Xia et al. [12] favoured carbon electrodes for the reduction of the Ce(IV)/Ce(III) system rather than the platinum electrode. They have found that the carbon electrode was more suitable for the Ce(IV)/Ce(III) system than a platinum electrode. However, they did not obtain a higher potential when the carbon electrode was used; it was relatively low. Hence, I will focus on the electrochemical behaviour of the Ce (IV)/Ce(III)

redox couple in sulphuric acid medium with various working electrodes, C, Au and Pt electrodes. Considering the fact that the nature of the electrode material is an important matter for electrolyte investigation, both analytical techniques CV and RDE will be used to compare the results obtained from these techniques.

4.2 Experimental Procedure

4.2.1 Instrumentation

CV measurements were performed using a Bioanalytical System (BAS) 100B voltammetric system. A rotating disc electrochemistry (RDE) stand was used in conjunction with the BAS 100B voltammetric system from Bioanalytical Systems, Inc.West Lafayette, Indiana, USA

4.2.2 Preparation of cerium (IV) sulphate [$Ce(SO_4)_2$] solution

Cerium (IV) sulphate [$Ce(SO_4)_2$] was dissolved in 0.5 M H_2SO_4 by continuous stirring. The solution was filtered and poured in to a small specially designed CV glass cell for CV and for RDE experiments. The electrodes used for CV and RDE experiments were the following: Platinum wire as counter electrode, Ag/AgCl as reference electrode and various working electrodes (carbon, gold and platinum) with a diameter of 3mm (Area was ca. 0.07 cm^2). The solutions were de-aerated by bubbling with nitrogen before and during experiments. Voltammetry measurements were performed using a BAS 100B voltammetric system. When the RDE was used, a RDE stand was used in conjunction with the BAS 100B voltammetric system.

4.3 Results and discussion of cyclic voltammetry experiments

4.3.1 Electrochemical evaluation of Ce(III)/(IV) redox couple using carbon electrode

The results below show the obtained cyclic voltammograms for the Ce(III)/(IV) redox couple in 0.5M sulphuric acid at three different electrodes (carbon, gold and platinum).

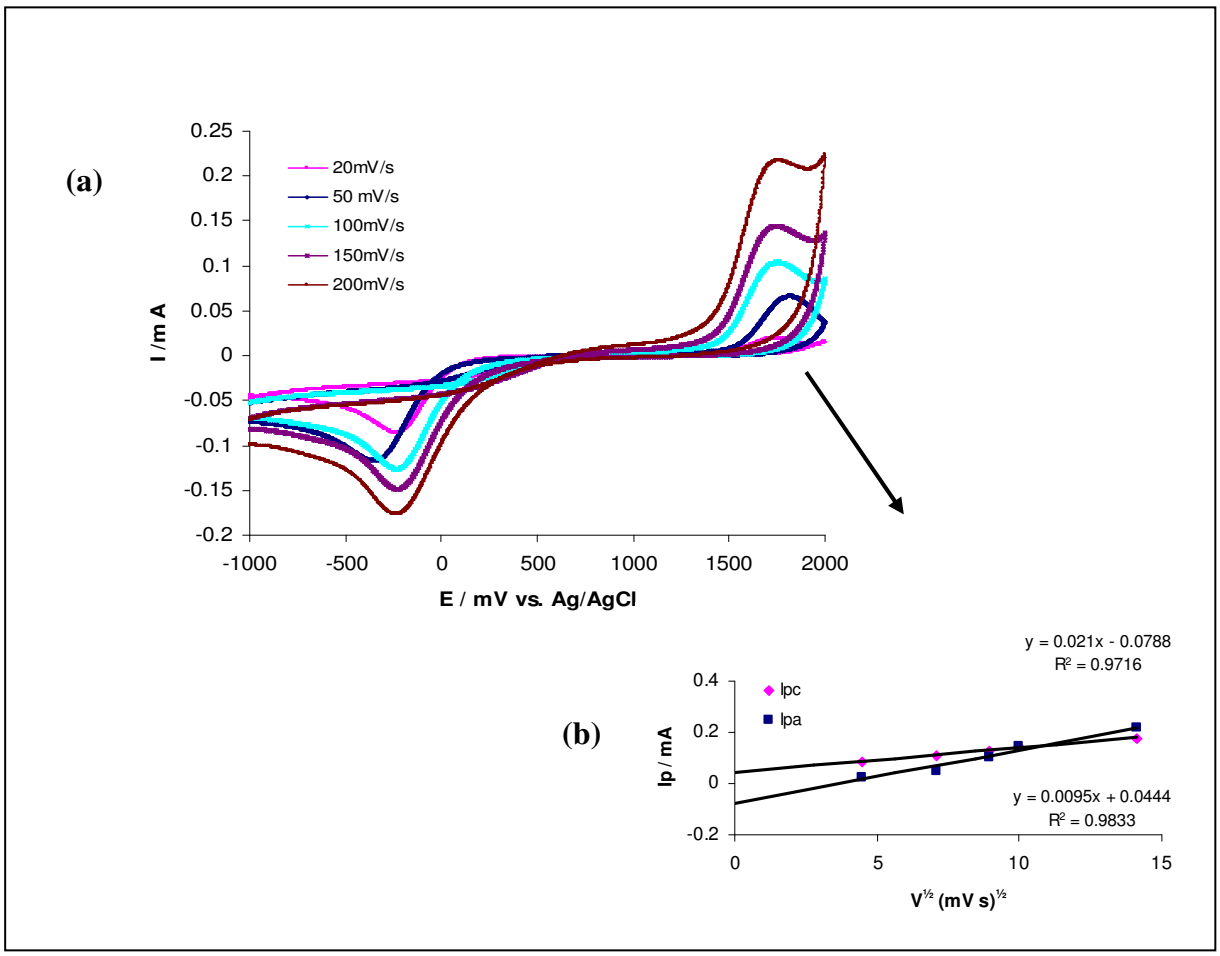

Figure 4.1: Cyclic voltammograms of a 0.1M $Ce(SO_4)_2$ solution in 0.5 M H_2SO_4 at a glassy carbon electrode: (a) at various scan rates 20-200 mV/s (b) Plot of peak current vs. square root of scan rate.

The cyclic voltammograms of the cerium (IV) sulphate in 0.5 M sulphuric acid are shown in ***Figure 4.1 (a) and (b).*** Forward scans reveal that the anodic peak associated with the oxidation of Ce^{3+} to Ce^{4+} occurs at approximately 1750 mV. On the reverse scan, the cathodic peak associated with the reduction of Ce^{4+} to Ce^{3+} occurs at approximately – 270 mV versus Ag/AgCl. ***Figure 4.1(b)*** shows that the anodic and cathodic peak potential changes slightly with different scan rates.

Table 4.1: Electrochemical parameters E, ΔE, and Ipc / Ipa evaluated by CV for $Ce(SO_4)_2$ on C-electrode

Scan rate	**Ec Reduction**	**Ea Oxidation**	**Ipc(Red)**	**Ipa,(Ox)**	**ΔE=Ea-Ec**	**√scan rate**	**Ipc/Ipa**
(mV/s)	(mV)	(mV)	(mA) x (10^{-1})	(mA) x (10^{-1})	(mV)	(mV/s)	
20	-300	1760	-0.6	0.3	2060	4.47	1.8
50	-358	1837	-1.07	0.6	2195	7.07	1.6
100	-256	1766	-1.25	1.04	2022	10.0	1.21
150	-274	1774	-1.48	1.45	2048	12.24	1.02
200	-286	1784	-1.73	2.17	2070	14.14	0.80

Therefore, the electrochemical process will be irreversible since the separation between the forward and reverse potential peak Δ*Ep* is more than 59 mV as shown in ***Table 4.1***, and the potential of the forward peak is independent of the scan rate. Pletcher et al. [16] reported a larger peak potential separation from the cyclic voltammograms of Ce(III)/Ce(IV) system obtained at carbon electrodes. A similar study of the Ce(III)/(IV) redox couple by Fang et al. [14] confirmed the irreversible nature of the Ce(III)/(IV) redox couple in the presence of sulphuric acid.

4.3.2 Electrochemical evaluation of Ce(III)/(IV) redox couple using Platinum electrode

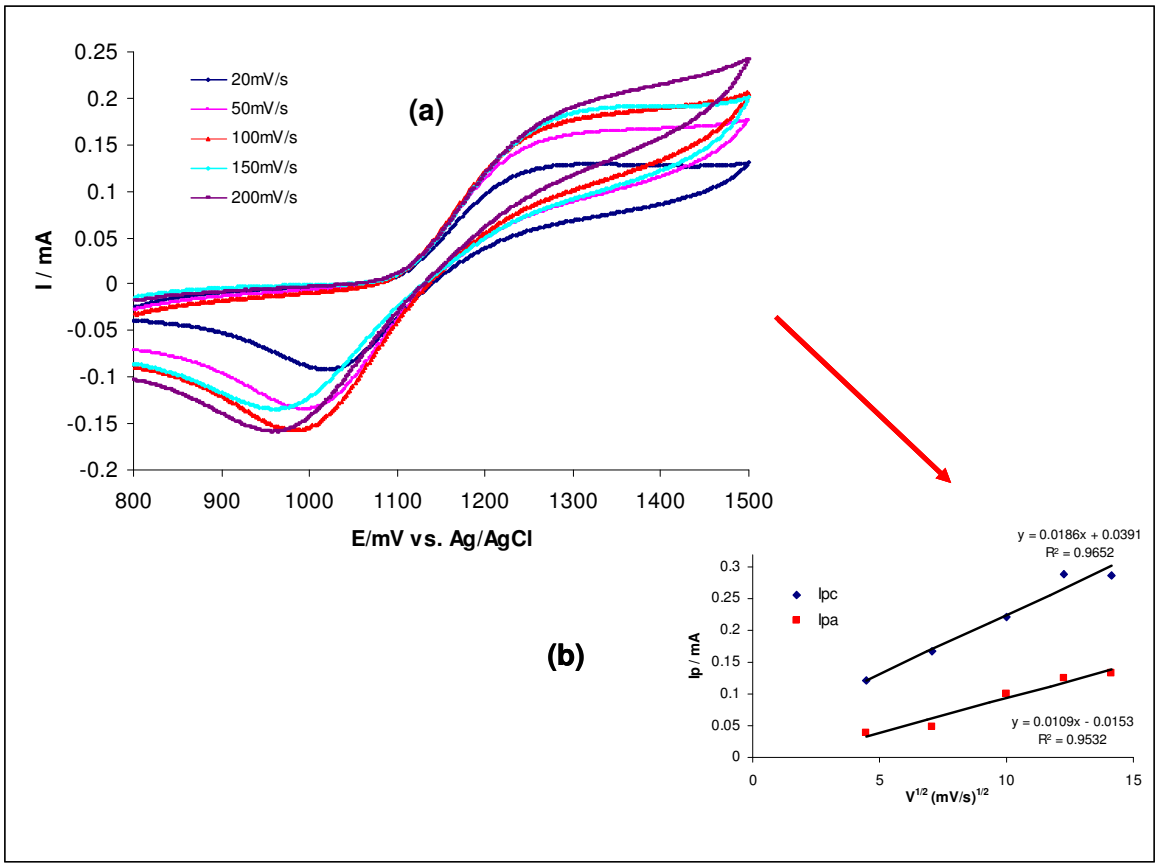

Figure 4.2: Cyclic voltammograms of 0.1M $Ce(SO_4)_2$ solution in 0.5 M H_2SO_4 at Pt-electrode in (a) at various scan rates 20-200mV/s (b) Plot of peak current vs. square root of scan rate.

Table 4.2 Electrochemical parameters E, ΔE, and Ipc/Ipa evaluated by CV for $Ce(SO_4)_2$ on Pt- electrode

Scan rate	Ec Reduction	Ea Oxidation	Ipc(Red)	Ipa,(Oxi)	ΔE=Ea-Ec	√Scane rate	Ipc/ Ipa
(mV\s)	(mV)	(mV)	(A) x (10^{-1})	(A) x (10^{-1})	(mV)		
20	966	1282	-0.9	1.2	272	4.47	0.76
50	974	1294	-1.32	1.6	320	7.07	0.82
100	978	1312	-1.34	1.62	334	10.0	0.83
150	982	1322	-1.36	1.8	340	12.25	0.75
200	984	1334	-1.56	2.2	350	14.4	0.71

The scan rate dependence of the peak currents and peak potentials is shown in ***Figure 4.2*** (b), peak splitting was found to increase with increasing scan rate. It also gives a linear correlation between the peak current and the square root of scan rate. From ***Table 4.2***, the Randles Sevcik equation predicted that the peak current should be proportional to the square root of scan rate (√ scan rate). The results obtained follow the Randles Sevcik prediction, where the peak height (ip) is proportional to √ scan rate. It indicates that the electrode process of Ce (III)/Ce (IV) is electrochemically irreversible. This is contrary to the report by Liu et al. [8] who reported a reversible electrochemical behavior of Ce (III)/Ce (IV) on the Pt-electrode.

4.3.3 Electrochemical evaluation of Ce(III)/(IV) redox couple using Au-electrode

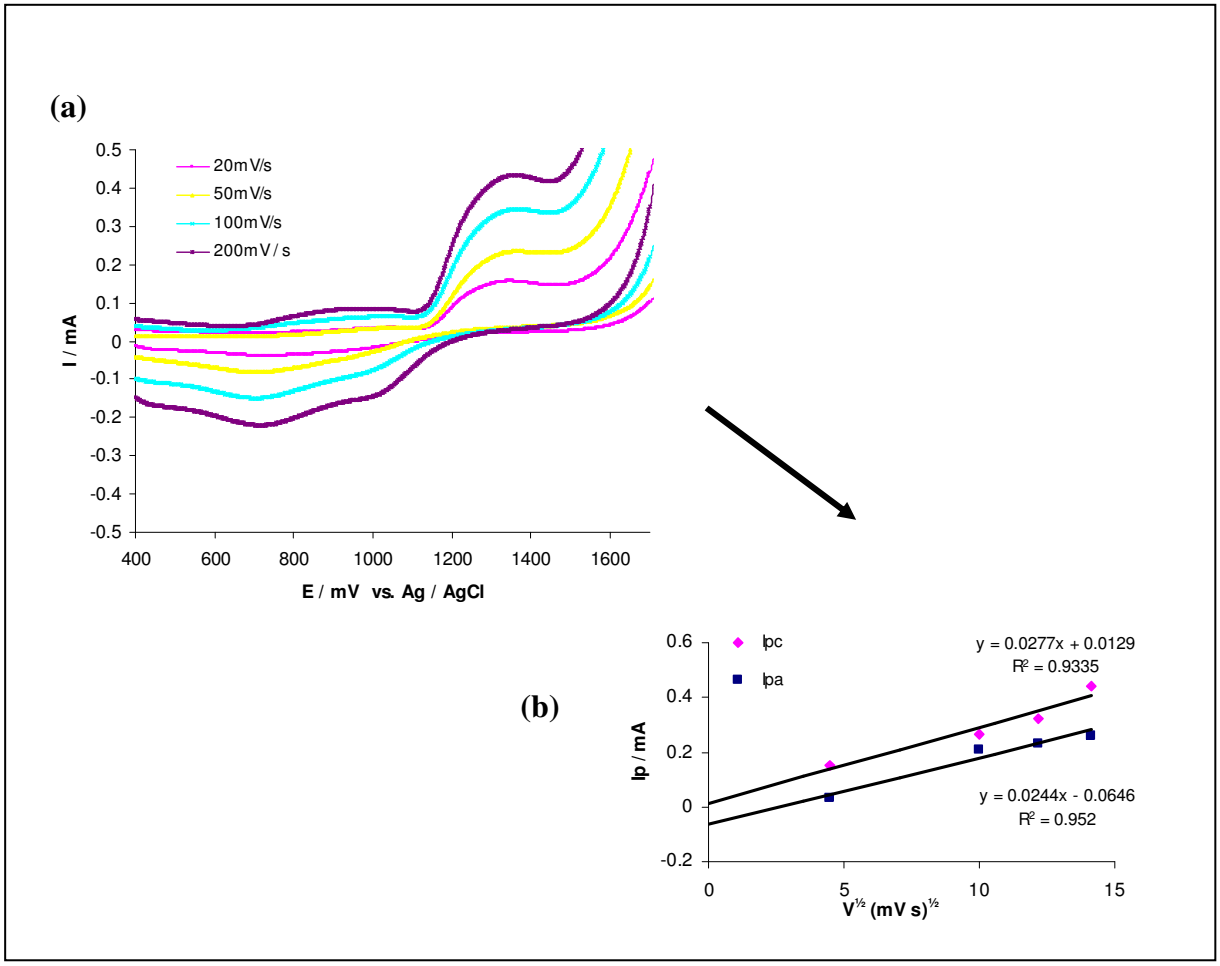

Figure 4.3: Cyclic voltammograms of 0.1M $Ce(SO_4)_2$ in 0.5 M H_2SO_4 at Au-electrode (a) at various scan rates 20-200 mV/s (b) Plot of peak current vs. square root of scan rate.

In ***Figure 4.3(a)*** the forward scan reveals that the reversible anodic peak associated with the oxidation of Ce^{3+} to Ce^{4+} occurs at approximately 1360 mV. On the reverse scan, cathodic peak associated with the reduction of Ce^{4+} to Ce^{3+} at approximately 710 mV versus Ag/AgCl. The scan rate dependence of the peak currents and peak potentials is shown in ***Figure 4.3 (b).*** Peak splitting between the cathodic (Ipc) peak and anodic peak (Ipa) was found to increase with increasing scan rate from the square root of scan rate of 10 to 15 $(mV/s)^{1/2}$. It also gives a linear correlation between the peak current and the square root of scan rate.

Table 4.3 Electrochemical parameters E, ΔE, and Ipc/Ipa evaluated by CV for $Ce(SO_4)_2$ on Au- electrode

Scan rate	Ec Reduction	Ea Oxidation	Ipc(Red)	Ipa,(Oxi)	ΔE=Ea-Ec	√Scane rate	Ipc/ Ipa
(mV\s)	(mV)	(mV)	(A) x (10^{-1})	(A) x (10^{-1})	(mV)		
20	682	1348	-0.32	1.56	666	4.47	0.239
50	686	1350	-0.8	2.34	664	7.07	0.345
100	692	1368	-1.49	3.44	676	10.0	0.433
200	722	1384	-2.2	4.32	662	14.14	0.51

It can be seen from ***Table 4.3*** that the anodic and cathodic peak potential changed slightly with a scan rate. A large peak potential separation was observed and it indicates that the electrode process of Ce (III)/Ce (IV) is electrochemically irreversible.

4.3.4 Comparison of the Ce (III)/Ce (IV) couple using various electrodes (C, Pt and Au)

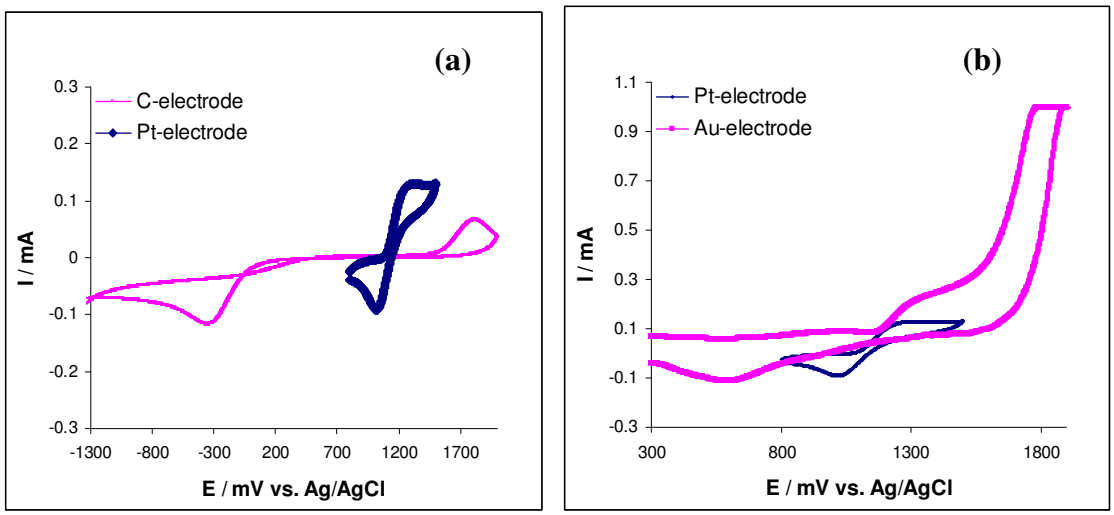

Figure 4.4: Cyclic voltammograms of 0.1M $Ce(SO_4)_2$ in 0.5M H_2SO_4 at a scan rate of 100mV/sec on (a) C and Pt- electrode (b) Pt and Au- electrode.

Comparing the carbon and Pt-electrode electrodes in ***Figure 4.4 (a)*** it can be seen that with the carbon electrode, a higher potential was observed at around 1780 mV, see ***Table 4.1***.the platinum electrode gave the highest potential which was observed around 1384 mV at a scan rate of 200 mV/s, see ***Table 4.2***. In ***Figure 4.4 (b)*** the platinum was also compared with the Au-electrode, and it was found that the platinum is still favoured compared to Au-electrode in relationship to over potentials generated.

4.4 Rotating Disc Electrode (RDE) Results

4.4.1 Electrochemical investigation of Ce (III)/Ce (IV) couple using C-electrode.

RDE will give information about the electron transfer mechanism in the absence of any mass restriction**.** In this section results for hydrodynamic voltammogram from RDE was used to confirm the results observed from similar CV. The RDE and CV results illustrate a reversible one electrode process only on the platinium electrode, where it is expected to show the potential separation (ΔEp). If the peak current (ip) and square root of the scan rate ($v^{1/2}$) is a constant value, independent of scan rate (v). The electrochemical behaviour is measured to be reversible, also if the electrons transfer rate is fast on the experiment time scale. The larger peak splitting indicates that the energy required increases. Therefore, the reaction is irreversible. In peak splitting an increase is caused by increasing the scan rate, which indicates a slow interfacial electron transfer.

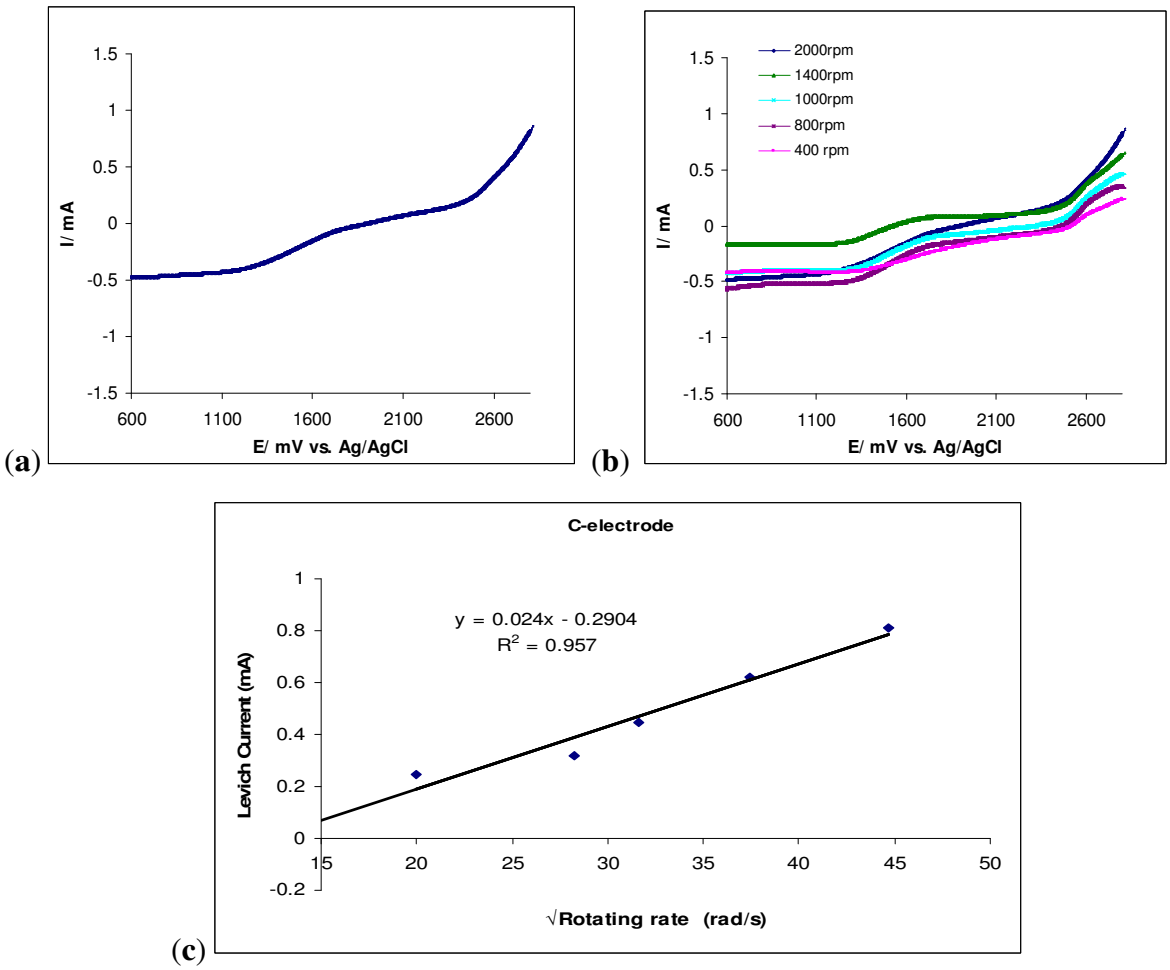

Figure 4.5: Hydrodynamic voltammogram for 0.1M of $Ce(SO_4)_2$ in 0.5 M H_2SO_4 at C-electrode (a) at a rotating rate of 1000 rpm (b) Rotating rate of 400-2000 rpm (c) Plot of Levich current vs. square root of rotating rate.

Table 4.4: RDE results for $Ce_2(SO_4)_3$ on a C-electrode

Rotating rate	IL	E(1/2)	Length of S-Shape	√Rotating rate
(mV\s)	(A) x (10^4)	(V)	(mm)	
400	8.08	1.196	40	20.0
600	6.44	1.20	38	24.49
800	7.20	1.197	29	28.28
1000	7.28	1.198	26	31.62
1400	8.07	1.26	20	37.41

Figure 4.5 (a) and (b) represent the hydrodynamic voltammograms obtained for different rotation rates (from 100 to 1000 rpm). From these measurements, it is possible to study the dependence between the limiting current density (i_L) and the rotation rate (ω). The relation between i_L and the square root of the rotation rate is linear as predicted, shown in ***Figure 4.5*** (c). The values of limiting current are tabulated in ***Table 4.4***. Values for the diffusion coefficient of Ce (III)/Ce (IV) at carbon electrode 2.97 x 10^{-6} cm2 s^{-1} was calculated using the Levich equation ***(see previous Equation 3.1)*** Where *w* is the rotation rate (s^{-1}) and the other units are the same as in ***Equation 3.1***

A Plot of *iL* vs. $w^{1/2}$ give a straight line with slope proportional to $D^{2/3}$. For a quasi-reversible process, the peak potential *Ep* is a function of scan rate, the difference between *Ep* and formal potential *Eo*, being related to the standard rate constant. The peak current may be also be expressed as in ***Equation (4.3)*** below

$$ip = (0.227)\, n\, F\, A\, C\, k\, exp\, [-(\alpha nF/RT)\, (E-Eo) \qquad \textbf{(4.3)}$$ [24]

A plot of *lni* vs potential *(E-Eo)* were constructed as shown in ***Figure 4.6*** and a straight line plot was obtained with a linear regression of 0.9516. This plot of ln*i* vs (*E-Eo*), determined at different scan rates, should have a slope of – *(αnF/RT)* with the intercept proportional to (*k*). The rate constant for the Ce(III)/(IV) was calculated to be 2.7 x10^{-4} cm s^{-1} as shown in ***Table 4.5*** for C-electrode and electron coefficient of (α = 0.36). Generally, it can be considered that for a metal, α is theoretically equal to 0.5 (α + β =1) [9]. Consequently, the value of 0.4 for glassy carbon is expected, since this material exhibits a metallic character.

Table 4.5: Data taken from cyclic voltammograms recorded on carbon electrode for calculation of rate constant (k)

$E_1 - E^0$	lni	αf(E-E°)	K (10^{-4})
1850	**6.9077**	-0.19434	**2.73**
1795	6.9501	-0.13972	2.74
1691	7.0013	-0.06135	2.74
1561	7.1005	-0.01489	2.75
1442	7.2013	-0.00736	2.76
1409	**7.3005**	-0.00593	**2.77**
1377	7.4013	-0.00541	2.77
1265	7.5005	-0.00506	2.78
1141	**7.6013**	-0.00475	**2.79**
1074	7.7005	-0.00442	2.79
980	7.8013	-0.00408	2.80
896	**7.9005**	-0.00351	**2.80**
810	8.0013	-0.00283	2.81
799	**8.1005**	-0.00199	**2.82**

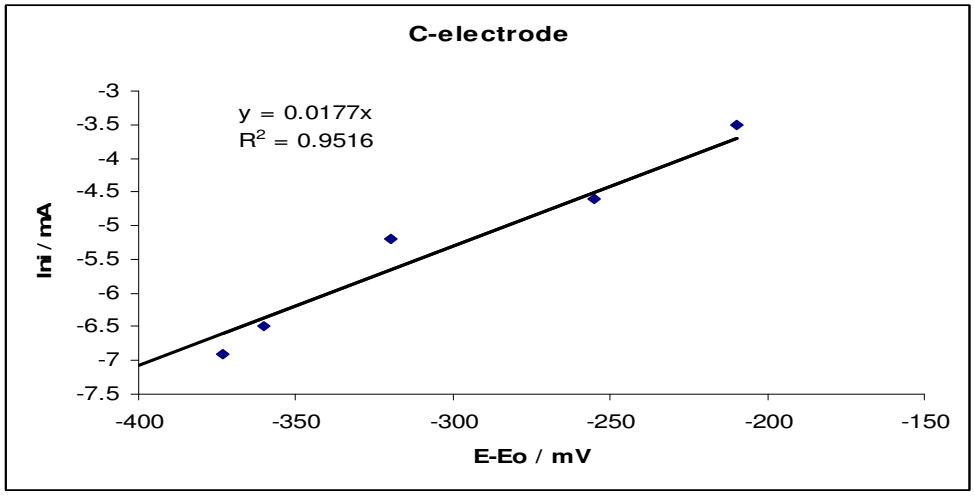

Figure 4.6 Plot of *Lni* vs. (E-Eo) for voltammogram in Figure 4.1 on C- electrode.

4.4.2 Electrochemical investigation of Ce (III)/Ce (IV) couple using Pt-electrode

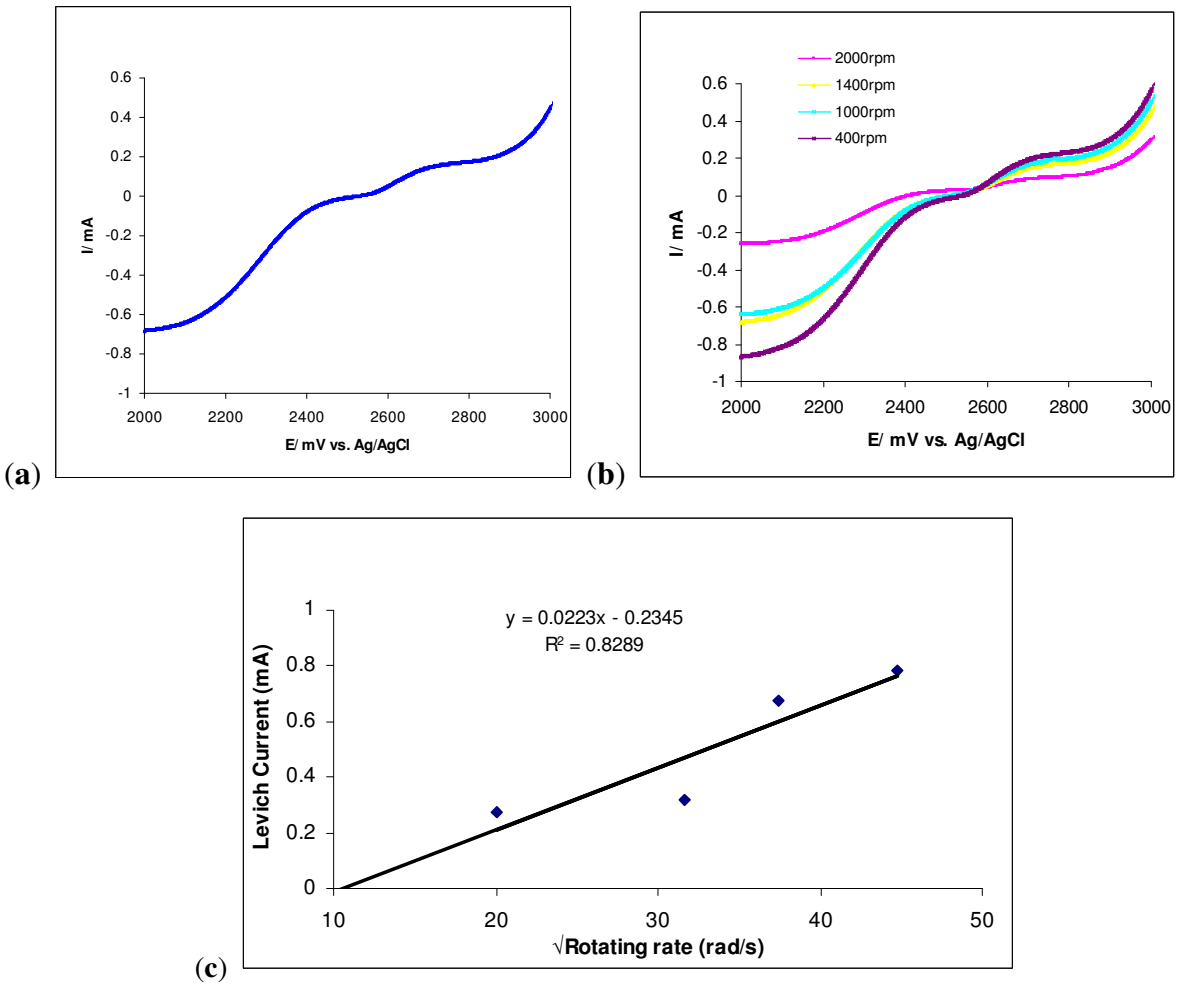

Figure 4.7: Hydrodynamic voltammogram for 0.1M of $Ce(SO_4)_2$ in 0.5 M H_2SO_4 at Pt-electrode (a) at a rotating rate of 1000 rpm (b) Rotating rate of 400-2000 rpm (c) Plot of Levich current vs. square root of rotating rate.

Table 4.6: RDE for $Ce_2(SO_4)_3$ on Platinum electrode

Rotating rate	IL	E(1/2)	Length of S-Shape	√Rotating rate
(mV\s)	(A) (10^4)	(V)	(mm)	
400	2.72	0.79	14	20.0
600	3.17	0.85	20	24.49
800	6.77	0.87	45	28.28
1000	7.84	0.89	61	31.62
1400	5.55	0.93	72	37.41

From the ***Figure 4.7 (a) and (b)*** it was possible to measure the limiting current and the rotation rate. The relation between i_L and the square root of the rotation rate is linear as expected and can be seen in ***Figure 4.7 (c)***. The values of limiting current are tabulated in ***Table 4.6***. Values for the diffusion coefficient of Ce (III)/Ce (IV) at the platinum electrode are 3.2 x 10^{-6} cm^2 s^{-1} as was calculated using the Levich equation (***Equation 4.3***).

Table 4.7: Data taken from cyclic voltammograms recorded on Pt-Electrode

$E_1 - E^0$	lni	αf(E-E°)	K (10^{-4})
72	-12.9202	0.2304	**3.128**
65	-13.2361	0.208	3.024
55	-13.8697	0.176	2.985
33	-14.018	0.1056	2.983
18	-14.1506	0.0576	**2.952**
4	-14.2973	0.0128	2.143
12	-14.4324	-0.0384	2.228
27	-14.5449	-0.0864	2.311
176	-14.7368	-0.5632	**2.398**
700	-14.9593	-2.24	2.989
1441	-15.2926	-4.6112	**2.711**
1893	-16.1052	-6.0576	2.803
2253	-17.7513	-7.2096	2.987
2840	-12.9202	-9.088	**2.999**

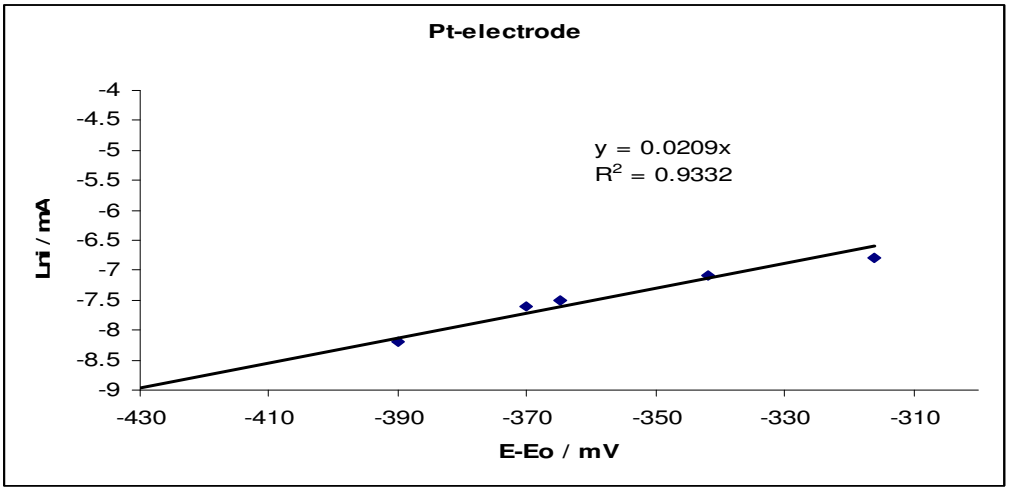

Figure 4.8 Plot of *Lni* vs. (E-Eo) for voltammogram in Figure 4.2 on Pt-electrode.

A plot of ln *i* vs (*E-Eo*) in ***Figure 4.8***, determined at different scan rates, should have a slope of – *(αnF/RT)* with the intercept proportional to (*k*), the intercept of ln*i* vs (*E-Eo*) is 0.227 *nFAck,* a straight line plot was obtained with a linear regression of 0.9332. The electron transfer coefficient (α) values were obtained from the same plot of lni vs potential (E-Eo), and found to be (α) = 0.4 , the rate constant for the Ce(III)/(IV) was calculated to be 1.9 x 10^{-4} cm^2 s^{-1} as shown in ***Table 4.7*** for Pt- electrode.

4.4.3 Electrochemical investigation of Ce (III)/Ce (IV) couple using Au-electrode.

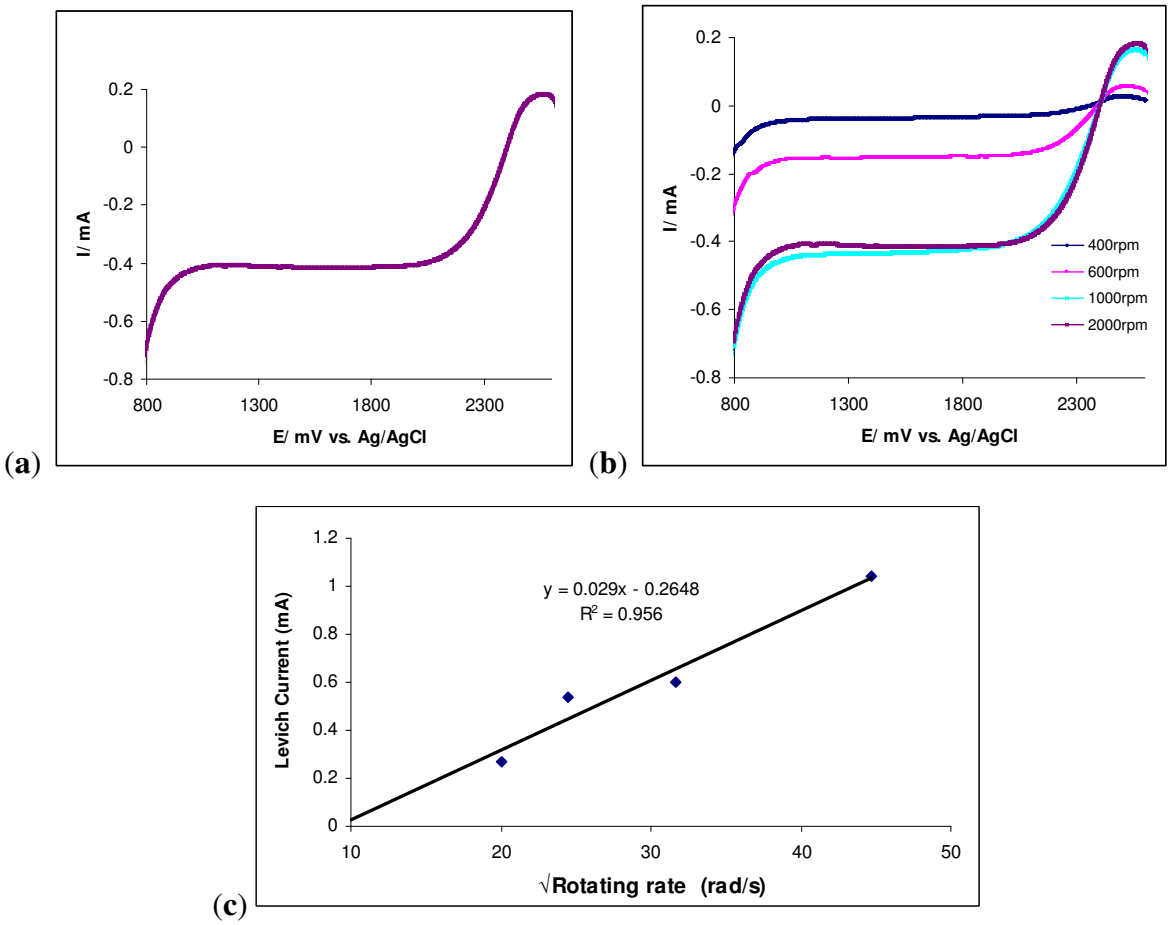

Figure 4.9 Hydrodynamic voltammogram for 0.1M of $Ce(SO_4)_2$ in 0.5 M H_2SO_4 at Au-electrode (a) at a rotating rate of 1000 rpm (b) Rotating rate of 400-2000 rpm (c) Plot of Levich current vs. square root of rotating rate.

Table 4.8: RDE for $Ce_2(SO_4)_3$ on Gold electrode

Rotating rate	IL	E(1/2)	Length of S-Shape	√Rotating rate
(mV\s)	(A) (10^4)	(V)	(mm)	
400	1.945	0.91	12	20.0
600	2.68	0.88	24	24.49
800	5.37	0.90	50	28.28
1000	5.99	0.92	56	31.62
1400	10.40	0.94	98	37.41

Figure 4.9 (a) and (b) for the hydrodynamic voltammogram of Ce (III)/Ce (IV) at gold electrode obtained for different rotation rates from 100 to 1000 rpm, from this voltammogram It is possible to measure the limiting current density (i_L) and the rotation rate (w). A straight line was observed as shown in ***Figure 4.9*** (c), this means there is linear relation between i_L and the square root of the rotation rate as predicted. The values of limiting current are tabulated in ***Table 4.8***. Values for the diffusion coefficient of Ce (III)/Ce (IV) at carbon were found to be 2.97 x 10^{-6} cm^2 s^{-1} which was calculated according to the Levich equation ***(Equation 4.2).***

Table 4.9: Data taken from cyclic voltammograms recorded on Au- Electrode

$E_1 - E^0$	Ln_i	$\alpha f(E-E^\circ)$	$K(10^{-4})$
60	12.3337	-0.192	3.13
33	12.2293	-0.1056	3.12
12	12.1442	-0.0384	3.11
18	12.0002	0.0576	3.04
47	11.8148	0.1504	2.99
66	11.6710	0.2112	2.95
76	11.5864	0.2432	2.90
84	11.5141	0.2688	2.86
93	11.4332	0.2976	2.81
141	10.9567	0.4512	2.76
156	10.8049	0.4992	2.72
182	10.5528	0.5824	2.67
211	10.2962	0.6752	3.07

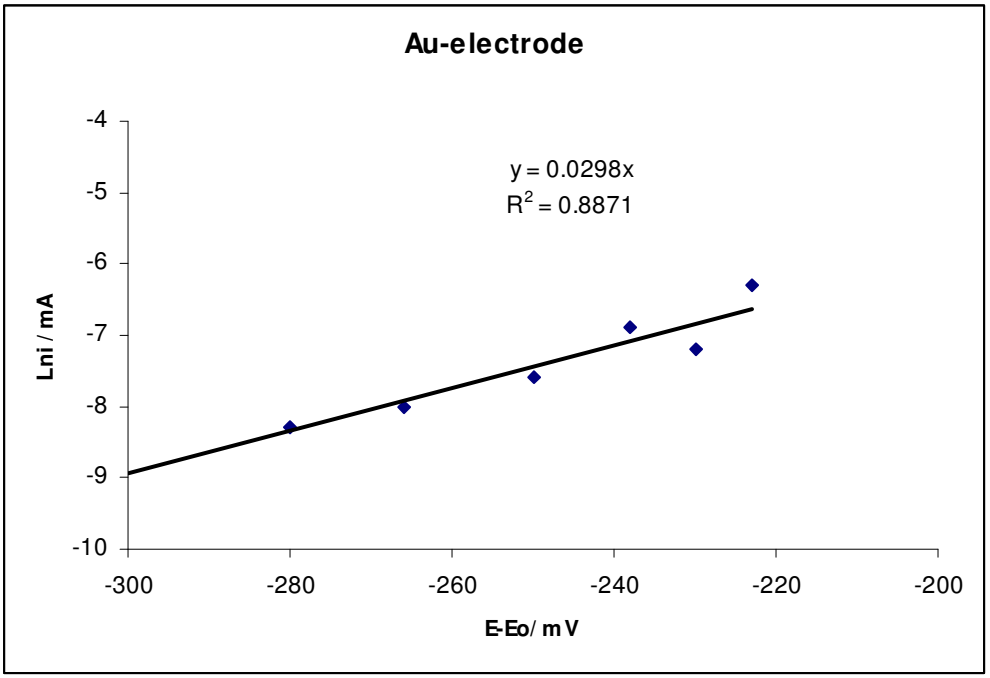

Figure 4.10 Plot of *Lni* vs. (E-Eo) for voltammogram in Figure 4.3 on Au- electrode.

The rate constant for the Ce(III)/(IV) was calculated to be 3.2 x10^{-4} cm s^{-1} as shown in ***Table 4.9*** for Au-electrode. A plot of ln_i vs potential (*E-Eo*) were constructed as shown in ***Figure 4.10*** and a straight line plot was obtained with a linear regression of 0.8871. The electron coefficient (α) value was found to be 0.32 obtained from the plot ln_i vs potential (E-Eo).

4.5 Calculations

Rate constant and electron coefficient was calculated from Butler-Volmer equation below [25].

$$i = lnFAkC\, e^{-\alpha f(E-E^{\circ})}$$

$$k = lni - lnFAC + \alpha f(E-E^{\circ})$$

Table 4.10: Data taken from cyclic voltammograms recorded on C, Au and Pt-electrode Calculation rate constant (k)

Carbon			**Platinum**			**Gold**		
Reaction type			**Reaction type**			**Reaction type**		
Irreversible			**Irreversible**			**Irreversible**		
$k(10^{-4})$ (cm/s)	$E_1 - E^0$	*Lni*	$k(10^{-4})$ (cm/s)	$E_1 - E^0$	*Lni*	$k(10^{-4})$ (cm/s)	$E_1 - E^0$	*Lni*
2.73E	1850	6.9077	2.13	72	-12.9202	2.81	93	11.4332
2.82E	1409	7.3005	3.92	18	-14.1506	2.94	141	10.9567
2.79E	1141	7.6013	3.99	176	-14.7368	3.72	156	10.8049
2.83E	896	7.9005	2.01	1441	-15.2926	2.67	182	10.5528
2.77E	799	8.1005	3.97	2840	-12.9202	3.87	211	10.2962

4.6 Comparison and discussion for CV and RDE

The nature of the electrode material is an important consideration for electrolyte examination. The investigation of cerium in sulphuric acid by CV and RDE has been carried out on three types of electrodes, including glassy carbon, gold and platinum. Some of these electrode type, electrode preparation is necessary, for example, by polishing electrode. **Table 4.10:** summarizes the values obtained for the kinetics of Ce(III)/(IV) at different electrodes C, Pt and Au-electrodes. The anodic transfer coefficient, the rate constant, diffusion coefficient, electron coefficient, and linear regression were calculated and discussed below. The reactions at C and Pt-electrode show a larger (k) value than at the gold electrode, meaning that the reaction will be faster to a certain extent when the carbon and Pt-electrodes are used rather than the Au-electrode.

Table 4.11: Electrochemical parameters of Ce(III)/(IV) at C, Pt and Au electrodes.

Electrodes	α	*D* [cm^2/s] (10^{-6})	Linear Regression	*K* ($10^4/cm^2\ s^{-1}$)
Carbon	0.36	2.79	0.9516	2.75
Platinum	0.41	3.2	0.9332	3.9
Gold	0.32	2.97	0.8871	3.2

The rate constant was calculated comparing the three electrodes, C, Au and Pt. The highest rate constant is obtained at Pt-electrode, which make it the favoured electrodes for cerium (III/IV) redox couple, with the reaction being faster. C and Au-electrode together came second as they are more similar since their rate constant values are close. The rate constant for all three electrode (C, Pt and Au) differ slightly as is shown in ***Table 4.11***. Unfortunately, the Au-electrode is corroded by the cerium (III/IV) solution when used for more than 5 min. Therefore, C and Pt-electrode should replace the Au-electrode. Even though there is an adsorption of cerium (IV) on Pt-electrode and formation of oxide on the surface of Pt-electrode the rate constant is still high, there was not much influence of the reaction during the process, the reaction remains fast. When using C-electrode, although there is no adsorption and no formation of oxide on the surface, the reaction will not be as fast as on a Pt-electrode. The electrochemical behaviour for cerium (III/IV) couple was electrochemically irreversible when using all three (C, Pt and Au) electrodes.

4.7 Conclusion

After evaluation of the three electrodes (C, Au and Pt), C had the highest over potential, for the reaction of cerium (III/IV) followed by Pt and then Au-electrode, The electrochemical behaviour for the Pt-electrode gave a better electrochemical reversibility than C-electrode, than means the kinetic reaction will be faster than when using the C-electrode, making the Pt–electrode the most preferable electrode. A high rate constant and a low diffusion constant for the cerium (III/IV) system were obtained when a Pt–electrode was used. A high rate constant for the cerium (III/IV) system was obtained with Pt and Au electrodes, which make Pt–electrode the most ideal electrode material for cerium (III/IV) redox couple; the C–electrode was the second preferred electrode. The rate constant for C-electrode and Au-electrode differs slightly. Unfortunately the Au–electrode is easily corroded by cerium (III/IV) solution.

4.8 Reference

[1] Randle T.H, Kuhn A.T, J. Chem. Soc., Faraday Trans. 79 (1983) 1741.

[2] Fenton A.J, Furman N.H, Anal. Chem. 29 (1957) 221.

[3] Lingane J.J, Langford C.H, Anson F.C, Anal. Chim. Acta 16 (1957)165.

[4] Ferro S, Battisti A.D, Phys. Chem. Chem. Phys. 4 (2002)1915.

[5] Mills A, Worsley D, J. Chem. Soc., Faraday Trans. 87 (1991) 3275.

[6] Meada Y, Sato K, Ramaraj R, Electrochim. Acta 44 (1999) 3441.

[7] Kiekens P, Steen L, Donche H, Temmerman E, Electrochim. Acta 26 (1981)841.

[8] Liu Y, Xia X, Liu H, J. Power Sources. 130 (2004) 299.

[9] Kunz H, J. Am. Chem. Soc. 53 (1931) 98.

[10] Mills A, Giddings S. Inorg. Chim. Acta 16 (1957) 165.

[11] Cai C, Mirkin MV, J Am Chem Soc. 127 (2006) 171.

[12] Xia X, Liu H, Liu Y, J. Electrochem. Soc. 149 (2002) A426.

[13] Chen Y. W. D, Santhanam K. S. V, Bard A. J, J. Electrochem. Soc. 128 (1981) 1460.

[14] Fang B, Iwasa S, Wei Y, Arai T, Kumagai M, Electrochim. Acta 47 (2002) 3971.

[15] Paulenova A, Creager S.E, J. Power Sources 109 (2002) 431.

[16] Pletcher D, Valder E, Electrochim. Acta 33 (1988) 499.

[17] Wei Y, Fang B, J.Appl. Electrochem. 35 (2005) 561.

[18] Abbaspour A, Mehrgardi M.A, Talanta 67 (2005) 579.

[19] Glentworth P, Wiseall B, Wright C.L, Mahmood A.J, J. Inorg. Nucl. Chem. 30 (1968) 967.

[20] Pletcher D, White J. C. P, Electrochim. Acta 37 (1992) 575.

[21] Cai C, Mirkin MV, J Am Chem Soc 127 (2006) 171.

[22] Zang JB, Wang YH, Zhao SZ, Bian LY, Lu J Diamond Relat Mater 16(2007)16.

[23] Murthy ASN, Srivastava T, J Power Sources 27 (1989) 119.

[24] Zanello P, Inorganic Electrochemistry Theory, Practice and Application, The Royal Society of Chemistry, Cambridge, 2003.

[25] Bard A.J, Faulkner L.R, Electrochemical methods fundamentals and applications, 2nd edition, John Wiley & Sons, New York (2001).

Chapter 5

Electrochemical Study of Cerium (IV) in the Presence of Ethylenediaminetetraacetic Acid (EDTA) and Diethylenetriaminepentaacetate (DTPA) Ligands [*]

Summary

The electrochemical behaviour of the complexation of cerium (IV) with EDTA and DTPA was studied using both cyclic voltammetry (CV) and rotating disc electrode (RDE). The Ce(IV)–DTPA complex at various scan rates, gave a linear correlation between the peak potential (Ep) and square root of the scan rate, showing that the kinetics of the overall process was controlled by mass transport. However, when the EDTA ligand was added to the Ce(IV) there was no specific change to the potential peak, i.e. the Ce(IV)–EDTA complex has the same redox potential as the Ce(IV)/(III) couple. Kinetic parameters such as potential, limiting current, diffusion coefficients, transfer coefficients and rate constants were studied. The results of RDE experiments confirmed that the parameters measured by CV are similar under hydrodynamic conditions and can be used to determine the kinetic parameters of the redox couples. The use of DTPA as a ligand for complexation of Ce(IV) gave more favourable results compared to the Ce–(EDTA) complex reported previously. The results of kinetic studies of the Ce(IV)–DTPA complex indicate what this complex may be useful as an electrolyte for redox flow batteries.

5.1 Introduction

The search for stable redox systems for use in redox flow batteries (RFBs) has been an active field of research for the past few years [1–7]. A typical battery makes use of two fully soluble redox couples, and consists of stacks, electrolytes, pumps and tanks. The storage capacity is determined by the electrolyte concentration and the size of the battery cells. The first study of redox flow batteries was reported by Thaller [2] who used Fe^{2+}/Fe^{3+} and Cr^{2+}/Cr^{3+} redox couples for the redox flow cell energy storage systems.

[*] This chapter has been published by Modiba P and Crouch A. M in the Journal of Applied Electrochemistry 38 (2008) 1293.

Later reports [3, 4] described a multiplicity of redox couple flow batteries (Fe^{2+}/Fe^{3+} and V^{4+}/V^{5+}), ($Fe^{2+}/Fe^{3+}$and Ti^{+3}/ TiO^{+2}), (Fe^{2+}/Fe^{3+} and V^{2+}/VO^{2+}), (Cr^{2+}/Cr^{3+} and $Cu(NH^3)^{2\ +}1$/ $Cu(NH^3)^{4\ +2}$) and (V^{2+}/VO^{2+} $Fe(O^3)^{-3}/Fe(O^3)^{-4}$) systems for redox cell development.

Reid et al. [5] also tried to use the Fe^{2+}/Fe^{3+} and Cr^{2+}/Cr^{3+} couples in redox flow batteries. In all these studies encountered the same problem of poor reversibility and the cross mixing of anolyte and catholyte through the separating membrane was encountered because of the use of two separate redox couples in a half cell.

The system also suffered from serious efficiency losses, which reduces the life time of expensive membranes. All these problems can be minimized by employing the same element in different oxidation states. In both half cells this approach requires the use of different complexing agents to provide a workable difference in redox potential. Quantities of redox couples based on a single species (all-vanadium, iron, chromium, cerium, and neptunium) have been reported in the literature [6–13]. Recently much of attention has been focused on the all−vanadium RFB [6, 7, 10, 11] due to its various advantages, where there is no decrease in capacity caused by the cross mixing of the positive electrolyte and negative electrolyte, meaning that there will be no energy efficiency loss during the process. The effect of cross-contamination for all vanadium RFB does not need catalysts for both electrode reactions, and there is no evolution of hydrogen gas, which needs rebalancing power and additional equipment. Even though these qualities exist for all-vanadium redox flow systems the open-circuit voltage for each single cell after full charging is about 1.4 V, which is relatively low.

Lui et al. [4] proved that vanadium could be replaced by cerium. Fang et al. [14] investigated the Ce(IV)/Ce(III) couple, which has a standard reduction potential of 1.74 V, which is higher than the all-vanadium RFB. Paulenova and Creager [15] evaluated the cerium couple in a RFB because of its positive redox potential, and the cell voltage was predicted to be approximately 1.9 V. The use of the Ce^{4+}/Ce^{3+} redox couple is attractive for RFB technology because of its large positive redox potential, which should result in a battery with a higher cell voltage and a greater energy storage capacity. Pletcher and Valder [16] reported the electrochemical behaviour of the Ce^{4+}/Ce^{3+} redox couple in aqueous nitrite media and the electrochemistry of the Ce^{4+}/Ce^{3+} couple in sulphuric acid solutions has been widely investigated [17–20].

The kinetics and mechanism of the oxidation of organic compounds by various oxidizing agents have also received considerable attention in recent years. In particular, the oxidation of different organic compounds using carboxylic acids and alcohol with Ce(IV) has been studied extensively. Abbaspour and Mehrgardi [18] investigated the electrochemical behaviour of Ce(III) ions in the presence of EDTA, and they determined the kinetic parameters such as transfer coefficients and rate constants for the electrocatalytic oxidation of the nitrite ion. Glenworth et al. [19] carried out a kinetic study of isotopic exchange reactions between lanthanide ions and lanthanide polyaminopolycarboxylic acid complex ions in aqueous solution to determine the chemical effect of nuclear transformation of Ce–EDTA and Ce–DTPA couples. This work was used as a point of departure to demonstrate the superior performance of the Ce–DTPA complex.

A literature search has revealed no report of an electrochemical study of Ce(IV) in the presence of DTPA as a ligand or complexone for use in redox flow batteries system. In this paper we report on the study of a Ce(IV) redox system using EDTA or DTPA as a ligand for redox flow batteries. This system was also used to compare Ce–DTPA and Ce–EDTA systems, to show that the former system Ce–DTPA is more promising than the latter Ce–EDTA in terms of its stability and electron transfer capability. A comparison was also made to similar systems of iron.

5.2 Experimental

5.2.1 Materials

All reagents were of analytical reagent grade unless stated otherwise. Ethylenediaminetetraacetic acid (EDTA), sulphuric acid, potassium ferricyanide ($K_3Fe(CN)_6$), potassium nitrate (KNO_3) sodium hydroxide, cerium(IV) sulphate and diethylenetriaminepentaacetic acid (DTPA) were obtained from Sigma-Aldrich (Steinheim, Germany).

5.2.2 Preparation of Ce(IV)–DTPA and Ce(IV)–EDTA

Cerium(IV) sulphate [$Ce(SO_4)_2$] and Ce(IV)–EDTA were prepared as described in the literature [21]. For the preparation of Ce(IV)–DTPA, DTPA was added to replace EDTA as per literature method [21], and dissolved in 1 M H_2SO_4. The solution was filtered and poured

in a small, specially designed cyclic voltammetry (CV) glass cell. Deionized water was prepared by passing distilled water through a Milli Q water purification system (Millipore from Bedford, MA, USA)

5.2.3 Preparation of Fe(III)–DTPA and Fe(III)–EDTA

Fe(III)–DTPA and Fe(III)–EDTA were prepared by dissolving potassium ferricyanide ($K_3Fe(CN)_6$) in 0.1 M potassium nitrate (KNO_3) solution. The specific quantities of EDTA and DTPA were added in a separate container to complex with the prepared iron solution.

5.3 Instrumentation

CV measurements were performed using a BAS 100B voltammetric system. A rotating disc electrochemistry (RDE) stand was used in conjunction with the BAS 100B voltammetric system from Bioanalytical Systems, Inc.West Lafayette, Indiana, USA.

5.3.1 Electrochemical measurements

The electrochemical behaviour of Ce(IV) ion in the presence of EDTA and DTPA was investigated with CV and RDE or hydrodynamic voltammetry techniques. The electrodes used for both CV and RDE experiments included: a platinium disc electrode with a diameter of 3 mm as a working electrode, Ag/AgCl as a reference electrode and a platinium wire as a counter electrode. The electrodes were initially hand polished with 600–1200 grit paper. Before each experiment they were polished again with a microcloth using 1, 0.3, and 0.05 μm alumina, followed by rinsing the electrodes with de-ionized water. Thereafter the electrodes were polished with 1 μm diamond polish slurry. The electrodes were rinsed again several times with de-ionized water and methanol to remove polishing residues. The surface activity was confirmed by recording CVs for $K_3Fe(CN)_6$ in 0.1 M KNO_3 solution. The solutions were de-aerated by bubbling with nitrogen before each experiment for 10 min. Analyses were carried out at room temperature at various scan rates from 20 to 200 mV s^{-1}.

5.4 Results and discussion

5.4.1 Cyclic voltammetry

The redox process of Ce^{3+} / Ce^{4+} on the platinum electrode is presented in ***Figure 5.1(a) and (b)*** It was observed that the peak potentials of cathodic and anodic were changed to more negative direction as the scan rate increases from 20 to 200 mVs^{-1}. Forward scans reveal that the anodic peak associated with the oxidation of Ce^{3+} to Ce^{4+} occurs at approximately 1020 mV. On the reverse scan, the cathodic peak associated with the reduction of Ce^{4+} to Ce^{3+} occurs at approximately 1290 mV. Therefore, the electrochemical process will be quasi-reversible since the separation between the forward and reverse potential peak ΔEp is more than 59 mV, and the potential of the forward peak is independent of the scan rate. Pletcher et al. [16] reported a larger peak potential separation from the cyclic voltammograms of Ce(III)/Ce(IV) in H_2SO_4 system obtained at carbon electrodes. A similar study of the Ce(III)/(IV) redox couple by Fang et al. [14] confirmed the irreversible nature of the Ce(III)/(IV) redox couple in the presence of sulphuric acid. Fang et al. also investigated the effect of sulphuric acid concentration on the formal potential of the cerium redox couple. The scan rate dependence of the peak currents and peak potentials in sulphuric acid is reported in ***Figure 5.1(c)***. There is a linear relationship between peak current and scan rate, indicating a diffusion controlled reaction.

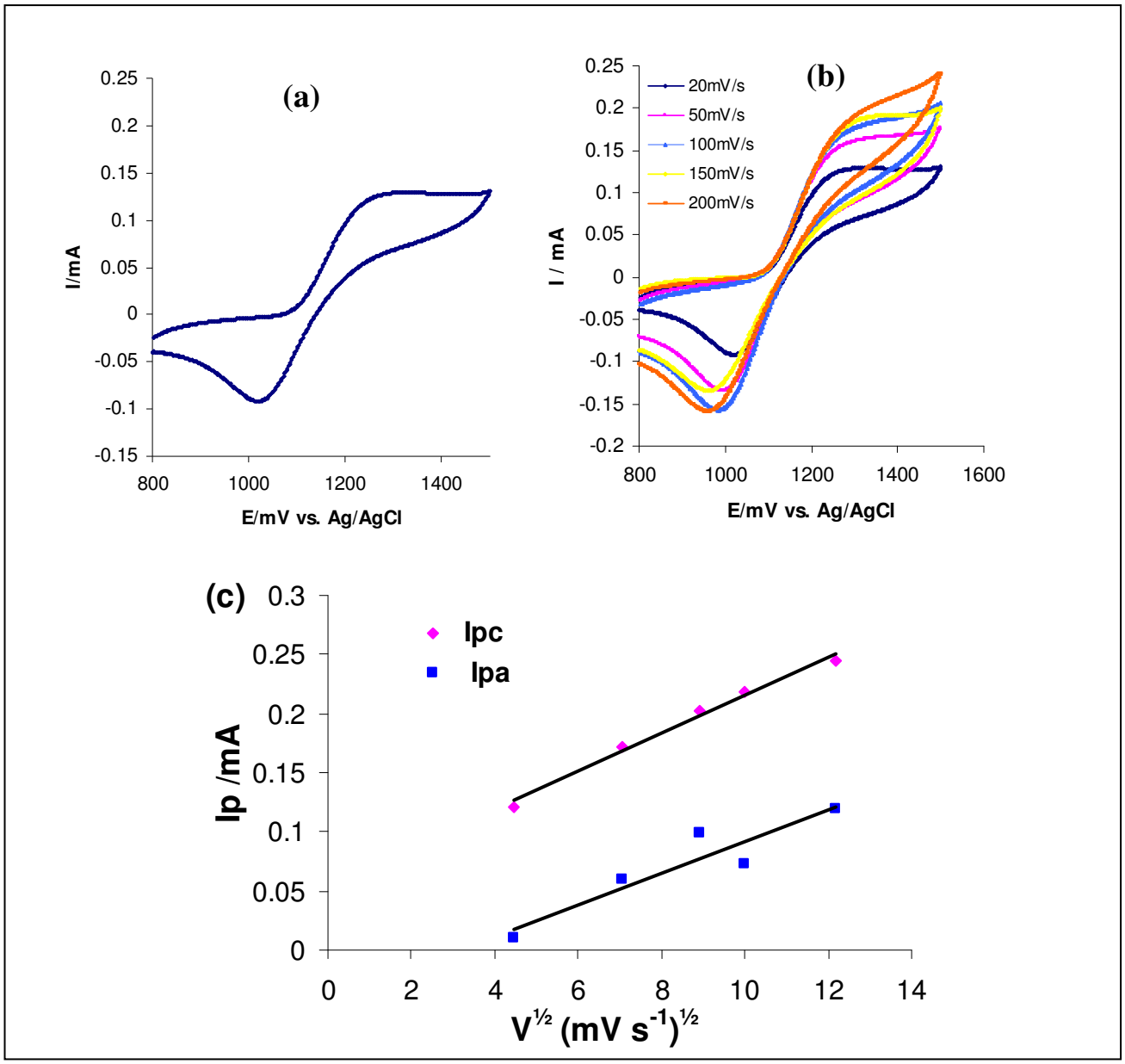

Figure 5.1: Cyclic voltammograms for a platinium electrode in: (a) 0.1 M $Ce(SO_4)_2$ solution in 1M H_2SO_4, at a scan rate of 100 mVs^{-1};(b) at various scan rates: 20, 50, 100, 150 and 200 mVs^{-1};(c) Plot of peak current vs. square root of scan rate for voltammogram of Ce $(SO_4)_2$ on Pt-electrode.

Figure 5.2(a) and b shows the voltammograms for the Ce(IV) aminocarboxylate complexes in 1 M H_2SO_4 solution .The peak potential Epa and Epc values are observed at around 1020 mV and 1290 mV. Both the cathodic peak and anodic peak potentials changed slightly with the scan rate as shown in ***Figure 5.2(b)***. Peak splitting was found to increase with increasing scan rate, meaning a larger peak separation was observed and the electrochemical process was irreversible. The redox reaction Ce(III) to Ce(IV) shows a quasi-reversible electrochemical behaviour, Ce(IV)–EDTA illustrates an irreversible behaviour, whereas the Ce(IV)–DTPA complex is quasi-reversible as shown in ***Figure 5.2(c).*** The cathodic peak potential shift

towards more negative potential values for the reduction step, the current ratio Ipa/ Ipc for the Ce(IV)–DTPA complex was found to be 0.84 and the transfer coefficient (a) from the Table 1 was found to be 0.42. This ratio and transfer coefficient supports the notion that the reaction shown in ***Figure 5.2(a)*** is quasi-reversible. Various concentrations of DTPA (1–3 mM) were added to the cerium solution and the colour of the solution changes after adding 3 mM DTPA, the colour changes from deep yellow to light yellow. The ionic strength was strictly kept constant, since the change in the rate constant could be due to the small changes in the ionic strength. Sodium hydroxide was used to adjust the pH of the solution to 4.5. Ce(IV)–DTPA complex provides better results at the pH 4.5 than the Ce(IV)–EDTA complex as shown in ***Figure 5.2***.

Glentworth et al. [19] studied the kinetics of lanthanide polyaminopolycarboxylic acid complex ions, claiming that the rate of exchange depends on the pH of Ce–DTPA and on the concentration of Ce–DTPA complex. The reason is that the ligands may be considered to be electrostatically bonded to the metal ion and it is probable that the carboxylate group is unstable, i.e. there is a continuous breaking and reforming of the bonds. The unstable carboxylate group will be vulnerable to attack by protons and the stability of the ligand will be increasingly reduced by successive protonation of the carboxylate group. Rao [22] studied the rate of exchange kinetics of EDTA, DTPA and its analogues with Ce(IV) in sulphuric acid medium using spectrophotometric methods. No electrochemical study is presented for Ce(IV)–DTPA. Rao confirmed that the rate constant depends on the nature of amino groups i.e. tertiary > secondary > primary. This implies that a ligand like EDTA will be less vulnerable to attack by an oxidizing agent like Ce(IV) in sulphuric acid than DTPA. Therefore the Ce(IV)–DTPA complex will be more stable and more suitable for redox flow batteries than the Ce(IV)–EDTA system. A plot of the peak current (ip) for the oxidation and reduction processes versus square root of scan rate ($V^{1/2}$) is given in ***Figure 5.2 (d)*** and ***(e)*** This shows the dependence of peak current for the oxidation and reduction process of the Ce(IV)–DTPA complex; the peak current is a linear function of the potential scan rate, confirming that the surface measures limit these processes. It also proves that the Ce(IV)–DTPA complex is a quasi-reversible redox process within the potential range and is controlled by a diffusion limited reaction.

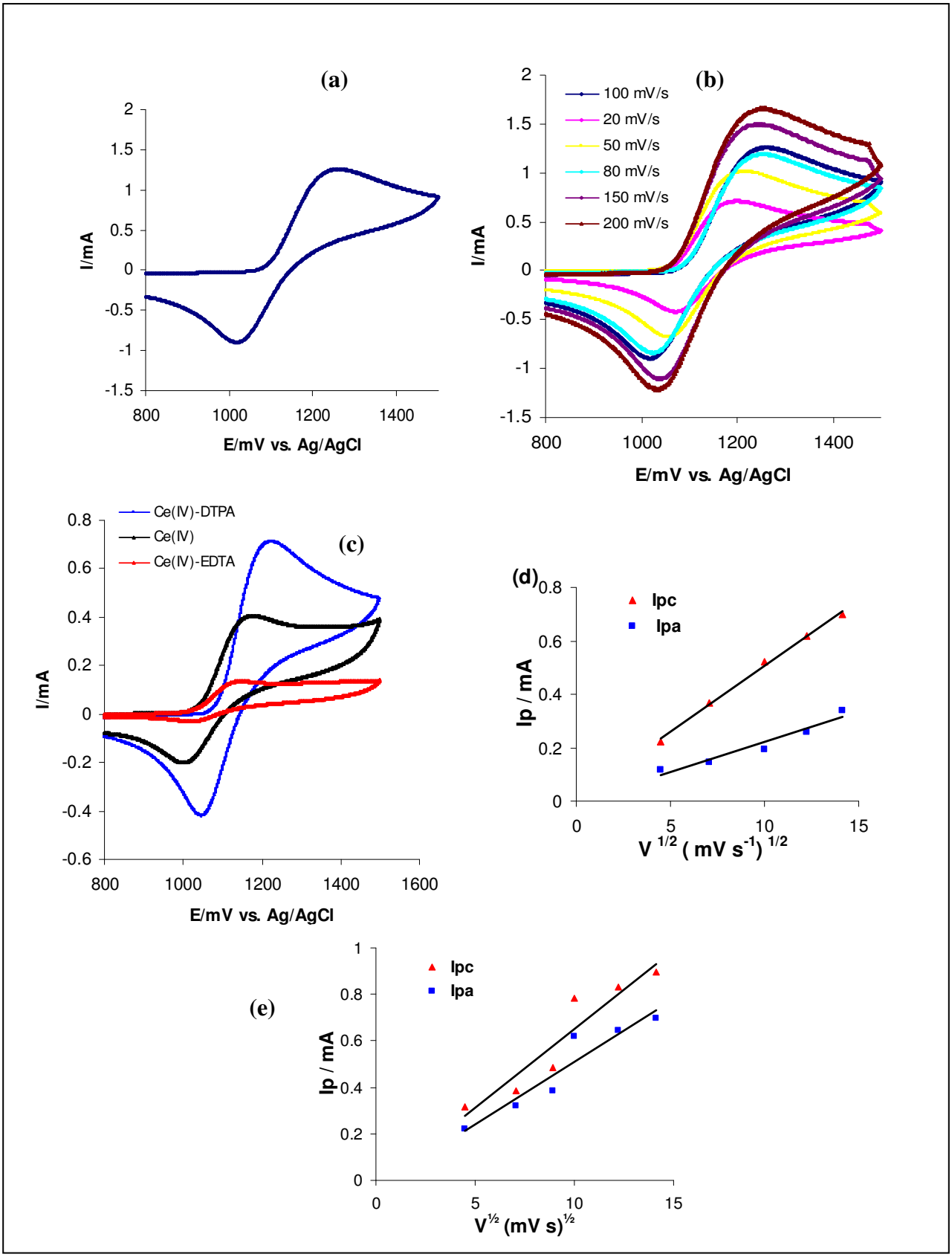

Figure 5.2: Cyclic voltammogram for a 0.1 M $Ce(SO_4)_2$ solution in 1 M H_2SO_4 at a platimium electrode. With (a) 0.03 M DTPA at a scan rate of 100 mVs^{-1} (b) at various scan rates: 20, 50, 100, 150 and 200 mV s^{-1} and (c) 0.1 M of $Ce(SO_4)_2$, Ce (IV)–EDTA and Ce (IV)–DTPA. (d) Randles plot for the redox reaction of Ce(IV)–EDTA. (e) Randles-Sevcik plot for the redox reaction of Ce(IV)–DTPA.

Figure 5.2(d) shows a large current separation between the anodic and cathodic lines indicating faster kinetics for the reduction process than the oxidation process for the Ce(IV)–EDTA complex. In contrast ***Figure 5.2(e)*** illustrates that the anodic ‘‘line’’ and cathodic ‘‘line’’ are close together and have similar slopes, indicative of relatively comparable electron transfer rates. However the Ce(IV)–EDTA complex is slightly limited by the surface processes and a poor linear response is achieved as shown in ***Figure 5.2(d)***. ***Figure 5.2(c)*** shows an overlap of the three voltammograms of the redox behaviour of Ce(IV) in sulphuric acid, the Ce(IV)–EDTA complex and the Ce(IV)–DTPA complexes respectively.

The anodic and cathodic peak currents of the Ce(IV)–DTPA complex is higher than the corresponding currents for the Ce(IV)– EDTA complex and Ce(IV) at the same concentration, indicating a faster electron transfer at the platinum working electrode for the former. This enhanced electron transfer compared to the other complexes is also supported by the electron transfer coefficient (α) for this reaction.

Table 5.I: Cyclic voltammogram data for different electrolytes determined using a platinum electrode

Electrolyte	**Diffusion coefficient ($10^6 D$ / cm^2 s^{-1})**		**Electron coefficient (α)**		**Standard rate constant ($10^4 k^o$ / cm^2 s^{-1})**	
	This study	***Literature values***	***This study***	***Literature values***	***This study***	***Literature values***
Ce(IV)	2.4	3.20[a] [21]	0.31	-	1.6	1.9 [21]
Ce(IV)-EDTA	1.3	-	0.36	-	1.9	1.9 [b] [18]
Ce(IV)-DTPA	1.1	-	0.42	-	3.1	-
Fe(III)	2.3	3.24[c] [25] 7.6 [26]	0.39	-	2.1	3.25 [25] 2.87 [d] [26]
Fe(III)-EDTA	1.9	1.50[e] [25]	0.48	0.49 [27]	2.6	1.9[f] [27]
Fe(III)-DTPA	0.28	0.20 [25]	0.51	-	2.3	156 [25]

[a] Diffusion coefficient of Ce(IV) at Au-electrode = 0.32 x 10^{-5}cm s^{-1} [21]

[b] The rate constant (k) of Ce(IV)–EDTA in 0.1M KCl = 1.9 s^{-1} [18]

[c] Diffusion coefficient of Fe(III) at Diamond-electrode = 7.6 x 10^{-6} cm^2 s^{-1} [26]

[d] The rate constant (k) of Fe(III at Diamond-electrode = 2.87 x 10^{-3} cm s^{-1} [26]

[e] Diffusion coefficient of Fe(III) at Pt-electrode = 1.50 x1 0^{-6} cm^2 s^{-1} [25]

[f] The rate constant (k) of Fe(III)–EDTA at Au-electrode = 1.9 cm s^{-1} [27]

The rate constant, diffusion coefficient and electron coefficient for Fe(III), Fe(III)–EDTA and Fe(III)–DTPA are shown in ***Table 5.1***. The values of (k) were obtained from the plot of $\ln_i$ vs potential (E-Eo), and found to be (k) = 2.1 9 10^{-4} cm/s Fe (III), Fe (III) EDTA (k) = 2.6 9 10^{-4} cm/s and Fe(III)DTPA (k) = 2.3 9 10^{-4} cm/s. The value of (α) were also obtained from the same plot of $\ln_i$ vs potential (E-Eo), and found to be (α) = 0.39 Fe(III), (α) = 0.48 Fe(III)EDTA and (α) = 0.51 Fe(III)DTPA as shown in ***Table 5.1***. In comparison the

Fe(III)EDTA complex species have a larger (*k*) value than the uncomplexed species, meaning that the reaction will be faster when the EDTA and DTPA complexes are used rather than the uncomplexed species of Fe(III).

5.4.2 Rotating disc voltammetry

The voltammograms of rotating disc electrochemistry were shown in ***Figure 5.3*** which was obtained at rotation rates between 200 and 4000 rpm. The limiting current results were plotted versus the square root of rotation rate as illustrated in ***Figure 5.3(c)***, a linear relationship has been found between the square root of rotation rate and the limiting current. This demonstrates that the Ce(IV)–DTPA reaction obeys the Levich equation below, ***Equation (5.1)*** *[*23]

$$i_L = (0.620)\ n\ F\ A\ D^{2/3}\ w^{1/2}\ v^{-1/6}\ C \qquad (5.1)$$

where iL is the Levich current, n is the number of electrons, F is the Faraday constant, A is the electrode area (in cm^2), D is the diffusion coefficient (in cm^2/s), *w* is the rotation rate (radians/s), v is the kinematic viscosity (cm^2/s), and C is the concentration of (mol/cm^3).

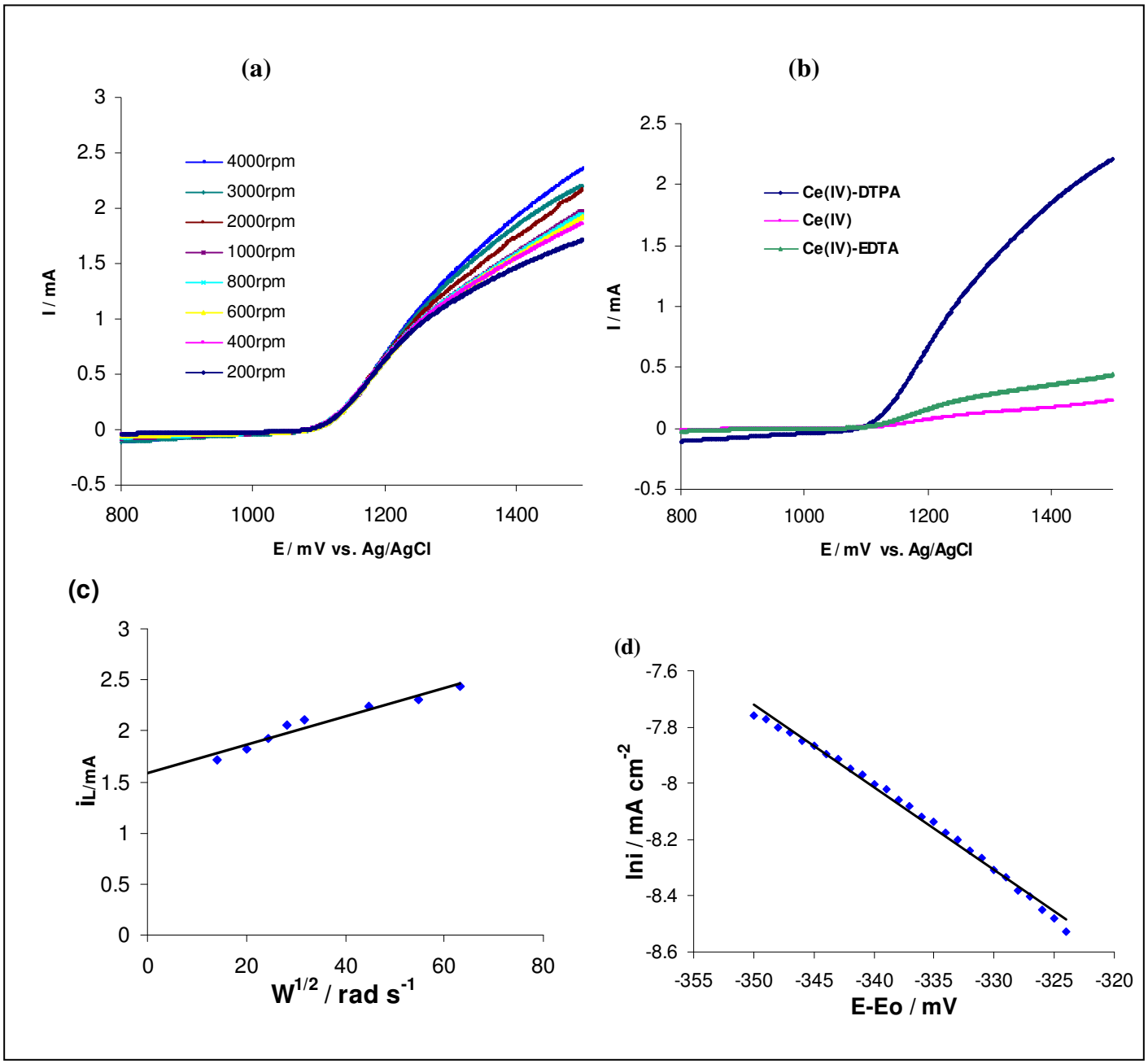

Figure 5.3: Hydrodynamic voltammograms of a 0.1 M $Ce(SO_4)_2$ solution in 1 M H_2SO_4 at a Plutinum electrode with (a) 0.03 M DTPA at various rotation rates: 200, 400, 600, 800, 1000, 2000, 3000 and 4000 rpm (b) in $Ce(SO_4)_2$, Ce (IV)–EDTA and Ce (IV)–DTPA at a rotation rate of 1000 rpm; (c) plot of Levich current vs. square root of rotation rate for the Ce (IV)–DTPA (d) a plot of lni vs. potential ($E-E_0$).

The values of the diffusion coefficient obtained from ***Figure 5.3(c)*** are shown in ***Table 5.1***. A plot of ln_i vs potential (E-Eo) were constructed as shown in ***Figure 5.3(d)***, a straight line plot was obtained with a linear regression of 0.9934. The rate constant (k) was calculated from the Levich plot and found to be in the range 1.6–3.1 10^{-4} cm^2/s, and is in good agreement with those found by earlier researchers [18, 20] as listed in ***Table 5.1***. Therefore, the process is

diffusion controlled. The diffusion coefficient of the uncomplexed Ce(IV) in 1 M H_2SO_4, calculated from the slope of the straight line, was found to be 2.4 x 10^{-6} cm^2/s as shown in ***Table 5.1***. This is lower than the value of 3.2 x 10^{-6} cm^2/s found in the literature [16, 17, 20]. A plot of i_L vs. $w^{1/2}$ gave a straight line with slope proportional to $D^{2/3}$. For a quasi-reversible process, the peak potential Ep is a function of scan rate, the difference between Ep and formal potential Eo, being related to the standard rate constant. The peak current may also be expressed as in **Equation (5.2)** [24].

$$ip = (0.227)\, n\, F\, A\, C\, k\, exp\, [-(anF/RT)\, (E-Eo) \qquad (5.2)$$

Plot of ln_i vs. (E-Eo), determined at different scan rates, should have a slope of -(anF/RT) with the intercept proportional to (*k*). The rate constant for the uncomplexed Ce(IV) in 1 M H_2SO_4 was calculated to be 1.6 x 10^{-4} cm/s as shown in ***Table 5.1***. This is a reasonable agreement with the value 1.9 x 10^{-4} cm/s found in the literature [20]. No kinetic and electrochemical data were available in the literature for the Ce(IV)–DTPA system for use in redox flow battery systems. Therefore the kinetics of uncomplexed Ce(IV) and Ce(EDTA) are the only points of reference, as shown in ***Table 5.1***. The Fe(III) EDTA and Fe(III)(DTPA) systems were also evaluated and used as a further point of reference. In comparison the Ce(IV)–DTPA complex species have a larger (*k*) value than the uncomplexed species, meaning that the reaction will be faster when DTPA is used as a complex rather than EDTA and uncomplexed species (Ce(IV).

5.5 Conclusion

The electrochemical behaviour of the complexation of Ce(IV) with EDTA and DTPA was studied using both CV and rotating disc electrochemistry (RDE). The results for cyclic voltammetry study of Ce(IV)–DTPA illustrate a quasi-reversible $1e^-$ transfer reaction electrode process on platinium. A potential separation (ΔEp) of greater than 59 mV was observed; this was dependent of scan rate. The Ce(IV)–DTPA complex at various scan rates gave a linear correlation between the peak current (Ep) and square root of scan rate, showing that the kinetics of the overall process was diffusion-controlled. RDE results also provided information about the electron transfer mechanism in the absence of any mass restriction. The kinetic tests also showed that the Ce(IV)–EDTA redox reaction at platinium was a relatively slow heterogeneous reaction. The electrochemical studies of the Ce(IV) in the presence of EDTA show irreversible behaviour. EDTA was therefore found not to be a suitable ligand for

use in electrolytes of RFB. In the Ce(IV) uncomplexed species the results show a quasi-reversible electrochemical behaviour with a lower electron transfer rate constant. The electrochemical study of Ce(IV), Ce(IV)–EDTA and Ce(IV)–DTPA at the platinum electrode indicated that the highest k value was between 1.6 and 3.1 x 10^{-4} cm/s and the diffusion coefficients between 1.1 and 2.4 x 10^{-6} cm/s. The Ce(IV)–DTPA complex species have a higher electron transfer rate constant than the Ce(IV)–EDTA complex and uncomplexed species Ce(IV), respectively. This indicates that the rate of electron transfer was fast. An all cerium redox couple in which the DTPA ligand will be used as an electrolyte for the redox flow battery system, has an advantage over the Ce–EDTA and Ce(IV) uncomplexed species. Hence the suggestion is that a redox flow battery employing the Ce(IV)–DTPA complex as the positive active species, with high voltage efficiency will satisfy an important requirement for a redox flow battery electrolyte.

5.6 References

[1] Rychcik M, Skyllas-Kazacos M, J. Power Sources 22 (1988) 59.

[2] Thaller LH, In: NASA TM-79143, National Aeronautics and Space Administration US, Department of Energy (1979).

[3] NASA TM-79067 National Aeronautics and Space Administration, US, Department of Energy (1977).

[4] Liu Y, Xia X, Liu H, J. Power Sources 130 (2004) 299.

[5] Reid MA, Thaller LH, NASA, Tech. Membr. No.809289 (1980) 1471.

[6] Sum E, Skyllas-Kazacos M, J. Power Sources 15 (1985) 179.

[7] Tsuda I, Nozaki K, Sakuta K, Kurokawa K, Sol. Energy Mater. Sol. Cells 47 (1997) 101.

[8] Hasegawa K, Kimura A, Yamamura T, Shiokawa Y, J. Phys Chem. Solids 66 (2005) 593.

[9] Yamamura T, Watanabe N, Shiokawa Y, J. Alloy Comp. 408 (2006) 1260.

[10] Skyllas-Kazacos M, Grossmith F, J. Electrochem. Soc.34 (1987) 2950.

[11] Kazacos M, Skyllas-Kazacos M, J. Electrochem. Soc.136 (1989) 2759.

[12] Doria J, De Andres MC, Armenta C, Proc. 9th Solar Energy Soc. 3 (1985) 1500.

[13] Chen Y.W.D, Santhanam K.S.V, Bard A.J, J. Electrochem. Soc.128 (1981)1460.

[14] Fang B, Iwasa S, Wei Y, Electrochim. Acta 47 (2002) 3971.

[15] Paulenova A, Creager SE, J. Power Sources 109 (2002) 431.

[16] Pletcher D, Valder E, Electrochim. Acta 33 (1988) 499.

[17] Wei Y, Fang B, J. Appl. Electrochem. 35 (2005) 561.

[18] Abbaspour A, Mehrgardi M.A, Talanta 67 (2005) 579.

[19] Glentworth P, Wiseall B, Wright C.L, et al. J. Inorg. Nucl. Chem. 30 (1968) 967.

[20] Kiekens P, Steen L, Donche H, et al. Electrochim. Acta 26 (1981) 841.

[21] Pletcher D, White J C P, Electrochim. Acta 37 (1992) 575.

[22] Rao G.N, Indian J. Chem. 8 (1970) 328.

[23] Bard A.J, Faulkner L.R, Electrochemical methods fundamentals and applications, 2nd edition, John Wiley & Sons, New York (2001).

[24] Zanello P, Inorganic electrochemistry theory, practice and application. The Royal Society of Chemistry, Cambridge (2003).

[25] Murthy ASN, Srivastava T, J. Power Sources 27 (1989) 119.

[26] Zang J.B, Wang Y.H, Zhao S.Z, Bian L.Y, Lu J, Diamond Relat. Mater. 16 (2007) 16.

[27] Cai C, Mirkin M.V, J. Am. Chem. Soc. 127 (2006) 171.

Chapter 6

Electrochemical Impedance Study of Ce(IV) with Other Aminopolycarboxylate Ligands for Redox Flow Battery Applications[*]

In this study the electrochemical behaviour of cerium with ethylenediamine disuccinate (Ce(IV)–EDDS) and nitrilotriacetic acid (Ce(IV)–NTA) on a platinum electrode were investigated by cyclic voltammetry (CV) and electrochemical impedance spectroscopy (EIS) for redox flow battery (RFB) applications. EDTA and DTPA results were used in this chapter to compare with other aminopolycarboxylate ligands like EDDS and NTA. The Ce(IV) redox system using EDDS and NTA as ligands for RFB was reported for the first time using EIS. The reversibility from the CV results was best when Ce(IV) was complexed with the DTPA ligand compared to the EDTA, EDDS and NTA ligands. The AC impedance spectra of these redox couples were analyzed and equivalent circuits proposed. Results of the EIS studies confirmed the results obtained from CV. Ce(IV)–DTPA showed the least resistance and faster electron transfer compared to Ce(IV)–EDTA, Ce(IV)–EDDS and Ce(IV)–NTA. The Ce(IV)–DTPA will therefore be a more suitable RFB electrolyte compared to Ce(IV), Ce(IV)–EDTA, Ce(IV)–EDDS and Ce(IV)–NTA due to its better electrochemical reversibility, lower resistance, higher potential, fast kinetic reactions, diffusion control and mass transfer.

6.1. Introduction

The complexes of metals with aminopolycarboxylic acid have attracted considerable attention [1-11]. The oxidation of various organic compounds using carboxylic acids with Ce(IV) has been extensively studied [1,3-4]. Abbaspour and Mehrgardi [1] investigated the electrochemical behaviour of Ce(III) ions in the presence of EDTA and determined the kinetic parameters such as transfer coefficient and rate constants for the electrocatalytic oxidation of the nitrite ion. The paper on Ce(IV) with the addition of DTPA complex has been published and in this is compared with uncomplexed Ce(IV) and Ce(IV)–EDTA, this all in the previous chapters and the paper [3]. Vanadium electrolyte was compared with the results observed from Modiba and Crouch [4] using charge/discharge characteristics of the electrolyte for battery performance, and found that the results are almost the same when comparing the vanadium and Ce(IV)–DTPA.

[*] Submitted to Electrochimica Acta, Modiba P, Matoetoe M, Crouch A.M. (2009).

It is important to study the kinetics and mechanism of different electrolytes for redox flow batteries, in order to be able to identify a suitable electrolyte that displays a high potential, high current and electrochemical reversibility. There are a few complications related to redox flow batteries (RBF), namely, mixing of electrolytes, and chemical degradation due to corrosion. An all–vanadium RFB system has been used to solve some of these difficulties [12-22], This system offers various advantages such as no decrease in capacity caused by the cross mixing of the positive and negative electrolyte, meaning that there will be no energy efficiency loss during the process. The effect of cross–contamination for all–vanadium RFB does not require catalysts for both electrode reactions, and there is no evolution of hydrogen gas, no need to rebalance power and additional equipment. Even though these qualities exist for all-vanadium redox flow systems the open-circuit voltage for each single cell after full charging is about 1.4 V, which is relatively low.

Liu and co-workers [23] investigated both cerium and vanadium, their CV results have confirmed the feasibility of replacing vanadium with a very high concentration of a cerium couple to produce a completely novel redox cell. Fang et al. [24] studied the Ce(IV)/Ce(III) couple, and obtained a formal potential of 1.2V and a coulombic efficiency of around 87%, which is higher than for the all–vanadium RFB. Kieken and co-worker [25] illustrated that the reduction of Ce(IV) to Ce(III) is independent of electrode materials using C, Pt and Au electrodes. They found that the charge transfer coefficient and the rate constant of all electrodes used were similar. Paulenova et al. [26] investigated the cerium couple for RFB, because of its larger positive redox potential, and the cell voltage was predicted to be approximately 1.9 V.

Glentworth et al. [2] examined the kinetics of isotopic exchange reactions between lanthanide ions and lanthanide as mentioned in ***Chapter 5, Section 5.1***. This work was used as a point of departure to demonstrate the superior performance of Ce(IV) with the addition of DTPA to form a Ce(IV)–DTPA complex. Also it should be useful to compare it with other ligands such as ethylenediaminetetraacetic acid (EDTA), ethylenediaminedisuccinic acid (EDDS) and nitrilotriacetic acid (NTA), My literature search has revealed no report of an electrochemical study of Ce(IV) in the presence of DTPA, EDTA, EDDS and NTA using electrochemical impedance spectroscopy (EIS) for redox flow batteries application. Generally the new battery technologies that are currently under development [3-4, 23-26], fluctuate in the use of different metals redox couples. The Ce^{4+}/Ce^{3+} redox couple is attractive for RFB technology because of its large positive redox potential, which should result in a battery with a higher cell

voltage and a greater energy storage capacity. Pletcher and Valder [26] reported on the electrochemical behaviour of the Ce^{4+}/Ce^{3+} redox couple in aqueous nitrite media, and the electrochemistry of the Ce^{4+}/Ce^{3+} couple in sulphuric acid solutions has been widely investigated [3-4, 23, 26-28]. A cerium couple is the most uncomplicated electrolyte for redox batteries, and it provides a relatively inexpensive and reliable power source. Although the production of cerium batteries is generally simple and has only a relatively low environmental impact, various disadvantages of cerium redox batteries do persist. To avoid these disadvantages associated with the cross contamination and relatively poor energy to volume ratio, alternative ligands can be used to complex cerium for example, cerium can be complexed with EDTA, EDDS or DTPA to achieve improved power levels.

In earlier work, by Modiba and Crouch [3] CV and RDE were used to evaluate the electrochemical kinetics of Ce(IV)–DTPA and Ce(IV)–EDTA complexes. In this chapter the electrochemical evaluation and electrochemical impedance spectroscopy of Ce(IV) with EDTA, EDDS, NTA and DTPA were used to determine their suitability as electrolytes for RFB. The AC impedance spectra of these redox couples have been analyzed and an equivalent circuit proposed.

6.2. Experimental

6.2.1 Materials

All reagents were of analytical reagent grade unless otherwise stated. Ethylenediaminetetraacetic acid (EDTA), ethylenediamine disuccinate (EDDS), nitrilotriacetic acid (NTA) and diethylenetriamine pentaacetic acid (DTPA) were obtained from (Fluka- Riedel-de Haen). Sulphuric acid, potassium ferricyanide ($K_3Fe(CN)_6$), potassium nitrate (KNO_3) sodium hydroxide, cerium (IV) sulphate [$Ce(SO_4)_2$] were purchased from Sigma–Aldrich (Steinheim, Germany).

6.2.2 Preparation of Ce(IV) with DTPA, NTA, EDDS and EDTA

Cerium (IV) sulphate [$Ce(SO_4)_2$] and Ce(IV)−EDTA were prepared as described in the literature [29]. For the preparation of Ce(IV)−DTPA , DTPA was added to replace EDTA as per literature method, and dissolved in 1 M H_2SO_4. The solution was filtered, and then poured into a small specially designed CV glass cell. Deionized water was prepared by passing distilled water through a Millipore water purification system (Bedford, MA, USA).

6.2.3 Instrumentation

CV measurements were performed using a BAS 100B voltammetric system (Bioanalytical Systems, Inc. West Lafayette, Indiana, USA). Electrochemical impedance spectroscopy (EIS) measurements were recorded with a VoltaLab PGZ 402 (Radiometer Analytical, France).

6.2.4 Electrochemical measurements

The electrochemical behaviour of the Ce(IV) ion in the presence of EDTA, NTA, EDDS and DTPA was investigated with CV and EIS. A three electrode system was used to perform all electrochemical experiments: a platinum electrode with a diameter of 3 mm was used as a working electrode, Ag/AgCl (3M NaCl type) as a reference electrode, and a platinum wire as a counter electrode.

Impedance measurements were performed in the frequency range from 100 kHz to 100 mHz at potential step from 800 −1300 mV, with an applied amplitude of 10 mV. All experiments were performed at room temperature and EIS results were recorded using Pt as working electrode. Alumina micro-polish and polishing pads (Buehler, IL, USA) were used for polishing the electrodes. The electrodes were sonicated for 15 min in water, followed by air-drying.

6.3. Results and discussion

6.3.1 Cyclic voltammetry

A cyclic voltammogram of Ce(IV) in the presence of EDDS at a Pt electrode showed anodic and cathodic peaks around 1232 and 490 mV, respectively, in ***Figure 6.1 (a)***. The anodic peak potential gradually increased from 1228 to 1244 mV with an increase in scan rate. A corresponding cathodic peak potential decrease was observed from 500 to 484 mV with an increase in scan rate from 20 −300 mV/s as shown in ***Figure 6.1 (b).*** These changes indicate that the potentials of the anodic and cathodic peaks are dependent upon the scan rates. The symmetric shape of the anodic and cathodic peaks reveals good electron transfer, but the potential separation (ΔE) shows poor reversibility between the anodic peak and the cathodic peak. The anodic peak current of the Ce(IV)−EDDS complex is greater than that of the cathodic peak and a variable change from the Ce(IV) is observed. The anodic peak showed a marked increase, whereas there was a slight increase in the cathodic peak current. This means that the addition of EDDS to Ce(IV), there was no effect in the chemical reaction. The Ce(IV)–EDDS results follow the same trend as the Ce(IV)–EDTA results reported earlier [3].

Both complexes of Ce(IV)–EDDS and Ce(IV)–EDTA are electrochemically irreversible; their surface processes are limited and they have poor linear response.

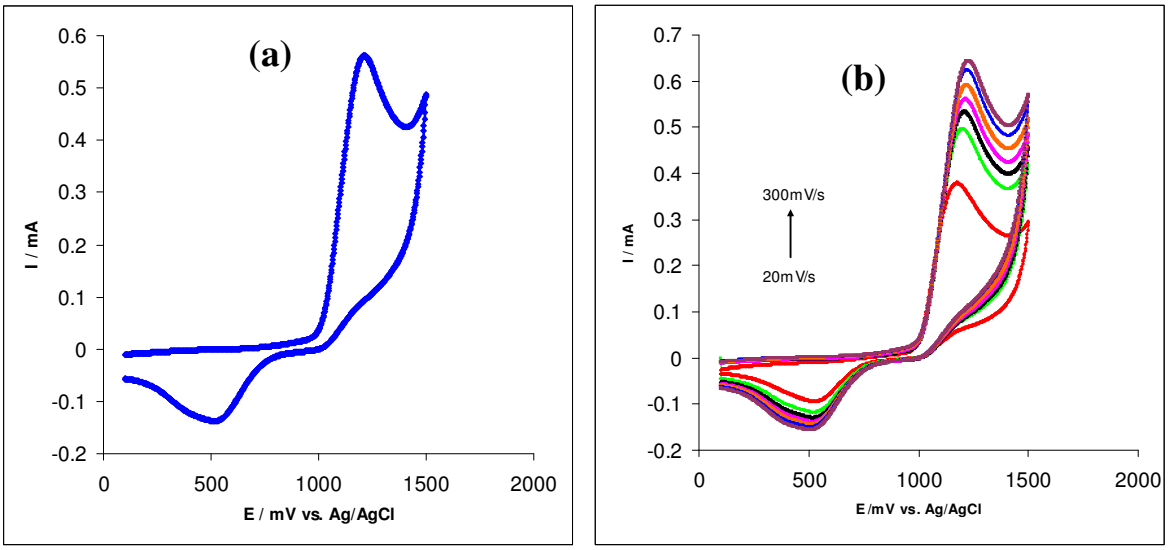

Figure 6.1: (a) Ce(IV)–EDDS cyclic voltammograms with a Pt –electrode are recorded at a scan rate of 100 mV/s and (b) at scan rates of 20, 50, 100, 150, 200, 250 and 300 mV/s respectively.

A voltammogram of Ce(IV) in the presence of NTA (Ce(IV)–NTA) is shown in ***Figure 6.2 (a)***. The anodic peak is observed around 1139 mV and the cathodic peak at around 942 mV. The Ce(IV)–NTA complex is electrochemically active, showing a quasi-reversible electrochemical behaviour. The peak current increases with scan rate as observed in ***Figure 6.2 (b)***.

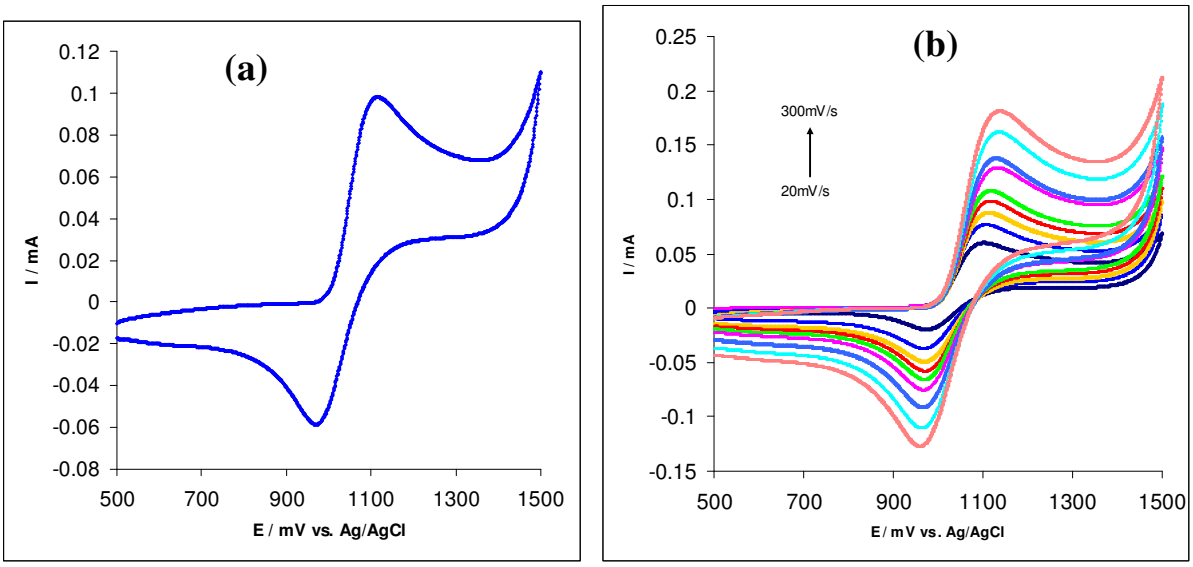

Figure 6.2: (a) Ce(IV) –NTA cyclic voltammograms with a Pt–electrode are recorded at a scan rate of 100 mV/s and (b) at scan rates 20, 50, 80, 100, 150, 200, 250 and 300 mV/s respectively.

Such changes indicate that the potentials of the anodic and cathodic peaks are independent of the scan rate, and the peak potential separation (ΔE_P) is more than 59 mV. If the peak potential separation (ΔE_P) is greater than 59 mV then the electrochemical reaction is considered to be quasi-reversible. The Ce(IV)–NTA complex and the Ce(IV)–DTPA complex had similar cyclic voltammogram shape [3]. Both complexes have a good reversible redox reaction, one electron (−1e) transfer reaction, which is mass transfer controlled and diffusion limited.

6.3.2 Comparison of the electrochemistry of Ce(IV) with various ligands (EDTA, EDDS, NTA, DTPA)

Studies of Ce(IV)–DTPA have shown that this complex has promising electrochemical properties, therefore comparison of this complex to other complexes was investigated [3]**.** A comparison of the cyclic voltammograms of the Ce(IV)–DTPA with Ce(IV) as an uncomplexed species, as well as with various aminopolycarboxylate ligands (EDTA, EDDS, NTA), are illustrated in ***Figure 6.3***. Ce(IV)–DTPA has the highest current, and its electrochemical reversibility is better than Ce(IV)–EDTA, Ce(IV)–EDDS, Ce(IV)–NTA and the uncomplexed Ce(IV) species. The Ce(IV)–DTPA cyclic voltammograms illustrate a quasi-reversible $1e^-$ transfer reaction electrode process with a ΔE_P of greater than 59 mV. This is an indication of reversible electrochemical behaviour, as stated in the literature [29-30].

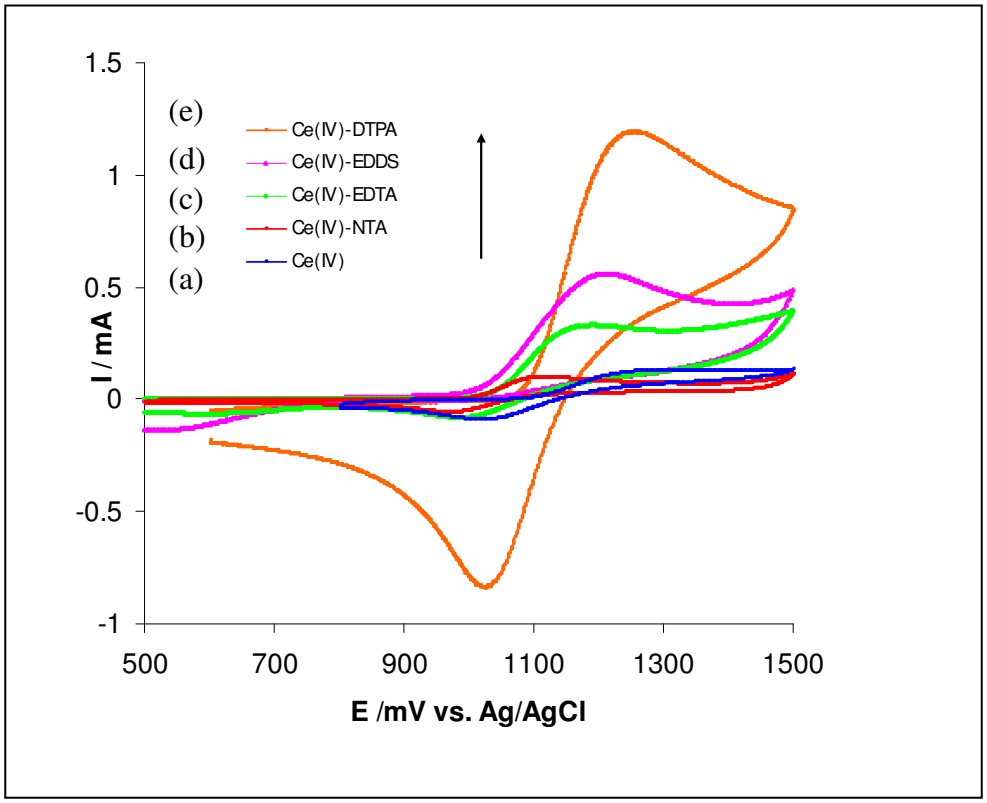

Figure 6.3: (a) Cyclic voltammogram of the following, recorded at a scan rate of 100 mV/s (a) Ce(IV), (b) Ce(IV)–NTA (c) Ce(IV) –EDTA, (d) Ce(IV)–EDDS, (e) Ce(IV)–DTPA (Concentration of cerium in all the above solutions is 0.1 M).

The Ce(IV)–DTPA complex showed a linear correlation between the peak current (Ep) and the square root of the scan rate, showing that the kinetics of the overall process was diffusion controlled.

The electrochemical parameters and kinetics of the Ce(IV) in the present of aminopolycarboxylate ligands (EDTA, EDDS, NTA and DTPA) are summarized in ***Table 6.1***.

Table 6.1: Electrochemical parameters and kinetics of Ce(IV) in the presence of aminopolycarboxylate ligands with a Pt–electrode.

Electrolyte	Epc (mV)	Epa (mV)	Ipc (A)	Ipa (A)	ΔE=Ea-Ec (mV)	Ipa/ Ipc	Dx10^6 /cm^{2}s^{-1}	kx10^4 /cm^{-1}
Ce(IV)	1002	1252	$-8.94\text{x}10^{-2}$	$1.22\text{x}10^{-1}$	249	1.36	2.4	1.6
Ce–EDTA	982	1192	$-3.37\text{x}10^{-1}$	$0.81\text{x}10^{-1}$	210	2.4	1.3	1.9
Ce–EDDS	490	1223	$-1.49\text{x}10^{-1}$	$3.44\text{x}10^{-1}$	733	2.3	1.5	2.1
Ce–NTA	957	1127	$-0.57\text{x}10^{-1}$	$0.97\text{x}10^{-1}$	170	1.69	1.2	2.6
Ce–DTPA	1080	1264	$-7.03\text{x}10^{-1}$	1.02	184	1.4	1.1	3.1

The peak ratios of the anodic and the cathodic peaks for all electrolytes are greater than 1, indicating that the anodic reaction is more favourable than the cathodic reaction. The peak potentials decrease as follows: Ce(IV)–DTPA > Ce(IV)–NTA > Ce(IV)–EDTA > Ce(IV) > Ce(IV)–EDDS. The current trend is as follows: Ce(IV)–DTPA > Ce(IV)–NTA > Ce(IV)–EDTA > Ce(IV)–EDDS > Ce(IV). Rao [11] confirmed that the rate constant depends on the nature of the amino groups, i.e. tertiary > secondary > primary. This implies that ligands like EDTA and EDDS will be less vulnerable to attack by oxidizing agents (like Ce(IV)) in sulphuric acid than DTPA and NTA. The Ce(IV)–DTPA complex and Ce(IV)–NTA complex species have higher rate constant (*k*) values than Ce(IV)–EDTA, Ce(IV)–EDDS and Ce(IV) uncomplexed species, meaning that the redox reactions of Ce(IV) will be faster when DTPA and NTA complexes are used rather than when EDTA and EDDS complexes are used. Therefore, the Ce(IV)–DTPA complex and Ce(IV)–NTA will be more stable and more suitable for redox reactions for flow batteries. However, Ce(IV)–NTA has the lowest current and potential compared to all five electrolytes used in this study, hence it will not be suitable as a storage electrolyte.

6.3.3 Electrochemical impedance

Based on the CV results, further studies were directed at determination of electrolyte resistance using EIS. Resistance studies of the five electrolytes Ce(IV), Ce(IV)–EDTA, Ce(IV)–EDDS, Ce(IV)–NTA and Ce(IV)–DTPA were performed and their application in RFB was assessed. In RFB low resistance and fast electron transfer of the electrolyte is favoured. Therefore an electrolyte that has low resistance to e^- transfer has superior impedance properties.

6.3.4 Electrochemical impedance of Ce(IV)

Results of impedance studies of the Ce(III)/(IV) redox couple are shown in ***Figure 6.4***. The Nyquist plot ***Figure 6.4 (a)*** for the Ce(IV) / Ce(III) couple at different potentials, from 0.9 V–1.3 V, measured at frequencies of 10^{-1} to 10^{5} Hz, displays single semicircles that represent the electron transfer resistance at the electrode surface between the electrolyte/electrode surface from the higher frequency to the lower frequency. This resistance controls the electron transfer kinetics of the redox process at the electrolyte/electrode interface.

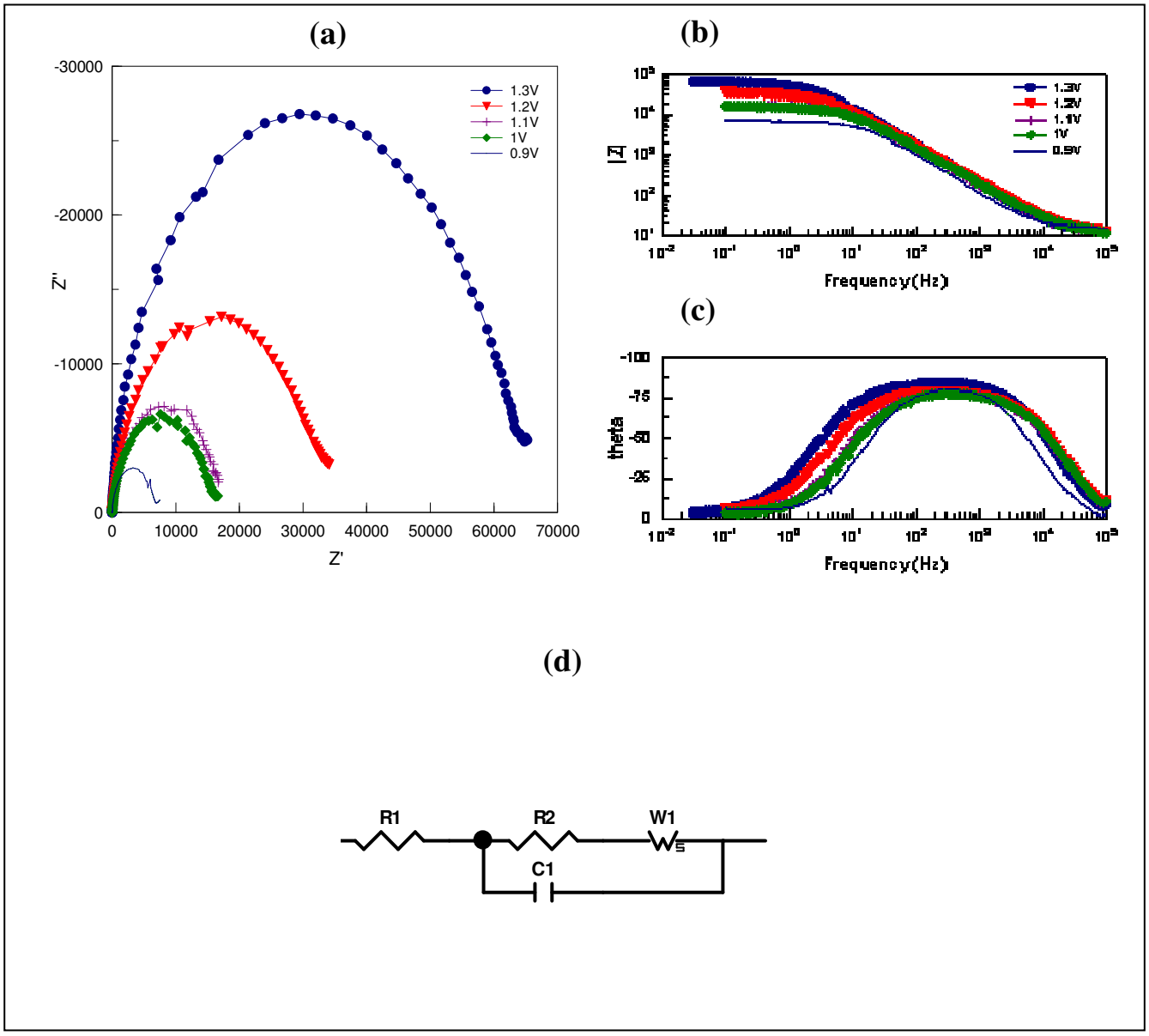

Figure 6.4: Results of Ce(III)/(IV) redox couple (a) Nyquist impedance plot, (b) Bode–magnitude plot, (c) Bode–phase plot and (d) Proposed equivalent circuit model diagram used for fitting the impedance data for the Ce(IV) electrolyte.

In this case, the lowest resistance is observed before the redox reaction (1.1V) at potentials of 1.0 and 1.2 V. The capacitance is also lower at 1.1 V, where the electron transfer is the fastest. ***Figures 6.4(b and c)*** shows corresponding Bode-magnitude plots, Bode–phase plot and the equivalent electrical circuit model used to determine the resistance.

Table 6.2: Electrical parameters from circle fitting for the Ce(IV) electrolyte

E (V)	R1 (Ω)	Error %	R2 (Ω)	Error %	C1 (F/cm^2)	Error %	W1 (Ω)	Error %
0.9	1.332	0.83	2.078	0.74	$2.6x10^{-6}$	5.18	143.46	2.67
1.0	1.267	0.25	2.348	0.56	$2.5x10^{-6}$	8.62	101.53	7.84
1.1	1.254	0.85	1.018	2.27	$2.3x10^{-6}$	11.25	783.5	5.81
1.2	1.474	0.92	3.404	0.25	$3.4x10^{-6}$	2.51	213.86	3.23
1.3	1.242	0.58	1.036	0.18	$2.7x10^{-6}$	4.27	143.76	13.79

R1: bulk solution resistance, and electrode resistance, C1: the capacitance at the contact interface between the electrode and the electrolyte solution (described as a capacitive constant phase element), R2: charge transfer resistance in parallel with C1, W1: Warburg diffusion element W1 attributable to the diffusion of ions.

Electrical parameters from circle fitting in ***Figure 6.4(d)*** is shown in **Table 6.2** . The higher resistance (R1) between the electrolytes and electrodes was observed at a potential of 1.2 V, R2 is also high from 0.9 to 1.1 V and from 1.2 to 1.3 V.

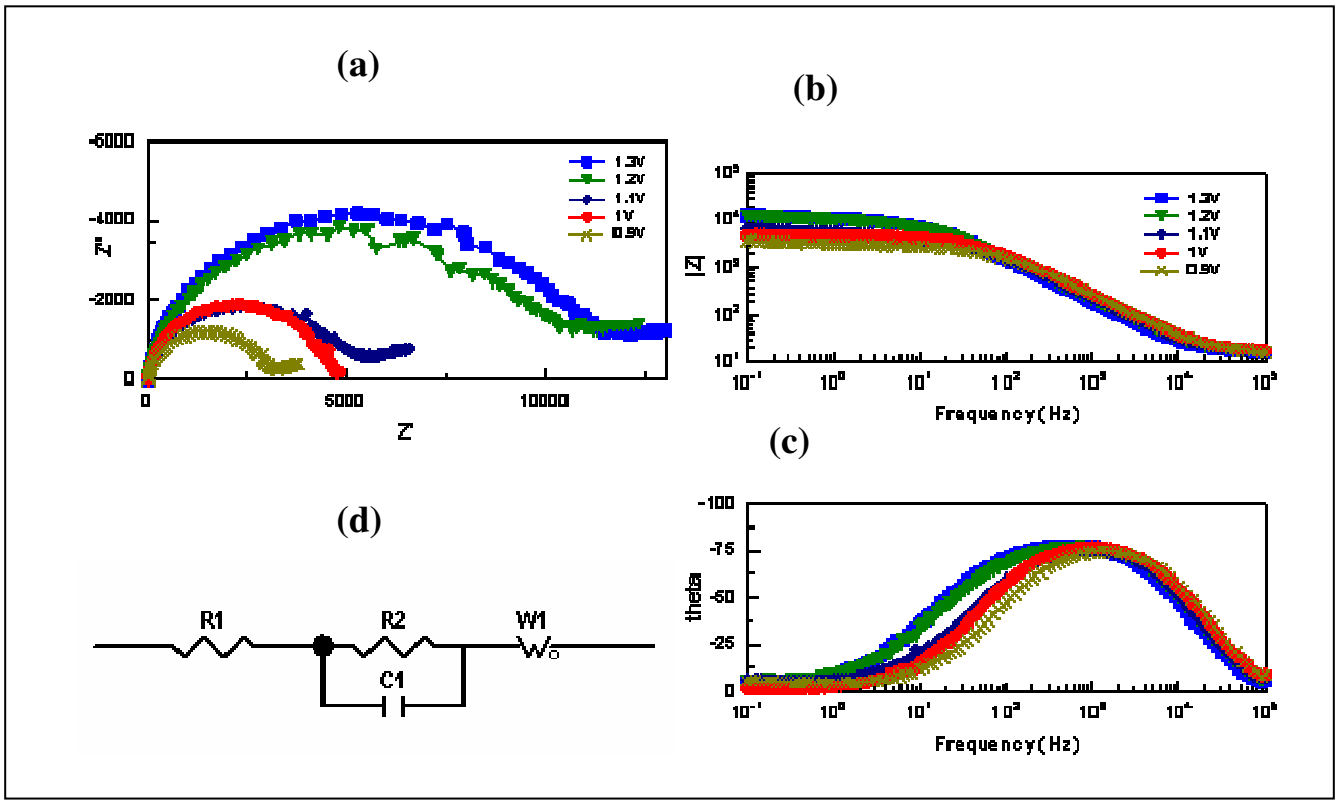

Figure 6.5: Results of Ce(IV)-EDTA (a) Nyquist impedance plot, (b) Bode–magnitude plot, (c) Bode–phase plot and (d) Equivalent circuit model used for fitting the impedance data for the Ce(IV)-EDTA electrolyte.

Figure 6.5(a) shows the Nyquist plot of a Ce(IV) couple in the presence of EDTA (Ce–EDTA) at different potentials from 0.9–1.3 V. Within the measured frequency range of 10^{-1} to 10^{5} Hz a single semicircle in the high frequency region is observed. The semicircle at high frequency represents the charge transfer process, which is usually described by the charge transfer resistance (R2). The response at low frequency is related to the diffusion process due to the Ce–EDTA layer that interrupts the access of the oxidizing species to the surface. At the potentials of 1.2 V and 1.3 V the arcs increased, and an increase in potential became wider in the high frequency region than in the lower frequency region of 0.9 – 1 V. At higher frequency the impedance is dominated by the electrolyte resistance, while at low frequency the surface electrode resistance (polarization resistance) dominates as shown in ***Figure 6.5(b-c).***

Table 6.3: Electrical parameters from circle fitting for the Ce(IV)-EDTA electrolyte

E (V)	**R1 (Ω)**	**Error %**	**R2 (Ω)**	**Error %**	**C1 (F/cm^2)**	**Error %**	**W1 (Ω)**	**Error %**
0.9	1.442	0.52	2.642	0.82	$2.4x10^{-6}$	8.88	135.39	5.81
1.0	0.966	0.83	1.9052	1.38	$2.3x10^{-6}$	4.62	101.35	3.94
1.1	1.125	0.66	2.723	5.62	$2.2x10^{-6}$	5.25	792.41	9.52
1.2	1.582	0.74	3.562	1.58	$2.1x10^{-6}$	1.82	225.15	2.89
1.3	1.032	0.15	2.968	8.48	$2.5x10^{-6}$	3.56	143.57	8.54

R1: bulk solution resistance, and electrode resistance, C1: the capacitance at the contact interface between the electrode and the electrolyte solution (described as a capacitive constant phase element), R2: charge transfer resistance in parallel with C1, W1: Warburg diffusion element W1 attributable to the diffusion of ions.

The values of the important parameters from equivalent circuit fitting in ***Figure 6.5(d)*** are summarized ***in Table 6.3***. It was found that the R1 value at 1.2 V is the higher than other potentials, and R2, C1 and W1 were higher than other potentials used.

6.3.5 Electrochemical impedance of the Ce(IV)-DTPA complex

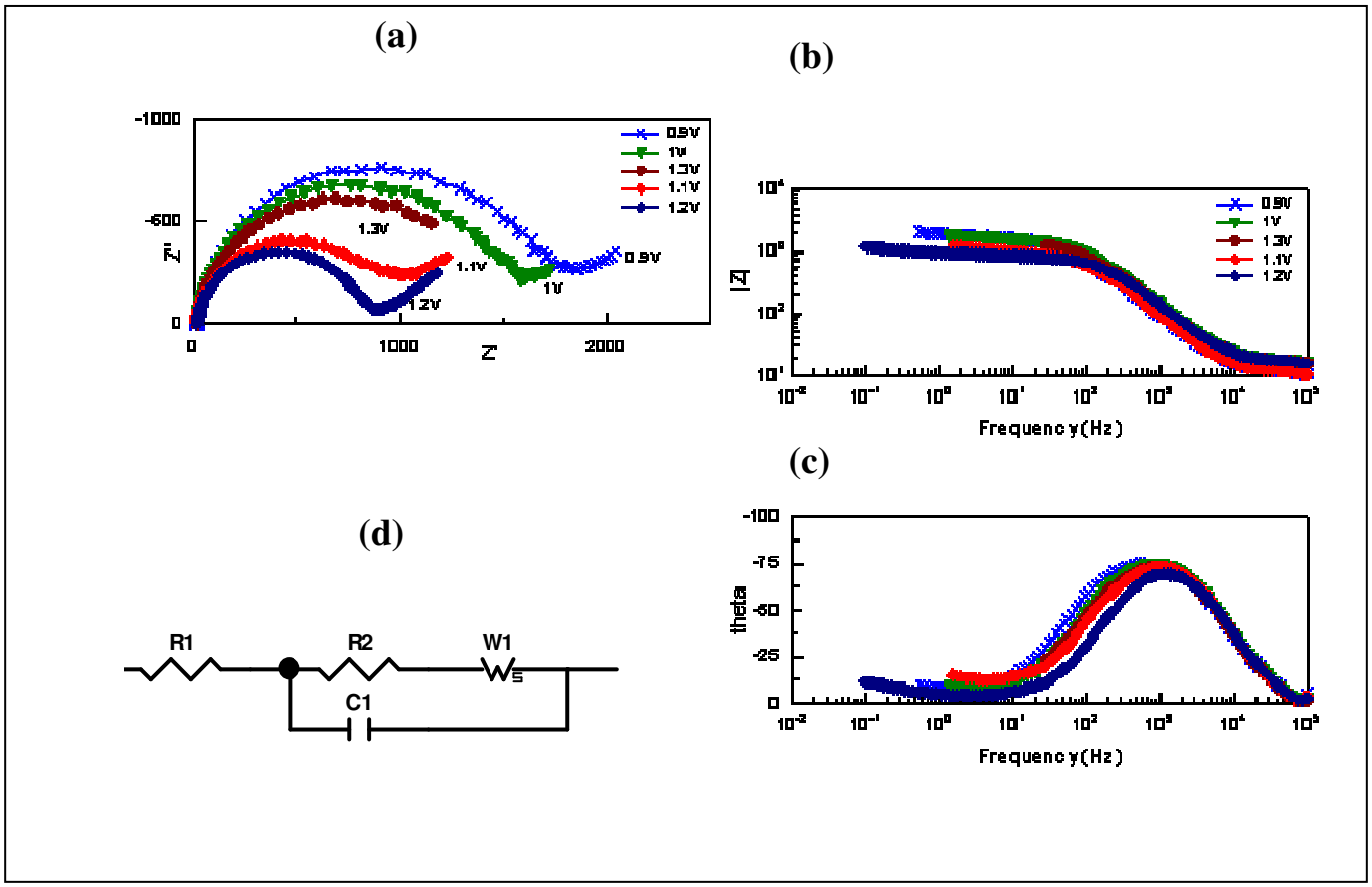

Figure 6.6: Results of Ce-DTPA (a) Nyquist impedance plot, (b) Bode–magnitude plot, (c) Bode–phase plot and (d) Proposed equivalent circuit model diagram used for fitting the impedance data for the Ce-DTPA electrolyte.

The Nyquist plot of the Ce(IV)/Ce(III) couple in the presence of DTPA at different potentials from 0.9 V–1.3 V appears to be a perfect Randles circuit equivalent (see ***Figure 6.6(a)***). In the measured frequency range of 10^{-1} to 10^{5} Hz, a single semicircle in the high frequency region and a straight line in the low frequency region are observed in all spectra, except at the potential of 1.3V where a depressed arc appears without a straight line. ***Figure 6.6(b)*** Bode-magnitude plot and ***Figure 6.6(c)*** bode–phase plot obtained from equivalent electrical circuit model in ***Figure 6.6(d)***.

Table 6.4: Electrical parameters from circle fitting for the Ce(IV)–DTPA electrolyte

E (V)	R1 (Ω)	Error %	R2 (Ω)	Error %	C1 (F/cm^2)	Error %	W1 (Ω)	Error %
0.9	1.203	1.12	1.950	0.52	$2.6x10^{-6}$	2.26	157.28	6.04
1.0	1.198	0.52	1.715	0.38	$2.5x10^{-6}$	5.42	112.35	5.93
1.1	1.197	1.02	1.802	2.08	$2.3x10^{-6}$	1.25	829.8	3.02
1.2	1.173	3.04	1.687	2.12	$2.3x10^{-6}$	8.12	705.5	8.89
1.3	1.205	0.98	1.925	5.06	$2.7x10^{-6}$	9.82	162.88	6.22

The corresponding data derived from the measurements of the equivalent circuits are presented in ***Table 6.4***. The lowest resistance (R1) between the electrolytes and electrodes was observed at a potential of 1.2 V. R2 is also low at the potential of 1.2 V, except all other remaining potential (0.9 – 1.1 and 1.3 V), C1 and W1 values are also high as shown in ***Table 6.4***. Further study was done to verify that the Ce(IV)–DTPA complex shows promise as an electrolyte for redox flow battery. Therefore, EIS was used in this work for more detailed information on the electron transport properties of the electrolyte, given that EIS is the best technique to determine reliable results for electrolytes electrochemical parameters.

6.3.6 Electrochemical impedance studies of the different complexes of Ce(IV) with EDDS, NTA, EDTA and DTPA

The perfect equivalent circuits model, characterised by a single semicircle and a straight line appear for all the electrolytes that were considered in this study, excluding the Ce(IV)–EDDS and Ce(IV)–NTA. A semicircle and a straight line in the EIS data were recorded for Ce(IV)–DTPA and Ce(IV)–EDTA. ***Figure 6.7(a)*** shows a single semicircle in the high frequency region and a long straight line with a slope of about 45º in the lower frequency region, this is an indication of an electrochemical process that is controlled by an electrochemical reaction and a diffusion step. In the Ce(IV)-DTPA complex corresponding Bode magnitude plots (logarithm of impedance versus logarithm of frequency) for all complexes are presented in ***Figure 6.7(b and c)***.

Table 6.5: Electrical parameters from circle fitting for various electrolytes in Figure 5 (d-f)

Electrolyte	R1 Ω	Error %	R2 Ω	Error %	C1 (-F/cm^2)	Error %	W1 Ω	Error %
Ce(IV)	1.474	0.58	3.404	0.35	$3.4x10^{-6}$	2.25	213.86	6.23
Ce(IV)-NTA	1.351	0.32	3.002	0.38	$2.3x10^{-6}$	5.52	188.94	8.12
Ce(IV)-EDTA	1.582	0.62	3.562	0.58	$2.1x10^{-6}$	9.12	225.15	3.05
Ce(IV)-EDDS	1.435	0.94	3.284	0.85	$3.2x10^{-6}$	7.98	208.52	9.52
Ce(IV)-DTPA	1.173	0.25	1.687	0.52	$2.5x10^{-6}$	3.58	705.51	4.13

Further detailed interpretation of the EIS measurements was performed by fitting the experimental plots, using the equivalent circuit depicted in ***Figure 6.7(d-f)***, from experimental data obtained from ***Figure 6.7(a)***. The data are summarised in ***Table 6.5***. The equivalent circuit for Ce(IV)-DTPA and Ce(IV) fitted very well in ***Figure 6.7(d)***, Ce(IV)-NTA and Ce(IV)-EDTA fitted well in ***Figure 6.7(e)***, and Ce(IV)-EDDS fitted satisfactorily in ***Figure 6.7(f)***.

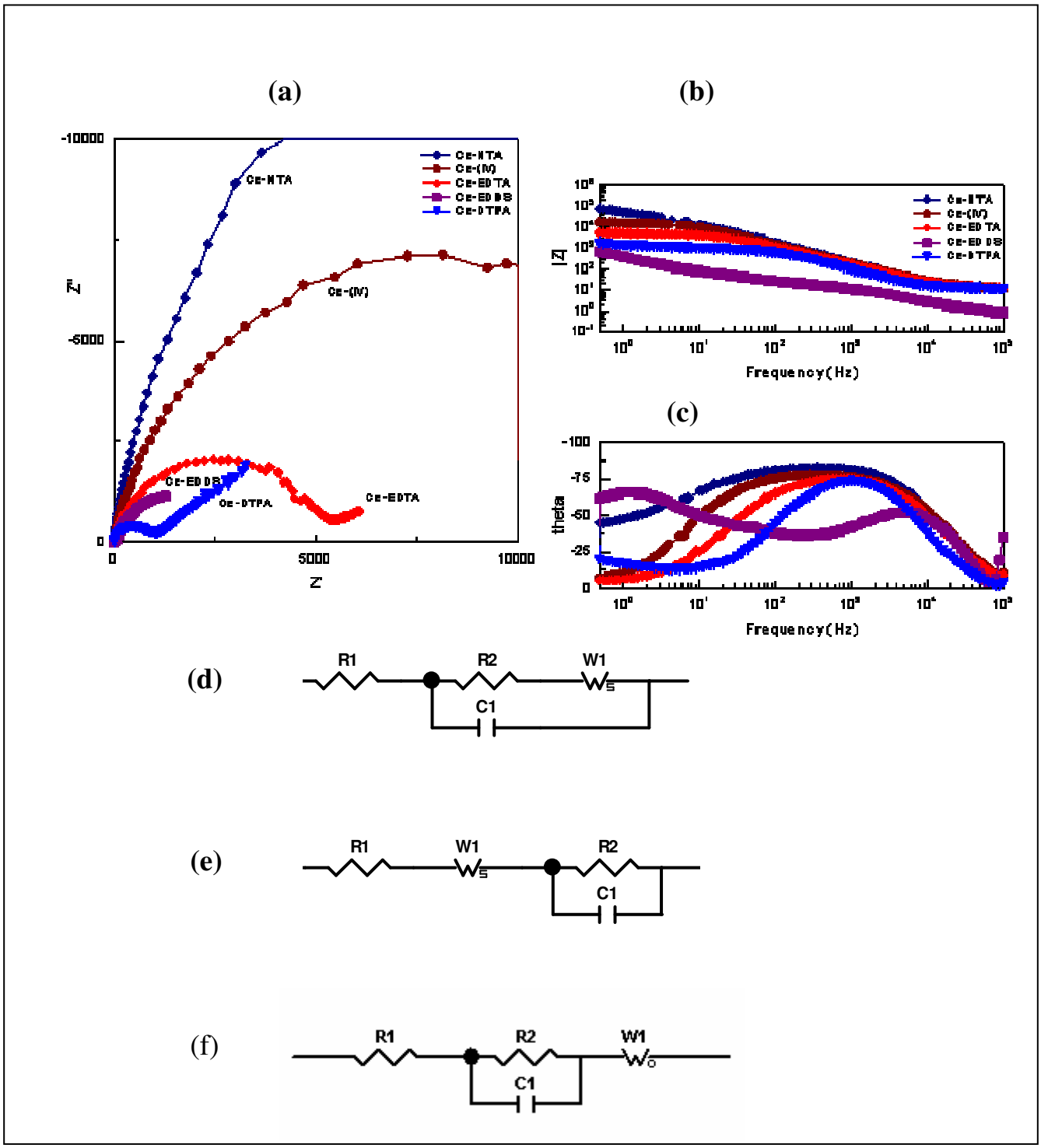

Figure 6.7: Results of Ce(IV) with (EDTA, EDDS, NTA and DTPA), (a) Nyquist impedance plot, (b) Bode–magnitude plot, (c) Bode–phase plot and plots (d-f) Proposed equivalent circuit model used for fitting the impedance data (d) Ce–DTPA, (e) Ce(IV) and Ce–EDTA, (f) Ce–EDDS and Ce–NTA.

.

Ce(IV)–DTPA has the lowest electrolyte resistance (R1) and charge transfer resistance (R2) values than other complexes, comparable with the values of C1 and W1 which are also low. Xue et al. [31] pointed out that when the resistance is low the potential will be high, and suggested that when the resistance of the electrolyte is high, the conductivity of the electrolyte will not be suitable. Therefore in Ce(IV)–DTPA, because the resistance is low, it means that the potential will be higher than the other complexes used in this study.

6.4. Conclusions

In this study the electrochemical behaviour of cerium with Ce(IV)–EDTA, Ce(IV)–EDDS, Ce(IV)–NTA and Ce(IV)–DTPA at a Pt–electrode was investigated by CV and EIS. The reversibility from the CV results was best when Ce(IV) was complexed with the DTPA ligand compared to the EDTA, EDDS and NTA ligands. The electron transfer was also faster for the Ce(IV)–DTPA couple compared to the other systems calculated from the electron diffusions and standard rate constants. The AC impedance spectra of Ce(IV)–EDTA, Ce(IV)–EDDS, Ce(IV)–NTA and Ce(IV)–DTPA were analyzed and equivalent circuits were proposed.

Equivalent circuit modelling for the Ce(IV)–DTPA complex illustrated that the process that takes place is a charge transfer process due to a combination of kinetics and diffusion processes. Furthermore, EIS results of analysis confirmed the results obtained from CV analysis. The Ce(IV)–DTPA showed the lowest resistance and faster electron transfer compared to Ce(IV)–EDTA, Ce(IV)–EDDS and Ce(IV)–NTA. Therefore, it is proposed that Ce(IV)–DTPA could be a suitable RFB electrolyte, better than Ce(IV), Ce(IV)–EDTA, Ce(IV)–EDDS and Ce(IV)–NTA, due to better electrochemical reversibility, lower resistance, higher potential, fast kinetic reactions, diffusion control and mass transfer.

6.5 References:

[1] Abbaspour A, Mehrgardi M.A, Talanta 67 (2005) 579.

[2] Glentworth P, Wiseall B, Wright C.L, Mahmood A.J, J. Inorg. Nucl. Chem. 30 (1968) 967.

[3] Modiba P, Crouch A M, J. Appl. Electrochem. 38 (2008) 1293.

[4] Modiba P, Crouch A.M, Proceedings of the 43rd Power Source Conference (2008) 71.

[5] Egan T.J, Barthakur S.R, Aisen P, J. Inorg. Biochem. 48 (1992) 241.

[6] Pierre J.L, Fontacave M, Biometals 12 (1999) 195.

[7] Neese F, Solomon E.I, J. Am. Chem Soc, 120 (1998) 12829.

[8] Metsarinne S, Rantanen P, Aksela R, Tuhkanen T, Chemosphere 55 (2004) 379.

[9] Vicente G, Povse A, Jose O, Transition Met. Chem. 23 (1998) 657.

[10] Engelmann M. D, Bobier R. T, Hiatt T, Cheng I. F, BioMetals 16 (2003) 519.

[11] Rao A.G.N, Indian J. Chemistry 8 (1970) 328.

[12] Chakrabarti M.H, Dryfe R.A.W, Roberts E.P.L, Electrochim. Acta 52 (2007) 2189.

[13] Skyllas-Kazacos M, Rychcik M, Robins R, Fane A, J. Electrochem. Soc. 133 (1985) 1057.

[14] Rychcik M, Skyllas-Kazacos M, J. Power Sources 22 (1988) 59.

[15] Kazacos M, Skyllas-Kazacos M, J. Electrochem. Soc. 136 (1989) 2759.

[16] Sum E, Skyllas-Kazacos M, J. Power Sources 15 (1985) 179.

[17] Sum E, Rychcik M, Skyllas-Kazacos M, J. Power Sources 16 (1985) 85.

[18] Tsuda I, Nozaki K, Sakuta K, Kurokawa K, Sol. Energy Mater. Sol. Cells 47 (1997) 101.

[19] Skyllas-Kazacos M, Grossmith F, J. Electrochem. Soc. 34 (1987) 2950.

[20] Skyllas-Kazacos M, Rychick M, Robins R, US Pat. No. 4,786,567 (1988).

[21] Hwang G.J, Ohya H., J. Memb. Sci. 120 (1996) 55.

[22] Zhu H.Q, Zhang Y.M, Yue L, Li W.S, Li G.L, Shu D, Chen H.Y, J. Power Sources 184 (2008) 637.

[23] Liu T.C, Pell W.G, Conway B.E, Electrochim. Acta 42 (1997) 3541.

[24] Fang B, Iwasa S, Wei Y, Arai T, Kumagai M, Electrochim. Acta 47 (2002) 3971.

[25] Kiekens P, Steen L, Donche H, Temmerman E, Electrochim. Acta 26 (1981) 841.

[26] Pletcher D, Valder E, Electrochim. Acta 33 (1988) 499.

[27] Wei Y, Fang B, J. Appl. Electrochem. 35 (2005) 561.

[28] Pletcher D, White J. C. P, Electrochim. Acta 37 (1992) 575.

[29] Bard J, Faulkner L.R, Electrochemical Methods Fundamentals and Applications Wiley Interscience Publications, New York, 2nd edition (2001).

[30] Zanello P, Inorganic Electrochemistry Theory, Practice and Application, Royal Society of Chemistry, Cambridge (2003).
[31] Xue F.Q, Wang Y.L, Wang W.H, Wang X.D, Electrochim. Acta 53 (2008) 6636.

Chapter 7

Electrochemical Properties of Metals (Cr, Fe, Mn, and V) for Redox Flow Battery Applications [*]

Summary

The electrochemical behaviour of Cr, Fe, Mn and V in the presence of DTPA ligand was investigated by cyclic voltammetry (CV) and electrochemical impedance spectroscopy (EIS) for use in redox flow battery (RFB) systems. Suitable electrolyte systems were initially chosen based on their electrochemical properties from CV results. Electrochemical reversibility, electron transfer and fast kinetic reactions are required. The results were compared with results for the Ce–DTPA system. From the EIS data, a feasible electrolyte was proposed based on its lower resistance. In Fe–DTPA and Mn–DTPA the electrochemical reversibility was much better than in the case of Cr–DTPA and V–DTPA, however, when V–DTPA was compared with Ce-DTPA, the Ce-DTPA complex was found to be better. Furthermore, EIS results confirmed the results obtained from CV. The Mn–DTPA, Cr–DTPA, Fe–DTPA and V–DTPA complexes had higher resistance than the Ce(IV)–DTPA complex. The Ce–DTPA is still the most preferable and suitable electrolyte compared to Mn–DTPA, Cr–DTPA, Fe–DTPA and V–DTPA, due to its better electrochemical reversibility, lower resistance, higher potential, fast kinetic reactions, diffusion control and mass transfer. For these reasons the cerium system with DTPA ligand, will still remain the better electrolyte in terms of performance and is a possible candidate for RFB application when compared to the other metal complexes mentioned above.

7.1. Introduction

A variety of redox couples have been used as an electrolyte for redox flow batteries [1-8]. Some couples have a lower cell voltage and a smaller energy storage capacity, but some have higher voltage but poor reversibility. Recently, the Mn(II)/Mn(III) couple's suitability was investigated as an electrode material [7]. The stability of the Mn(II)/Mn(III couple is poor, however the poor stability of Mn(III) is due to a spontaneous disproportionate reaction that produces Mn(II) and manganese dioxide.

[*] Submitted to J. Power Source Modiba P, Matoetoe M, Crouch A.M (2009).

Selim and Lingane [8] reported that Mn(III) could be present in sulphuric acid with concentrations of 4–8M. The lowest disproportionation reaction rate of Mn(III) was in 6.3M sulfuric acid and containing manganous sulphate, this mixture was used as the electrolyte.

An all-vanadium electrolyte system has been developed as a commercial system [9-13]. Chakrabarti at el. [12] reported that the performance of the all-vanadium system was significantly better than an all-chromium system, however they did observe cross-contamination of active electrolytes. Doria et al. [14] used an all-chromium redox system (Cr(II)/Cr(III) and Cr(III)/Cr(VI)) in a chloride medium for redox flow battery applications, and proposed a slow kinetic reactions for both chromium couples. Bae et al. [15] also investigated a chromium couple with the addition of EDTA ligand. They found that the redox reaction of the Cr(III)–EDTA/Cr(II)–EDTA couple was fast, had a higher energy output and longer life than a conventional Fe–Cr redox system. The kinetic reactions with Cr(V)–EDTA/Cr(III)–EDTA was however slow.

Several researchers have studied the complexes of metals with aminopolycarboxylic acid [16-17]. The oxidation of selected organic compounds using carboxylic acids and alcohol with Ce(IV) has been widely studied and is currently a very interesting prospect. In previous papers that we have published [1-2], Ce(IV) with the addition of DTPA complex was reported, the Ce(IV)–DTPA was also established and compared with uncomplexed Ce(IV) and Ce(IV)–EDTA [18]. Kiekens et al. [19] reported on the cerium system using various electrodes on different electrodes as mentioned in the previous chapter.

It is important to study the kinetics and thermodynamics of electrolyte for redox flow batteries in order to be able to identify a suitable electrolyte to give of high potential, current, and electrochemical reversibility to the reaction. In several cases, the thermodynamic properties of other complexes have also been examined electrochemically [20-23]. However in several cases the influence of complexation on the thermodynamic properties has not been competently comprehensible, because of the complicated mechanism of the complexation in the reaction that is taking place during the whole process.

In earlier studies by Modiba and Crouch [1]; CV and RDE were used to evaluate the electrochemical kinetics of Ce(IV)–DTPA, Ce(IV)–EDTA and uncomplexed Ce(IV). More recently we studied the electrochemical processes of Ce(IV) in the presence of DTPA, EDTA, EDDS, NTA using EIS and confirmed and extended the results from CV. We found that the Ce(IV)–DTPA complex was a suitable electrolyte when compared to Ce(IV)–EDTA,

Ce(IV)–EDDS, Ce(IV)–NTA complex and uncomplexed Ce(IV) species, due to better electrochemical reversibility, higher potential and lower resistance [18].

The cerium complexes of DTPA have been investigated [1-2, 18] and found to be a suitable electrolyte for redox flow batteries. In this chapter, the investigation and confirmation of a suitable electrolyte will be best favoured for the application of redox flow battery using CV and EIS techniques. It was considered advantageous to look into the chelating tendencies of other metal species with the DTPA ligand and to compare them with cerium-DTPA. Therefore, various electrochemical and physical measurements were conducted to investigate the appropriate electrolytes. Consequently various metals with DTPA ligands were examined and it was interesting to study the reaction between the metal and the ligand, since they all react differently with different metal species and the complex formation is different. Nevertheless, by using CV and EIS it was possible to compare and select a suitable electrolyte that will be more favorable than all other electrolytes mentioned above.

7.2. Experimental

7.2.1 Materials

All reagents were of analytical grade unless stated otherwise. Diethylenetriaminepentaacetic acid (DTPA) was obtained from (Fluka and Riedel-de Haën).Sulphuric acid, potassium ferricyanide ($K_3Fe(CN)_6$), potassium nitrate (KNO_3) sodium hydroxide, cerium(IV) sulphate [$Ce(SO_4)_2$], chromium sulphate Cr(III) sulphate, manganese (II) sulphate ($MnSO_4$), vanadium vanadate, (V_2SO_5) vanadium vanadyl ($VOSO_4$), were all purchased from Sigma–Aldrich (Steinheim, Germany).

7.2.2 Preparation of various metal species with DTPA

Chromium (III) sulphates, manganese (II) sulphate, cerium(IV) sulphate, potassium ferricyanide, potassium nitrate and ammonium vanadate were prepared as described in the literature [21]. For the preparation of all metals (Mn, Cr, Ce, Fe and V) with the ligand DTPA, the same procedure was used as in ***Chapter 5 Sections 5.2.2 and 5.2.3***.

7.2.3 Instrumentation

CV measurements were performed using a BAS 100B voltammetric System from Bio-analytical Systems, Inc., West Lafayette, Indiana, USA. Electrochemical impedance spectroscopy (EIS) measurements were recorded with a VoltaLab PGZ 402 (Radiometer Analytical, France).

7.2.4 Electrochemical measurements

Studies were performed using CV and EIS. A three–electrode system was used to carry out all the electrochemical experiments: a platinum electrode with a diameter of 3 mm as a working electrode, Ag/AgCl (3M NaCl type) as a reference electrode, and a platinum wire as a counter electrode.

Impedance measurements were performed in the frequency range of 100 kHz – 100 MHz at a potential step from 800 to 1300 mV, with an applied amplitude of 10 mV. All experiments were performed at room temperature and EIS results were recorded using Pt as the working electrode. Alumina micro-polish and polishing pads (Buehler, IL, USA) were used for polishing the electrodes. The electrodes were sonicated for 15 min in water, followed by air-drying.

7.3 Results and discussion

7.3.1 Cyclic voltammetry

7.3.1.1 Iron (Fe(II)/(III) couple

Figure 7.1(a) shows the cyclic voltammograms of the Fe(II)/(III) redox couple, anodic and cathodic peaks were observed around 260mV and 120mV, respectively , these results were compared with the EIS results. The anodic and cathodic peaks increased with increasing scan rate. The potential slowly increased from 240 to 280mV. Indications were that the potentials of the anodic and cathodic peaks were almost independent of the scan rate. The symmetric shapes of the anodic and cathodic peaks revealed that the ratios of the anodic and cathodic current peak heights are close to 1, indicating a reversible redox reaction of the Fe(II)/(III) couple occurred in the system. In ***Figure 7.1(b)*** the cyclic voltammogram of iron in the

presence of DTPA (Fe-DTPA complex) an oxidation peak was observed around 230 mV and cathodic peak around 60 mV.

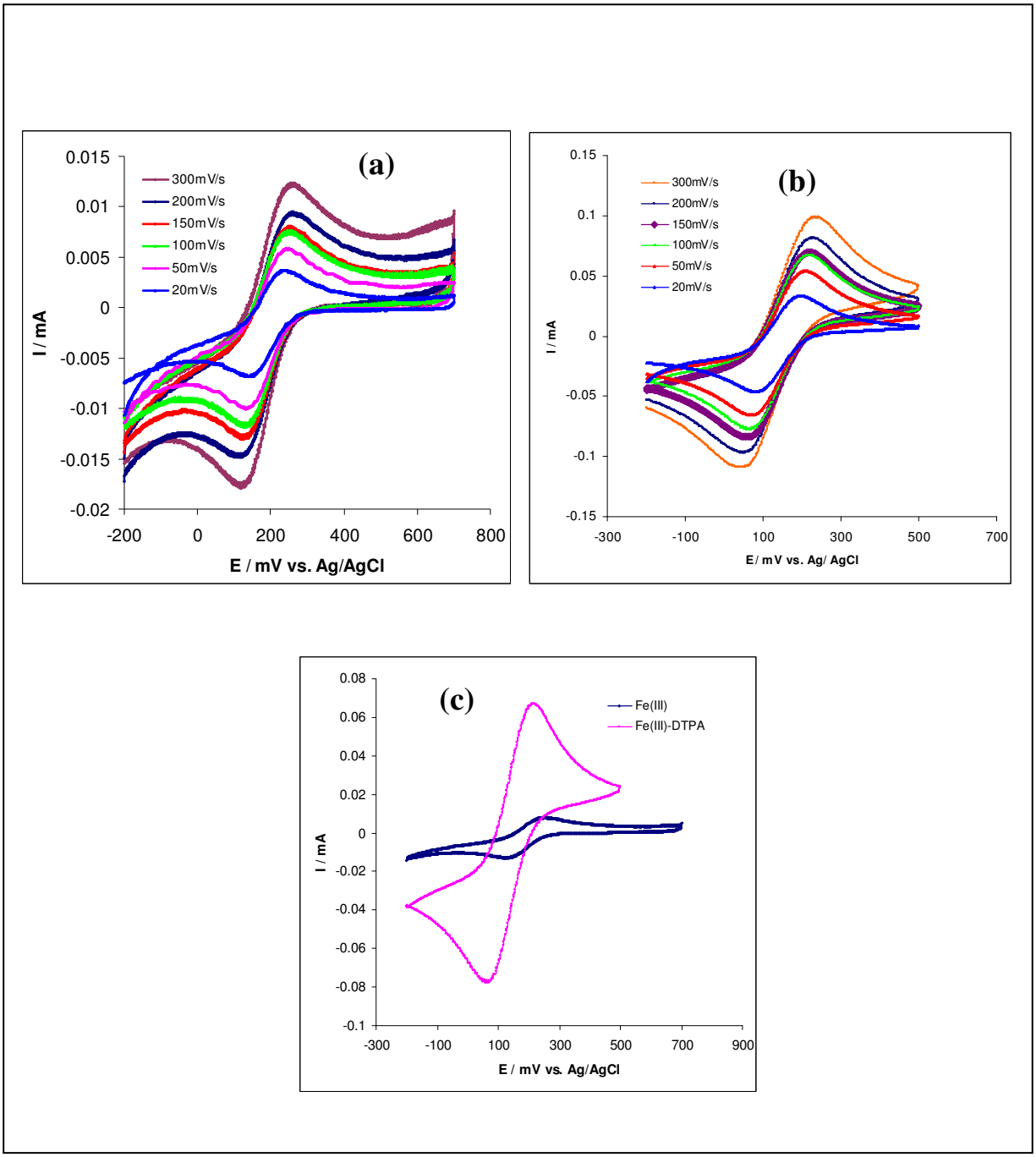

Figure 7.1: Cyclic voltammograms for a 0.1M Fe(II)/(III) solution in 1M H_2SO_4 recorded at a scan rate of 20–300mV/s: (a) Fe(II)/(III) couple, (b) Fe–DTPA, (c) Fe–DTPA and Fe(II)/(III) couple at the scan rate of 100 mV/s on Pt electrode.

The anodic cathodic potential difference (ΔEp = Epc – Epa) of the Fe(II)/(III) couple was in the region of ~140mV versus Ag/AgCl. ***Figure 7.1(c)*** shows an overlap of two

voltammograms, of the redox behaviour of Fe(II)/(III) couple and Fe–DTPA complex. The potential difference between the anodic and the cathodic peaks (ΔEp) was more than 59mV, from the scan rate of 20mV/s to 300mV/s for both the Fe(II)/(III) couple and the Fe–DTPA complex. Such changes indicate that the potentials of the anodic and cathodic peaks are independent of the scan rate, shown in ***Figure 7.1(a-b.)*** Hence, it is considered that the electrochemical reaction of the Fe(II)/(III) couple is a diffusion-controlled process, similar to that in the corresponding solutions. It is a single electron transfer quasi-reversible electrochemical process [22-23]. The electrochemical reaction is considered to be quasi-reversible for both systems the Fe(II)/(III) couple and the Fe–DTPA complex. The diffusion coefficient (*D*) and rate constant (*k*), for the Fe(II)/(III) couple and the Fe–DTPA are shown in ***Table 7.1***. The *D* value of the uncomplexed species (Fe(II)/(III) couple), calculated from the slope of the straight line, was found to be 2.3 x 10^{-6} cm/s and the complex species (Fe–DTPA) to be 2.8 x 10^{-6} cm/s. This is lower than the value of 3.92 m^2/s found previously by De Strycker et al. [24] for Fe(II)/(III) couple. The values of (*k*) were: Fe(II)/(III) couple (*k*) = 2.1 x10^{-4} cm/s, and Fe–DTPA (*k*) = 2.3 x10^{-4} cm/s. In comparison, the Fe(III) DTPA complex species have a larger (*k*) value than the uncomplexed species, meaning that the reaction will be faster when the DTPA complexes are used rather than the uncomplexed species of the Fe(II)/(III) couple.

7.3.2 Electrochemical impedance spectroscopy

The electrochemical impedance of 0.1M Fe(II)/(III) solution in 1M H_2SO_4 couple with and without 0.03M DTPA was investigated using EIS, ***Figure 7.2(a)*** shows the Nyquist plot of the Fe(II)/(III) couple and Fe–DTPA complex .

7.3.2.1 Iron (Fe(II)/(III) couple

A long straight line is observed in ***Figure 7.2(a)***, from higher to lower frequency region with a slope of about 45°. This is indicative of an electrochemical process that is controlled by an electrochemical reaction and diffusion step for the Fe–DTPA complex.

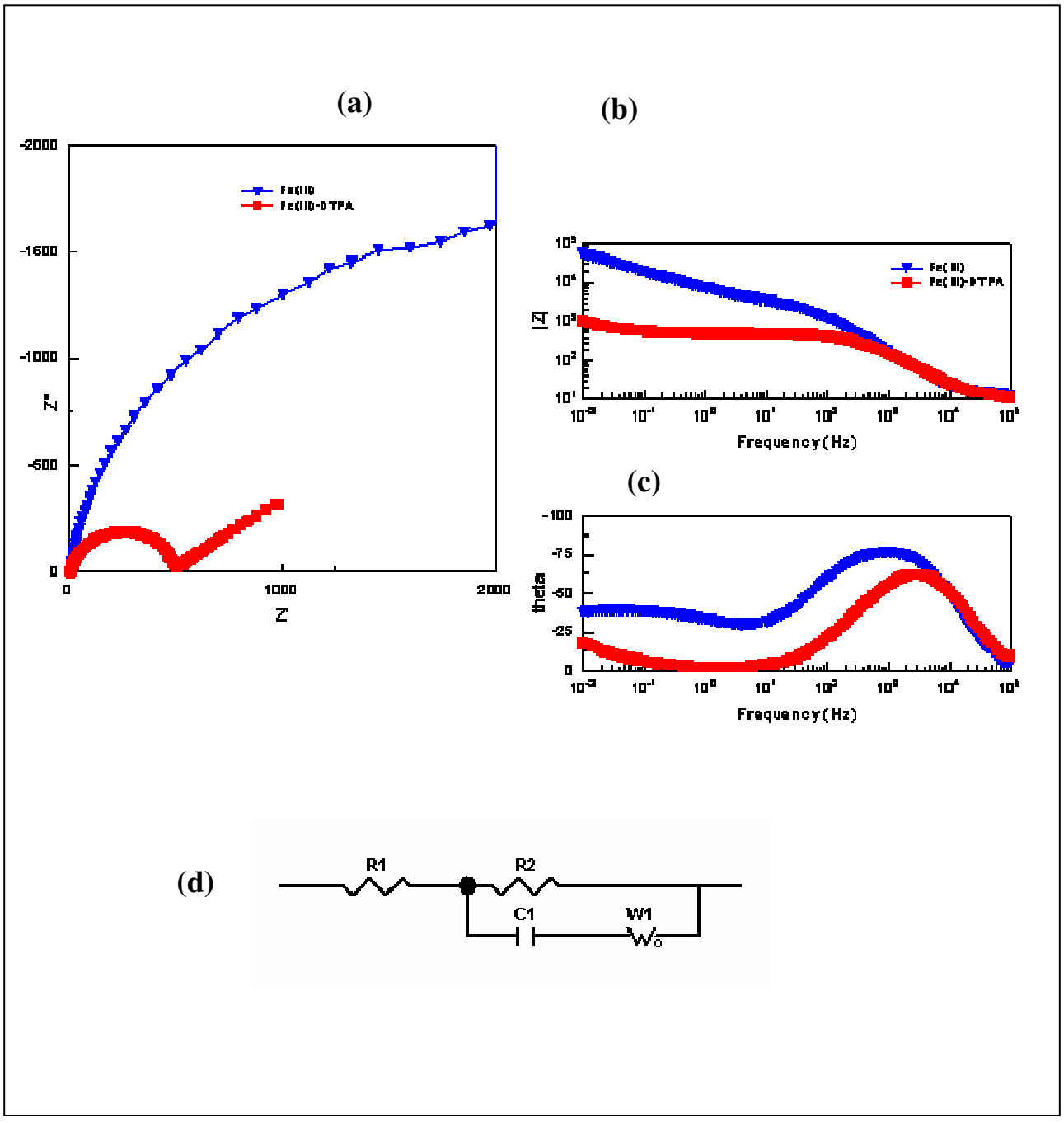

Figure 7.2: Results of 0.1M Fe(II)/(III) solution in 1M H_2SO_4 couple with and without 0.03M DTPA (a) Nyquist impedance plot for, (b-c) Bode plots, (d) Proposed equivalent circuit model used to fit the EIS data.

However for the Fe(II)/(III) couple a straight line with a slope of about 90º is observed in the higher frequency region. ***Figure 7.2(b)*** bode-magnitude plot and ***Figure 7.2(c)*** Bode–phase plot where obtained from the equivalent electrical circuit model in ***Figure 7.2(d)***. In this circuit; R1 is the solution resistance between the working electrode and the reference electrode; R2 is the charge-transfer resistance reflecting the electrochemical reaction of the Fe(II)/(III) couple at the electrode/solution interface; W is the Warburg impedance; and C1 models the double-layer capacitance, which is substituted for the capacitors to fit more exactly the high-frequency capacitive loop. All the results of the Fe(II)/(III) couple and the Fe–DTPA complex are in accordance with the predictions of the electrochemical mechanism, and the theory is best demonstrated by the fitting in ***Table 7.1***.

7.3.3 Cyclic voltammetry

The electrochemical behaviours of Cr, Fe, Mn and V in the presence of DTPA were investigated in effort to improve the electrochemical reversibility of these metal species. Research has proved that the use of DTPA improves the electrochemical properties of Ce(IV) [1-2].

7.3.3.1 Chromium (Cr(II)/(III) couple

Cyclic voltammograms of Cr(II)/(III) couple and Cr–DTPA complex are shown in ***Figure 7.3***. The forward scan reveals that the anodic peak associated with the oxidation of Cr(II) to Cr(III) at approximately 760 mV versus Ag/AgCl is shown in ***Figure 7.3(a)***. On the reverse scan, a cathodic peak associated with the reduction of Cr(III) to Cr(II) occurred at approximately –860 mV versus Ag/AgCl. There was another minor reduction peak around –116mV versus Ag/AgCl. The anodic and cathodic peak potential changed slightly when using different scan rates. The peak splitting increased with increasing scan rate, meaning that a larger peak separation was observed, therefore, the electrochemical process of Cr(II)/(III) couple will be irreversible.

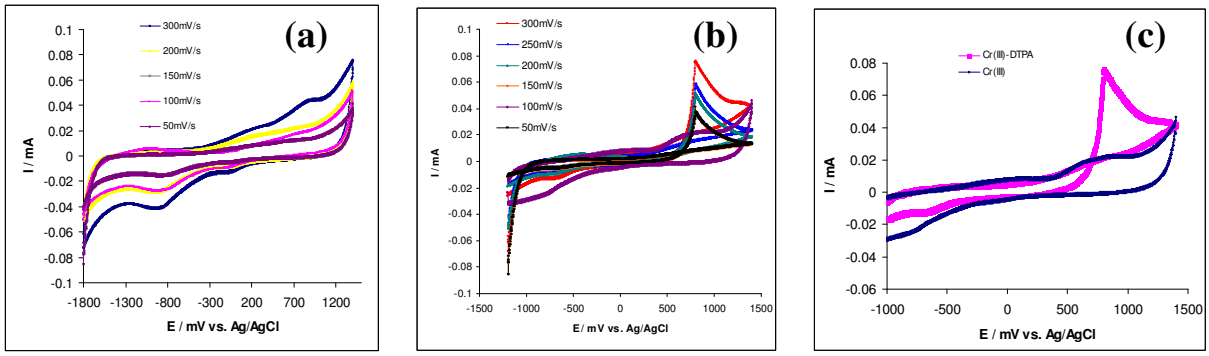

Figure 7.3: Cyclic voltammograms of 0.1M $(Cr_2SO_4)_3$ solution in 1M H_2SO_4 (a) without DTPA, (b) with 0.03 M DTPA, (c) Cr–DTPA and Cr(II)/(III) couple at the scan rate of 100 mV/s on Pt electrode.

The voltammogram of the Cr–DTPA complex showed a large oxidation and a slight reduction peak of Cr(II)/(III) couple at around 760 mV and –860 mV respectively as shown in ***Figure 7.3(b)***. Therefore, the electrochemical behaviour will be irreversible since the separation between the forward and reverse potential peak (ΔEp) is more than 59 mV. According to the literature [22], the potential of the forward peak is independent of the scan rate when the (ΔEp) is more than 59 mV, which is an indication of an irreversible electrochemical behaviour. An overlap of two voltammograms of the redox behaviour of Cr(II)/(III) couple and Cr–DTPA complex are shown in ***Figure 7.3(c)***. The observation illustrates that the anodic peak decreases in the absence of DTPA and increases significantly in the presence of DTPA (results are summarised in ***Table 7.1***).

Table 7.1: Electrochemical parameters E, ΔE, and Ipc/Ipa evaluated by CV using a Pt–electrode

Electrolyte	Epc (mV)	Epa (mV)	Ipc (A)	Ipa (A)	ΔE=Ea-Ec (mV)	Ipc/ Ipa	$D\ 10^{-6}$ cm^2s^{-1}	$k\ 10^{-4}$ cm^{-1}
Ce(IV)	-570	393	-5.58E-03	1.74E-03	963	3.2	2.4	1.6
Ce-DTPA	1080	1264	-1.21E-00	1.65E-00	184	0.73	1.1	3.1
Mn(III)	-643	-338	-3.62E-01	2.28E-01	305	1.6	3.8	2.3
Mn-DTPA	-585	-390	-2.06E-01	1.13E-01	195	1.8	3.1	2.7
Cr(II)	-792	786	-2.54E-02	2.18E-02	1576	1.1	2.5	1.8
Cr-DTPA	-686	798	-1.19E-02	7.51E-02	1484	0.2	1.9	2.1
Fe(III)	-116	238	-1.26E-02	6.6E-03	354	1.9	2.3	2.1
Fe-DTPA	44.0	229	-7.59E-02	6.61E-02	185	1.1	2.8	2.3
V(IV)	-589	354	-5.62E-03	1.7E-03	943	3.3	5.4	1.7
V-DTPA [(1)]	-757	-587	-2.64E-02	1.72E-02	170	1.5	4.9	2.2
V-DTPA [(2)]	-593	114	-2.40E-02	5.10E-02	707	0.5	6.5	9.1

[(1)] First peak for V(IV)–DTPA/V(V)–DTPA couple

[(2)] Second peak V(IV)–DTPA/V(V)–DTPA couple

The peak current increased upon oxidation of Cr(II)–DTPA to Cr(III)–DTPA, while on the reduction of Cr(III)–DTPA to Cr(II)–DTPA, no peak current increase was observed. This is due to the chelate nature of DTPA and to the lack of hydrogen atoms on the amine groups. It was not constructive using Pt–electrode for Cr(III) species, because only a small fraction of Cr(III) gave peak current that continuously decreases even at different scan rates. The diffusion coefficient (*D*) of Cr(III)–DTPA was calculated to be 1.9 x 10^{-6} cm^2/s and the rate constant (*k*) was 2.1 x 10^{-4} cm/s as shown if ***Table 7.1*** .

Bae et al. [15] used a graphite rod electrode for Cr(II)/(III)–EDTA couple and observed a reversible one–electron transfer reaction, and a fast redox reaction, with a diffusion coefficient (*D*) of 8.1 x 10^{-6} cm^2/s for Cr(III)–EDTA and 5.6 x 10^{-5} cm^2/s for Cr(II)–EDTA. Pletcher and White [21] have proven that the organic chemistry of the Cr(II)–DTPA and Cr(II)–EDTA complexes are similar in the cases of the reduction process. Therefore, the rate constant of Cr–DTPA was compared with that of Cr–EDTA, since there is no literature value for the rate constant (*k*) of Cr–DTPA to compare with the *k* values of Cr–DTPA observed in this study. Zhang et al. [25] found the *k* value to be 0.45 cm/s, while Anderson and Bonner. [26] found it to be around 2 x 10^{-5} M^{-1}/s, Hupp and Weaver [27] found the k value was 3 x 10^{-}

^{6} cm/s. Meier et al. [28] reported that Cr(III/II)–EDTA rate constant was found to be 0.462 cm/s and the diffusion coefficient (*D*) to be 2 x 10^{-7} m/s using a glassy carbon electrode. The (*k)* value differs due to different kinetics at different material used for electrode surfaces. This is the reason that the Pt–electrode was used in this study instead of glassy carbon electrode.

7.3.4 Electrochemical impedance spectroscopy

The electrochemical impedance of various metal species with and without DTPA ligand was investigated using EIS to determine the electrical parameters, such as the resistance and the capacitance of various electrolytes.

7.3.4.1 Chromium (Cr(II)/(III) couple

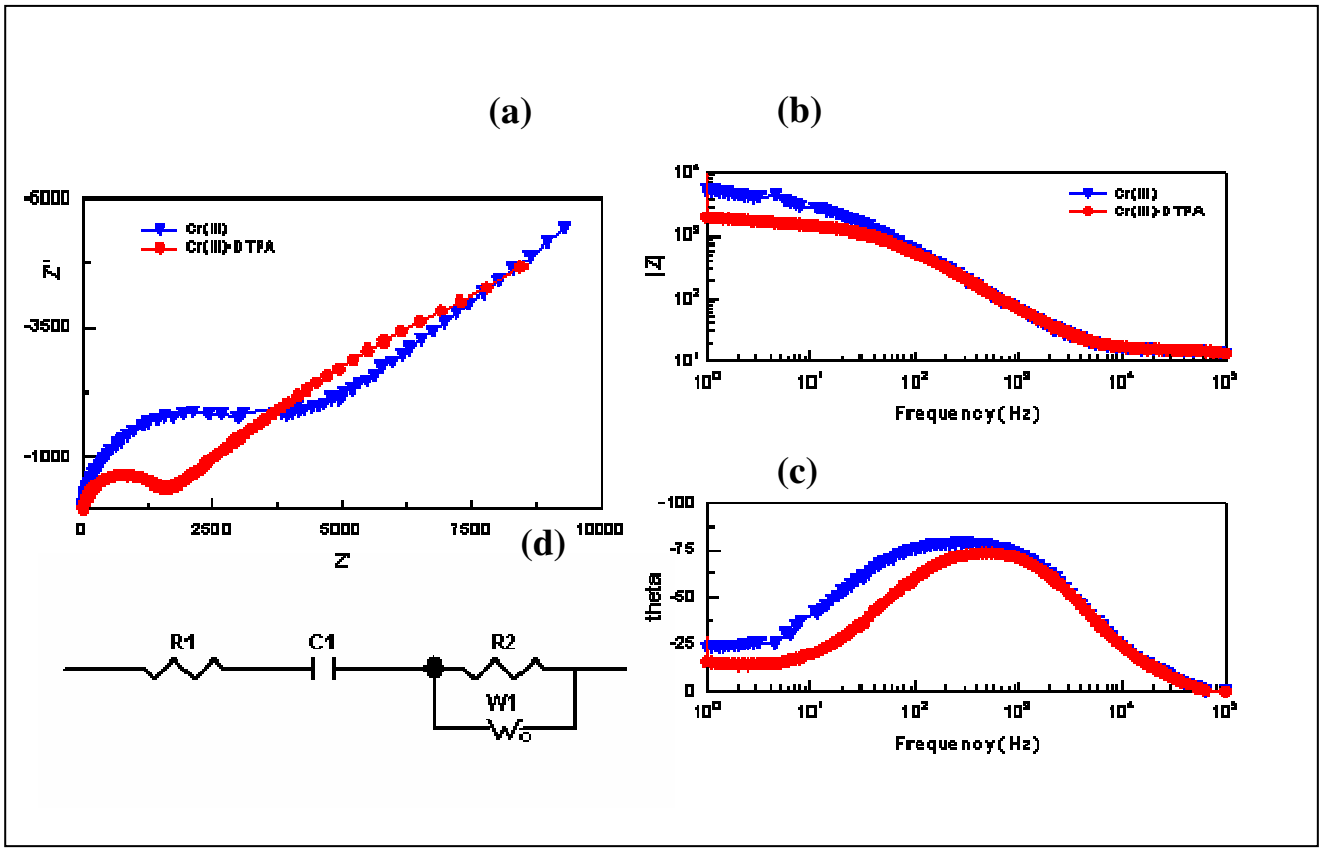

Figure 7.4: Results of 0.1M Cr(II)/(III) solution in 1M H_2SO_4 couple with and without 0.03M DTPA, (a) Nyquist impedance plot for, (b-c) Bode plots, and (d) An equivalent circuit model diagram used for fitting the experimental impedance data.

The Nyquist plots of the Cr(II)/(III) couple and Cr(II)-DTPA complex are shown in ***Figure 7.4(a)***. The measured frequency between 10^{-1} and 10^{5} Hz where the Cr(II)-DTPA displays a single semicircle in the high frequency region, and a straight line with a slope of about 45º in the low frequency region. The electrochemical process is controlled by an electrochemical reaction and diffusion step. For the Cr(II)/(III) couple, a semicircle that is open with a straight line was observed from high frequency to lower frequency. At the higher frequency region the impedance is dominated by the electrolytes resistance and at low frequency the surface of electrode resistance dominates as shown in ***Figure 7.4(b and c).*** The low charge-transfer resistance confirmed the existence of a fast Faradic reaction on the surface of the Pt–electrode. At lower frequencies, the straight line had a finite slope near 1, which represents the diffusive resistance of electrolyte at the electrode surface. Further detailed interpretation of the EIS measurements was performed by fitting the experimental plots using the equivalent circuit depicted in ***Figure 7.4(d)***. Where R1 is the electrolyte resistance, C1 is charge-transfer resistance, for the constant phase element of the interface between the electrode and the electrolyte, R2 is the charge transfer resistance, and W1 is the Warburg diffusion element for the resistance of the diffusion step.

7.3.5 Cyclic voltammetry

Cyclic voltammetry of the Mn(II)/(III) couple was carried out in the presence and absence of DTPA, as illustrated in ***Figure 7.5(a-b)***. The voltammogram show one electronic process that takes place at the redox reaction of the Mn(II)/(III) couple between the electrode surface and the electrolyte.

7.3.5.1 Manganese (Mn(11)/(111)) couple

The electrochemical properties of the Mn(II)/(III) couple and Manganese in the presence of DTPA (Mn–DTPA complex) were examined by cyclic voltammogram as illustrated in ***Figure 7.5(a-b)***. In this figure, an oxidation peak of Mn^{2+} to Mn^{3+} was observed at around –420 mV and the reduction peak at around –560 mV. The anodic / cathodic potential difference (ΔEp) = Epa – Epc gives the formal polaropraphic half wave potential of the Mn(II)/(III) couple, it was approximately ~ 143 mV, which is larger than 59 mV for reversible one–electron Nerstian transfer. These waves are best described as a quasi-reversible electrochemical reaction.

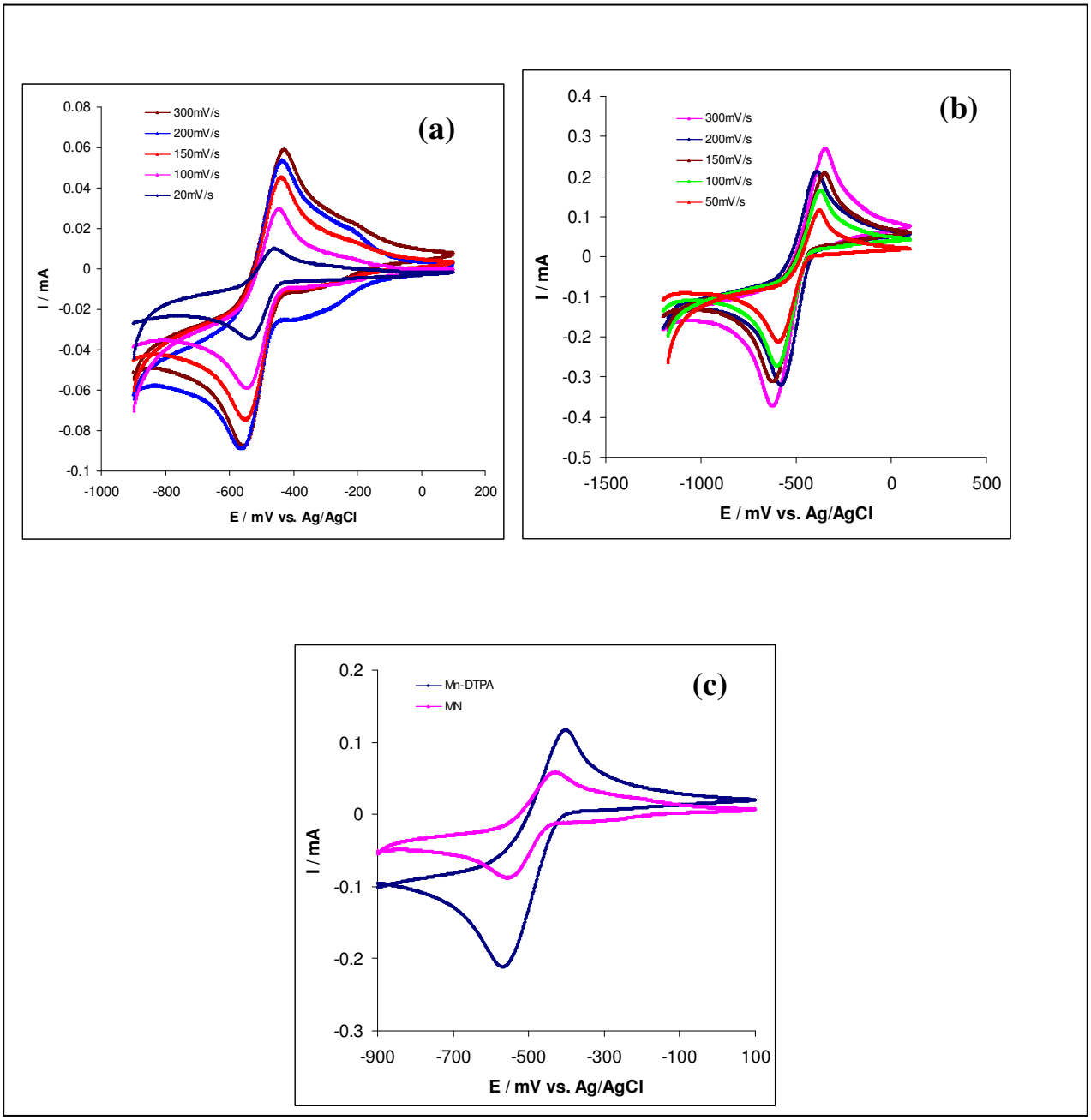

Figure 7.5: Cyclic voltammograms for 0.1M Mn(II)/(III) solution in 1M H_2SO_4 at the scan rate of 20–300mV/s (a) without DTPA, (b) with 0.03M DTPA, (c) Mn-DTPA and Mn(II)/(III) couple recorded at the scan rate of 100mV/s on platinum electrode.

A cyclic voltammogram of manganese in the presence of DTPA (Mn–DTPA complex) is depicted in ***Figure 7.5***. In the presence of DTPA, peak potentials showed a positive shift; the oxidation peak was observed around –390 mV and the cathodic peak around –570 mV. There was a minimum change in peak potential difference (ΔEp = Epc – Epa) of the Mn(II)/Mn(III)

couple. The diffusion coefficient (*D*) and the rate constant (*k*) for the Mn(II)/(III) couple and Mn(III)–DTPA are shown in ***Table 7.1***.

A closer inspection of the Mn(II)–DTPA complex here was similar to the Mn(II)–DTPA complex reported earlier [8] both showed good reversibility of the redox reaction, one electron transfer with mass transfer, and were controlled by a diffusion limited reaction and fast electron transfer. The anodic and cathodic peak currents of the Mn–DTPA complex are higher than the corresponding currents for the Mn(II)/(III) couple, indicating a faster electron transfer at the platinum working electrode than in case of the previous reaction of Mn(II)/(III) couple.

7.3.6 Electrochemical impedance spectroscopy

7.3.6.1 Manganese (Mn(11)/(111)) couple

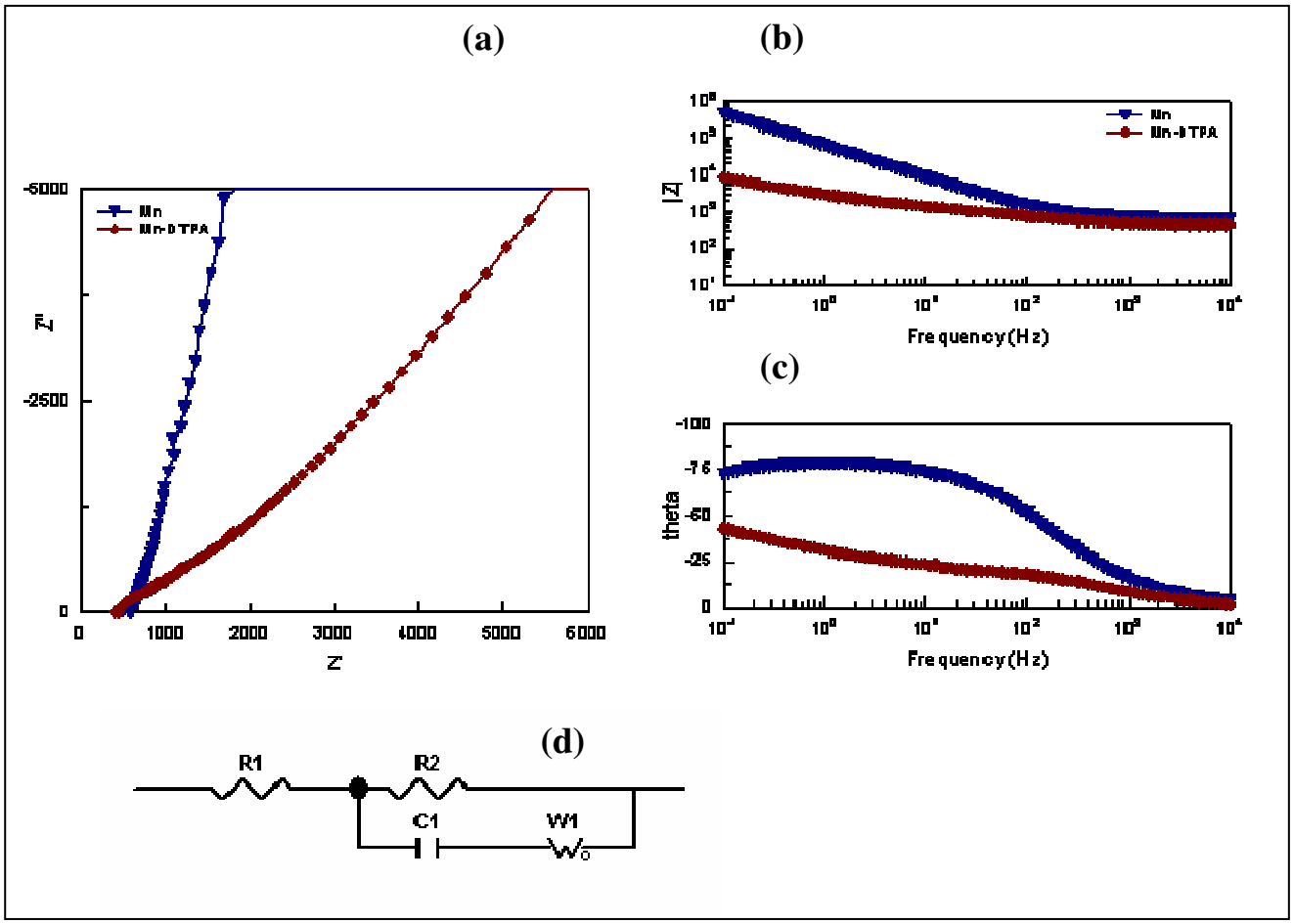

Figure 7.6: Results of 0.1M Mn(II)/(III) solution in 1M H_2SO_4 couple with and without 0.03M DTPA, (a) Nyquist impedance plot for, (b-c) Bode plots, and (d) Equivalent circuit model used for fitting the impedance data.

The Nyquist plot for the Mn(II)/(III) couple and Mn(III)–DTPA complex electrode are shown in ***Figure 7.6(a)***, where the Mn(II)/(III) couple exhibits a straight line with a slope of more than 45° from the higher to a lower frequency region. The Mn(III)–DTPA complex contains a capacitive loop in the higher frequency and a straight line with a slope of 45° at a lower frequency region. This means that the Warburg impedance phase angle of 45° is under diffusion control at the lower and higher frequency, that is observed from ***Figure 7.6(b-c)***. The R1, R2, C1 and W explanations have been stated early (in ***this Chapter Section 7.3.4***)

The Mn(II)/(III) couple from the higher to lower frequency region, with the appearance of the Warburg impedance phase angle of slightly more than 45°, indicates that the Mn(II)/(III) couple system was also under diffusion control similar to the Mn(III)–DTPA complex . The above mentioned two impedance spectra fitted well by the equivalent circuit in ***Figure 7.6(d)***. R1 is the solution resistance between the working electrode and the reference electrode.

7.3.7 Cyclic voltammetry

7.3.7.1 Vanadium (V(1V)/V(V)) couple

The results of electrochemical behaviour for the V(IV) species at a platinum electrode in 1M H_2SO_4 solution, are included in ***Table 7.1***. The anodic peak around –460 mV corresponds to the oxidation of V (IV) to V (V) and the cathodic peak occurs around –590mV corresponding to the reduction of V (V) to V (IV). There was another cathodic peak at about 180mV that could be associated with another reduction of V(IV) to V(III) observed in ***Figure 7.7(a)***. The peak potentials for the oxidation of V(IV) remains almost unchanged with increasing scan rate, although the reduction of V(V) changed with scan rate, indicating that the transformation reaction between V(IV) and V(V) is relatively irreversible.

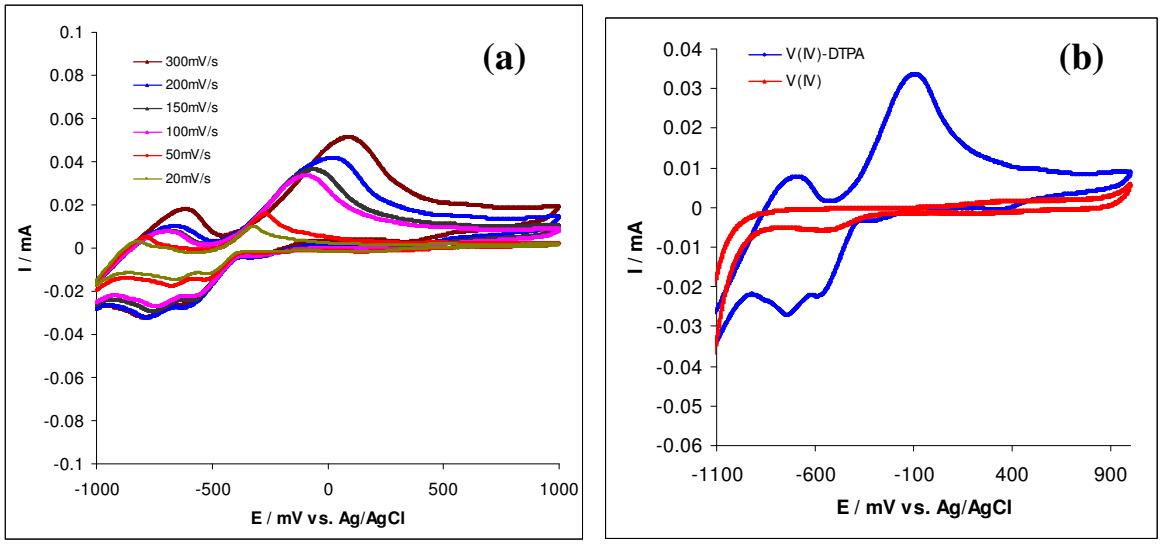

Figure 7.7: Cyclic voltammograms of 0.1M V(IV)/(V) solution in 1M H_2SO_4 at the scan rate of 20–300 mV/s (a) with 0.03 M DTPA (b) with and without DTPA, at the scan rate of 100 mV/s on Pt–electrode.

The cyclic voltammograms of vanadium in the presence of DTPA ligand, the results reveals two irreversible anodic processes, the first at around –670mV and the second at around -100mV versus Ag/AgCl. A comparison of the complex vanadium and uncomplex vanadium are shown in ***Figure 7.7(b)***. The complexed vanadium experiences two separate reduction and two oxidation reactions, all having features of chemical irreversibility in the cyclic voltammetric time scale. Diffusion coefficient and rate constant, for the V(IV)/V(V) and V(IV)–DTPA / V(V)–DTPA couples are shown in ***Table 7.1***. The V(IV)–DTPA / V(V)–DTPA complex become progressively more complex, and revealed that there is a formation of a new bond. The absorbed complex couple changes the peak–to–peak separation structure, to a state were the significant electron transfer become irreversible, therefore, this fact suggests that the electrochemical behaviour process is affected by the addition of DTPA ligand. No detailed studies have yet been carried out on the fundamental mechanism of the electrochemical behaviour of vanadium complexes with DTPA. These redox transformation could correspond to the sequence V(I)–DTPA / V(II)-DTPA / V(III)–DTPA / V(IV)–DTPA / V(V)–DTPA [23]. As far as the reduction processes are concerned, it is also likely that metal vanadium is positioned in the central point of the amino carboxylic ligands.

7.3.8 Electrochemical impedance spectroscopy

7.3.8.1 Vanadium (V(1V)/V(V)) couple

The electrochemical impedance of the V(IV)/(V) couple and the V(IV)–DTPA complex was investigated using EIS and ***Figure 7.8(a)*** shows the Nyquist plot of V(IV)/(V) couple and V(IV)–DTPA complex. A long straight line with a slope of more than 45° from higher to lower frequency region was observed for the V(IV)/(V) couple. This is the indication of an electrochemical process that is controlled by an electrochemical reaction and a diffusion step. However, for the V(IV)–DTPA complex, an incomplete semicircle was observed from a higher to lower frequency region. ***Figure 7.8(b)*** Bode-magnitude plot and ***Figure 7(c)*** Bode-phase plot obtained from the equivalent electrical circuit model in ***Figure 7.8(d)***, where R1, R2 and C1 are fitted in the circuit, and the was no Warburg diffusion in the circuit, that is an indication of a simple Randles equivalent circuit.

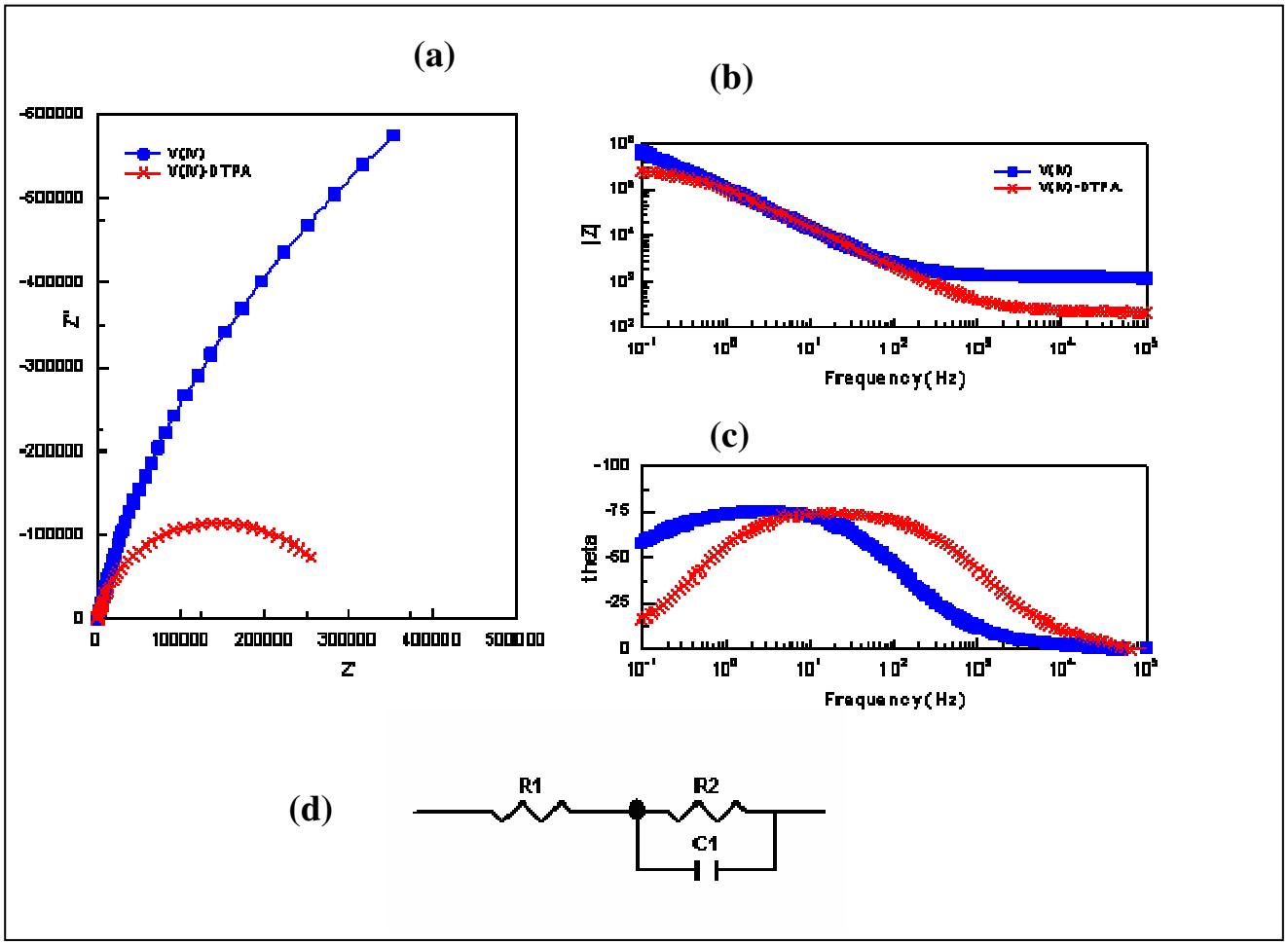

Figure 7.8: Results of 0.1M V(IV)/(V) solution in 1M H_2SO_4 couple with and without 0.03M DTPA, (a) Nyquist impedance plot (b-c) Bode plots, and (d) Proposed equivalent circuit model used for fitting the EIS experimental data.

The impedance results were fitted to a simple equivalent circuit consisting of a parallel combination C1, and R1, in series with R2, representing the ohmic drop in the electrolyte. ***Figure 7.8(d)*** shows all the fittings. The values of the V(IV)–DTPA are shown in ***Table 7.2***. The R1 and C1 values for V(IV)–DTPA are lower than in the case of uncomplexed V(IV) species.

7.3.9 Cyclic voltammetry

7.3.9.1 Effect of DTPA in the electrochemical behaviour of the metals

A comparison of the cyclic voltammograms of Mn, Cr, Fe, V, and Ce in the presence of DTPA ligand is illustrated in ***Figure 7.9***. the curves for Mn–DTPA, Fe–DTPA and Ce–DTPA have a better cyclic shape, which means that their electrochemical reversibility is much better than that of Cr–DTPA, and V–DTPA. All complexes with full cyclic shape voltammograms, illustrate a quasi-reversible electrochemical performance with a one electron transfer (1 e^-) reaction electrode process.

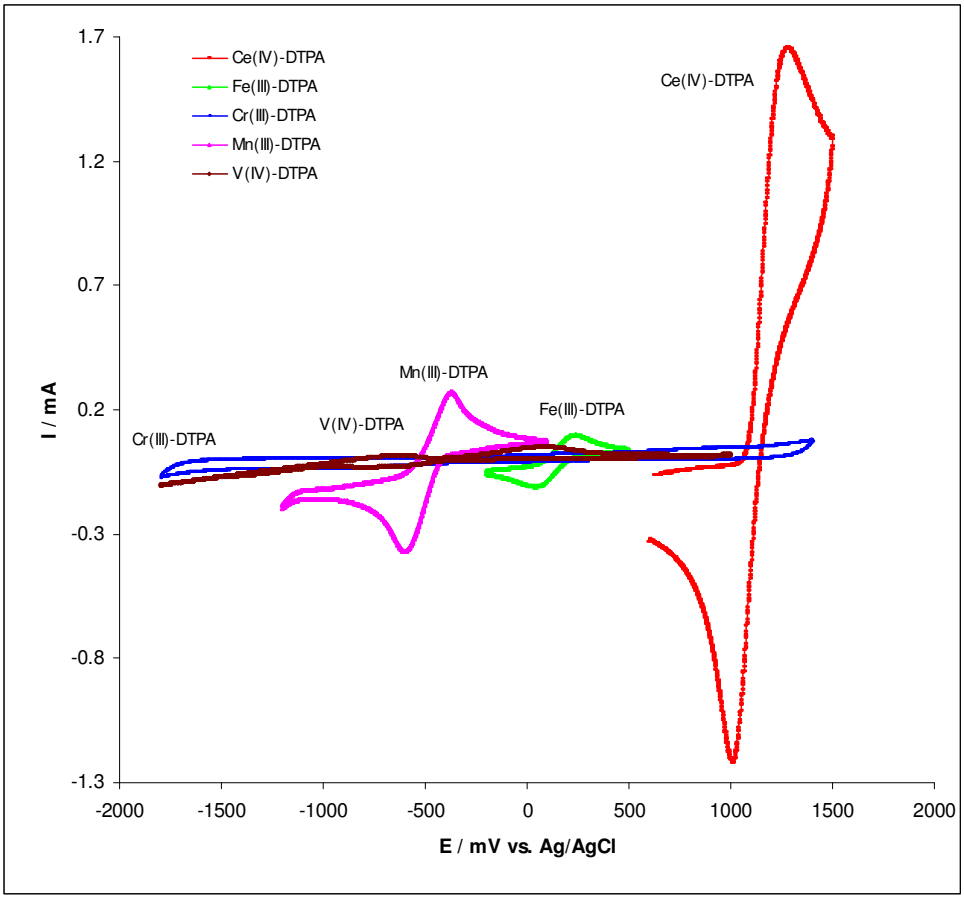

Figure 7.9: Cyclic voltammograms for the Mn–DTPA, Fe–DTPA, Cr–DTPA, V–DTPA, and Ce–DTPA recorded at a scan rate of 100mV.

A summary of the electrochemical parameters and kinetics are depicted in ***Table 7.1***. The peak ratios of the anodic and the cathodic peak for all electrolytes are greater than 1, indicating the favourable electrochemical reversibility, the most suitable electrolytes that are around 1. The peak potentials decrease from Ce–DTPA > Mn–DTPA > Fe–DTPA > V–DTPA > Cr–DTPA. The current trend is as follows; Ce–DTPA > Fe–DTPA >Mn–DTPA > V–DTPA > Cr–DTPA. Zanello [23] stated that transition metal complexes are stable in different oxidation states. The cerium specie acts as an oxidizing agent to remove electrons from another species, a trend, and affinity to add electrons measured by the standard reduction / oxidation potentials. Therefore the redox agent is based on the standard potential of the redox process of Ce-DTPA, therefore Ce-DTPA is be considered as the most appropriate of the stable metal complexes used in this study. This implies that a ligand like DTPA will be more exposed to attack by an oxidizing agent like Ce(IV) in sulphuric acid than other metal species mentioned used in this study (Fe, Mn, Cr and V).

7.3.10 Electrochemical impedance spectroscopy

7.3.10.1 Effect of DTPA on the electrochemical behaviour of the metals

The electrochemical impedances of Mn–DTPA, Cr–DTPA, Fe–DTPA, V–DTPA and Ce–DTPA are shown in ***Figure 7.10(a)***. Semicircles at the higher frequency and a straight line with a slope of about 45º in the lower frequency region were observed for Ce–DTPA and Fe–DTPA. This is an indication of an electrochemical process that is controlled by electrochemical reaction and a diffusion step.

Table 7.2:Electrical parameters from circle fitting for various electrolytes in Figure 5(d-g)

Electrolyte	R1(Ω)	Errors %	R2 (Ω)	Errors %	C1 (F/cm2)	Errors %	W1 (Ω)	Errors %
Ce(IV)	1.924	0.526	2.145	0.38	$3.7x10^{-6}$	2.98	679.27	5.36
Ce-DTPA	1.173	0.26	1.687	0.62	$2.5x10^{-6}$	3.61	705.51	3.22
Mn(III)	20.12	0.35	21.31	0.35	$2.1x10^{-4}$	6.28	389.24	9.52
Mn-DTPA	18.32	0.72	13.02	0.24	$2.7x10^{-5}$	5.14	414.00	6.13
Cr(II)	12.30	1.25	14.18	0.82	$3.6x10^{-2}$	1.23	211.88	8.58
Cr-DTPA	10.98	0.92	12.52	0.52	$5.1x10^{-3}$	3.87	225.15	11.02
Fe(III)	18.35	0.88	14.72	1.26	$3.8x10^{-5}$	5.12	128.78	8.13
Fe-DTPA	16.535	0.29	10.74	2.37	$1.6x10^{-6}$	7.26	145.52	5.36
V(IV)	14.84	0.58	13.76	0.58	$1.6x10^{-1}$	9.58	117.06	6.52
V-DTPA	11.925	0.62	14.25	1.98	$7.2x10^{-2}$	5.21	129.00	9.23

In the case of Cr–DTPA, an incomplete semicircle was observed from a higher to lower frequency region. A straight line with a slope of about 90º was observed in the case of the Mn–DTPA and V–DTPA from a higher to lower frequency region. Further detailed interpretation of the EIS measurements was performed by fitting the experimental plots using the equivalent circuit depicted in ***Figure 7.10(d-g)*** from experimental data obtained from ***Figure 7.10(a)***. Values of equivalent circuit parameters such as R1, R2, C1 and W1 were all calculated from the impedance data during the charge process, as summarized in ***Table 7.2***.

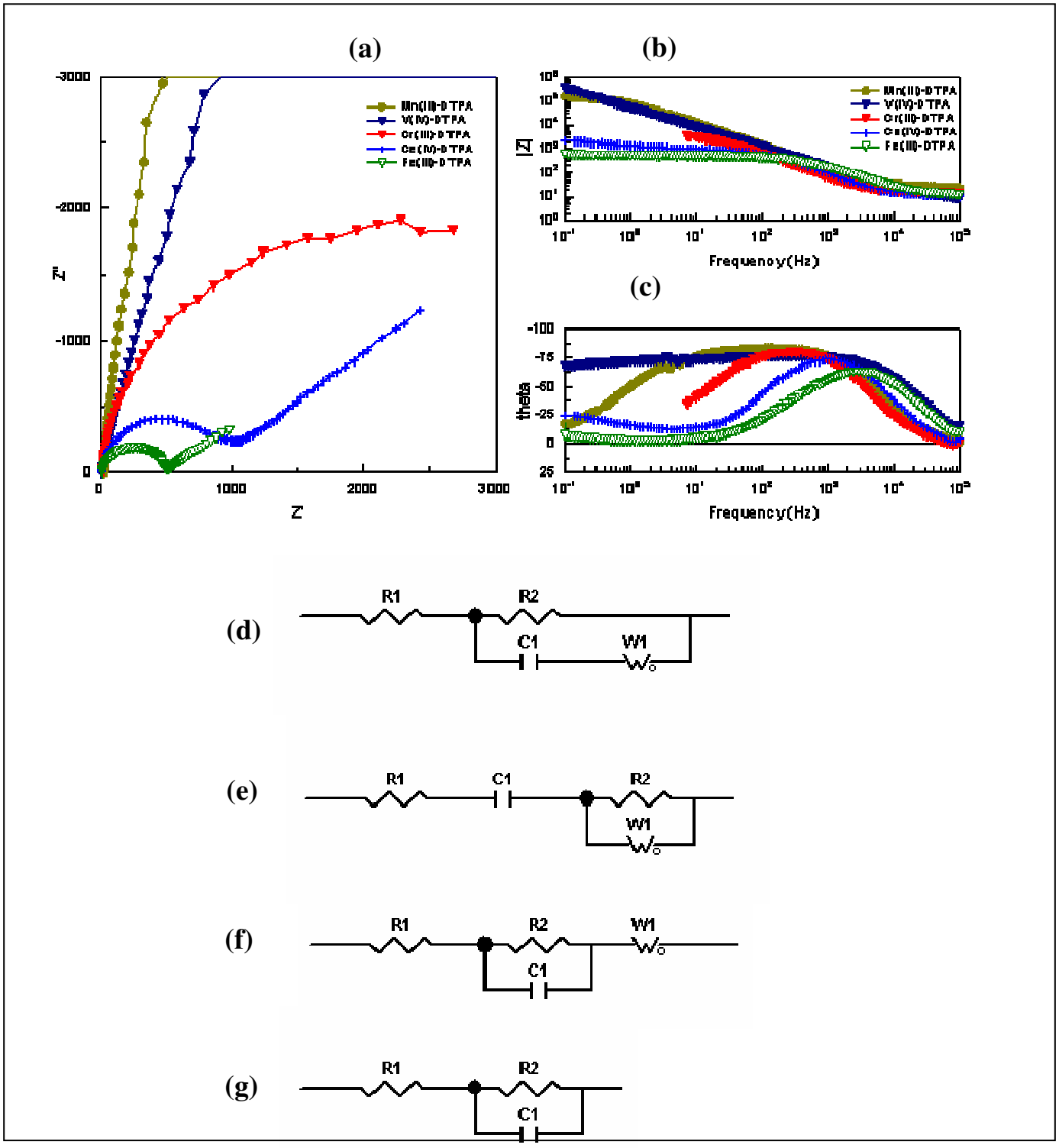

Figure 7.10: Results of Mn–DTPA, Fe–DTPA, Cr–DTPA, V–DTPA and Ce–DTPA, (b) and (c) Bode plots, (d-g) Equivalent circuit model diagrams used for fitting the impedance data (d) Ce–DTPA and Fe–DTPA, (e) Mn–DTPA, (f) Cr–DTPA, (g)V–DTPA.

The equivalent circuit for Ce(IV)–DTPA fitted best in ***Figure 7.10(d)***. Mn–DTPA and Fe-DTPA fitted both fine in ***Figure 7.10(e)***. Cr–DTPA fitted in ***Figure 7.10(f)***, and V-DTPA fitted in ***Figure 7.10(g)***. Ce(IV)–DTPA has the lowest electrolyte resistance (R1) and charge transfer resistance (R2) values as compared to the other complexes, similarly its C1 and W1 values are also low. Xue et al. [29] pointed that, when the resistance is low the potential will be high. The conductivity of the electrolyte will not be suitable for the V–DTPA system, given that the Ce(IV)–DTPA resistance is low, that means the potential will be higher than other complexes used in this study. It is clear that when the DTPA ligand is present in cerium species, the electrolyte resistance increases and hence the corrosion inhibition effect is pronounced. In addition, the capacitance decrease is due to the absorption that is taking place during the process at the electrolyte/electrode surface area. Therefore in Ce(IV)–DTPA the resistance is low, meaning that the potential will be higher than other complexes used in this study.

7.4 Conclusion

Due to better electrochemical reversibility, lower resistance, higher potential, fast kinetics reaction, diffusion control, and mass transfer. The Ce–DTPA complex is the most favoured electrolyte for redox flow batteries when compared to Cr–DTPA, Fe–DTPA, Mn–DTPA and V–DTPA complexes. CV and EIS results showed that the Ce–DTPA complex has the best electrochemical behaviour and lowest resistance, respectively, compared to the other metal–DTPA complexes used in this study. Hence the Ce–DTPA complex remains the most preferable electrolyte in terms of performance and as a possible candidate for RFB applications when compared to the other metal–DTPA complexes used in this study.

7.5 References:

[1] Modiba P, Crouch A.M, J. Appl. Electrochem 38 (2008)1293.

[2] Modiba P, Crouch A.M, Proceedings of the 43rd Power Source Conference (2008) 71.

[3] Fang B, Iwasa S, Wei Y, Electrochim. Acta 47 (2002) 3971.

[4] Skyllas-Kazacos M, Grossmith F, J. Electrochem. Soc. 34 (1987) 2950.

[5] Wei Y, Fang B, J.Appl. Electrochem. 35 (2005) 561.

[6] Chen Y. W. D, Santhanam K. S. V, Bard A. J, J. Electrochem. Soc. 128 (1981) 1460.

[7] Hasegawa K, Kimura A, Yamamura T, Shiokawa Y, J. Phys. Chem. Solids 66 (2005) 593.

[8] Selim R.G, Lingane J. J, Coulometry 21(1959) 536.

[9] Skyllas-Kazacos M, Rychick M, Robins R, All-vanadium redox battery, US Patent 4,786,567 (1988).

[10] Sum E, Skyllas-Kazacos M, J. Power Sources 15 (1985) 179.

[11] Sum E, Rychcik M, Skyllas-Kazacos M, J. Power Sources 16 (1985) 85.

[12] Chakrabarti M.H, Dryfe R.A.W, Roberts E.P.L, Electrochim. Acta 52 (2007) 2189-2195.

[13] Kazacos M, Skyllas-Kazacos M, J. Electrochem. Soc. 136 (1989) 2759.

[14] Doria J, De Andres M.C, Armenta C, Proc. 9th Solar Energy Soc. 3 (1985) 1500.

[15] Bae C.H, Roberts E.P.L, Dryfe R.A.W, Electrochim. Acta 48 (2002) 279.

[16] Abbaspour A, Mehrgardi M. A, Talanta 67 (2005) 579.

[17] Glentworth P, Wiseall B, Wright C.L, Mahmood A.J, J. Inorg. Nucl. Chem. 30 (1968) 967.

[18] Modiba P, Matoetoe M, Crouch A.M, Submited to Electrochim. Acta (2009).

[19] Kiekens P, Steen L, Donche H, Temmerman E, Electrochim. Acta 26 (1981) 841.

[20] Rao A G.N, Indian J. Chemistry 8 (1970) 328.

[21] Pletcher D, White J. C. P, Electrochim. Acta 37 (1992) 575.

[22] Bard J, Faulkner L.R., Electrochemical Methods Fundamentals and Applications 2nd ed., John Wiley & Sons, New York (2001).

[23] Zanello P, Inorganic Electrochemistry Theory, Practice and Application, The Royal Society of Chemistry, Cambridge (2003).

[24] De Strycker J, Westbroek P, Temmerman E, J. Electroanal. Chem. 565 (2004) 149.

[25] Zhang X, Yung H, Bard A.J, J Am. Chem. Soc. 109(1987) 1917.

[26] Anderson A, N. Bonner A, J Am. Chem. Soc. 76(1954) 3826.

[27] Hupp J.T, Weaver M.J, J. Phys. Chem. 88 (1984) 6128.

[28] Meier R, Werner G, Otto M, Electrochim. Acta 236 (1990) 315.

[29] Xue F-Q, Wang Y-L, Wang W-H, Wang X-D, Electrochim. Acta 53 (2008) 6636.

Chapter 8

Charge/Discharge Characteristics of Cerium (IV) and its Complexes with Ethylenediaminetetraacetic Acid (EDTA) and Diethylenetriaminepentaacetate (DTPA) Ligands as Potential Electrolytes for Redox Flow Batteries. [*]

Summary

The results of kinetic studies of the Ce(IV)–DTPA complex shows promise as an electrolyte for redox flow batteries. Charge/discharge characteristics and species formed during the charge-discharge cycle are reported.

8.1 Introduction

In all the new battery technologies that are currently under development[1–3], RFB systems vary in the manner in which they store energy electrochemically, by a mechanism that uses the oxidation and reduction of one or two soluble redox couples for both charging and discharging. Energy compartment chemicals used in redox flow batteries are stored in separate liquid tanks, and the liquid pumped to the cell in which the electrolyte is separated by an ion-conductive separator for both charging and discharging. The power of the system is determined by the size of the battery cells, whereas the energy storage capacity is determined by the concentration and volume of the electrolyte. RFB's offer the following advantages: as large-scale energy storage system for a wide range of applications, long life, reliability, simplicity, environmentally friendly, low maintenance and high-efficiency [1-9].

A cerium couple is the most uncomplicated electrolyte for redox batteries; it provides a relatively inexpensive and reliable power source. In order to improve the ratio of power to weight, these ligands can be complexed with EDTA, EDDS or DTPA to gain an improved power level. In this work, the charge/discharge performance in a small laboratory scale, a sandwich type cell was tested to determine the performance of the Ce–DTPA and the Ce–EDTA systems.

[*] Published as proceedings of the 43rd Power Source Conference, Philadelphia, New York, 7-10 July (2008), Modiba P, Crouch A.M.

8.2 Experimental

8.2.1 Cyclic voltammetry and rotating disc electrode

The procedures used to study the electrochemical kinetic parameters of the Ce(III)/Ce(IV) redox couple, of the Ce(IV)–EDTA and Ce(IV)–DTPA complexes by using CV and RDE with Pt electrodes were the same as described in ***Chapter 4 Section 4.2.***

This work was undertaken in view of the interest in the study of the electrochemical kinetic parameters of the Ce(III)/Ce(IV) redox couple using CV and RDE with different electrodes (C, Au and Pt electrodes).

8.2.2 Charge/discharge

In this study, systems that were found to exhibit fast kinetics were tested for their charge/discharge characteristics in a small specially fabricated sandwich cell. A Nafion 117 membrane was used as a separator. At the beginning of the charge/discharge, test 20ml of a solution of 0.1M $Ce(SO_4)_2$ and 0.03 M DTPA in 1 M H_2SO_4 was pumped into the cathode side. In addition, a 20ml of solution of 0.1M $Ce(SO_4)_2$ with 0.03 M DTPA in 2M H_2SO_4 was pumped into the anode side. Measurements were recorded at a current density of 20 mA cm^{-2}.

.3 Results and discussion

8.3.1 Cyclic voltammetry and rotating disc electrode

Cyclic voltammetry and rotating disc electrochemistry for these systems (Ce(III)/Ce(IV) couple, Ce(IV)–EDTA and Ce(IV)–DTPA complexes are similar to that discussed in ***Chapter 4, Sections 4.3 and 4.4***. Where the redox reaction of Ce(III) to Ce(IV) shows a quasireversible electrochemical behaviour, the Ce(IV)-EDTA illustrate an irreversible behaviour. The Ce(IV)-DTPA complex however show a quasi-reversible behaviour. It was also found that there is a linear relationship between the peak current and the scan rate, indicating a diffusion controlled reaction. The anodic and cathodic peak currents of the Ce(IV)-DTPA complex is higher than the corresponding currents for the Ce(IV)- EDTA

complex and Ce(IV) at the same concentration, indicating a faster electron transfer at the platinum working electrode for the former. This enhanced electron transfer compared to the other complexes is also supported by the electron transfer coefficient (α) for this reaction.

8.3.2 Charge/Discharge performance of the Cerium redox battery system

To investigate the reason why the performance of the best suitable battery electrolyte is good, the EIS was used to determine the resistivity of the Ce(IV), Ce(IV)–EDTA and Ce(IV)–DTPA electrolyte. The charge/discharge battery test was also used to determine the battery performance. The assembled cell was first charged and then discharged at a constant current of 20 mA in various electrolytes of Ce(IV), Ce(IV)–EDTA and Ce(IV)–DTPA, A lower current was used during the discharge process to prevent the cell voltage from dropping rapidly to zero. The Ce(IV), Ce(IV)–EDTA and Ce(IV)–DTPA electrolyte were compared according to the voltage generated by each electrolyte.

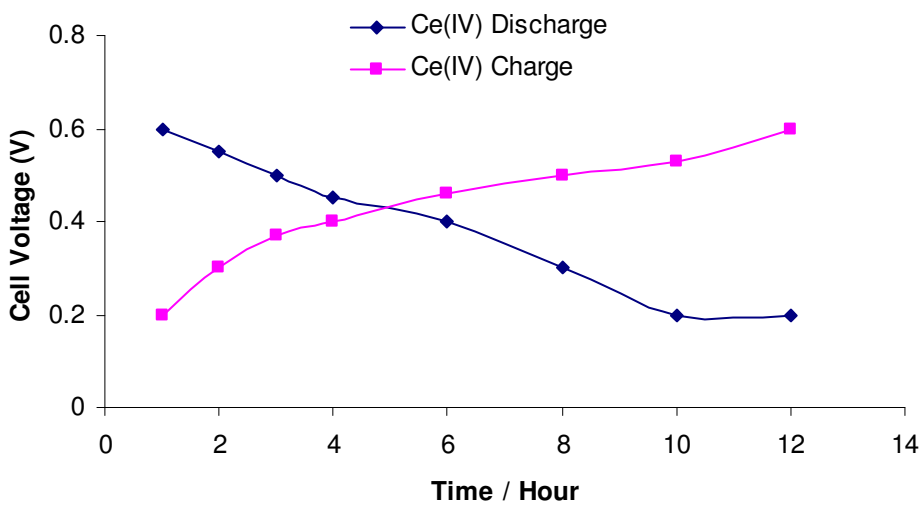

Figure 8.1(a): Charge/Discharge curves of the single cell Ce(IV) as redox couples at a current density of 20 mA cm^{-2}.

The cell potential versus time curve for the charge/discharge curves of the Ce(IV) electrolyte is shown in ***Figure 8.1(a).*** During the charge process of the Ce(IV) electrolyte, the cell voltage increases from 0.2V to 0.6V, and decreases from 0.6V to 0.2V through the discharge process. An energy efficiency of approximately 59%, a voltage efficiency of 45 % and a coulombic efficiency of 81 % were obtained as shown in ***Table 8.1.*** This is a poor

performance when compare with the corresponding complexes of Ce(IV)–DTPA electrolytes but better than the Ce(IV)–EDTA electrolyte.

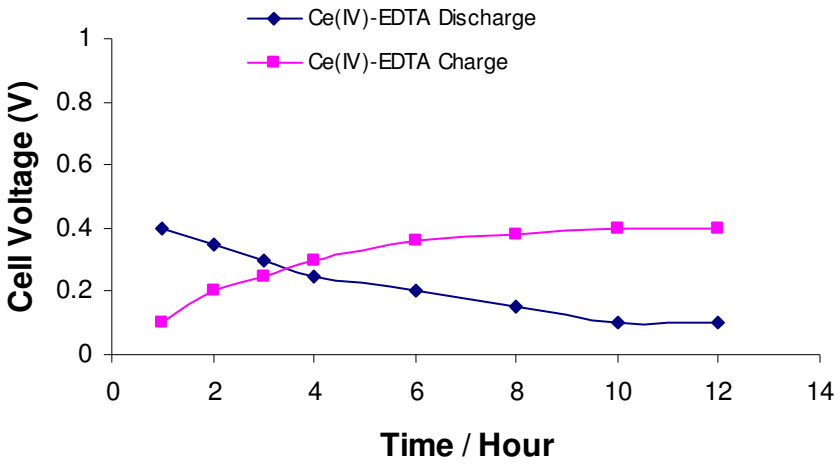

Figure 8.1(b): Charge/Discharge curves of the single cell Ce(IV)–EDTA as redox couples at a current density of 20 mA cm^{-2}.

During the charge/discharge process of the Ce(IV)-EDTA electrolyte in **Figure 8.1(b)**, when the battery cell is charged, the voltage increases from 0.2V to 0.4V, and throughout the discharge process it decreases from 0.4 to 0.2V. The lowest energy efficiency of approximately 36%, the voltage efficiency of 45 % and the advanced coulombic efficiency of 81 % were obtained. This was a very poor performance when compared with the Ce(IV) and Ce(IV)–DTPA electrolytes.

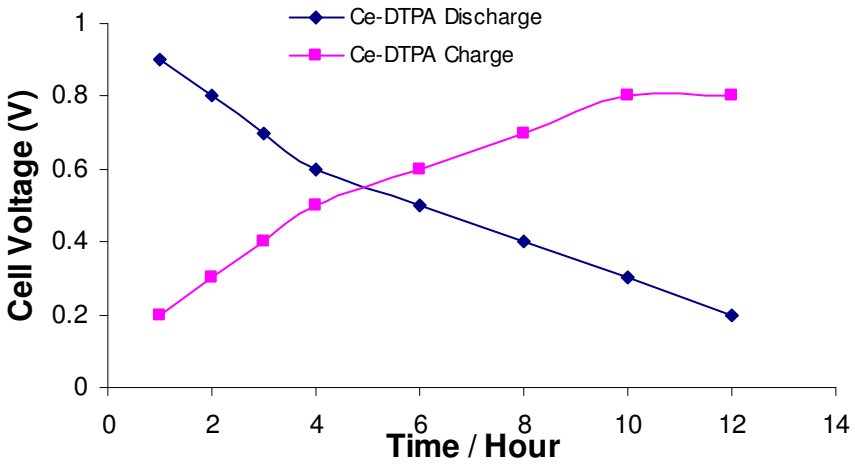

Figure 8.1(c): Charge/Discharge curves of the single cell of Ce(IV)–DTPA and as redox couples at a current density of 20 mA cm^{-2}.

The charge/discharge characteristics of the Ce(IV)–DTPA electrolyte is shown in **Figure 8.1(c)**. At the beginning of the charging process, the maximum voltage achieved is about 1V. Throughout the discharge process, the voltage decreases to 0.2V. The highest energy efficiency of approximately 85% as well as voltage efficiencies of 93%, and coulombic efficiencies of 92 % were obtained. The open circuit voltage after charging was high at 1 V, and the cell voltage remained above 0.2V during the duration of the discharge process. This was a very good performance when compared with Ce(IV) and Ce(IV)–EDTA electrolytes.

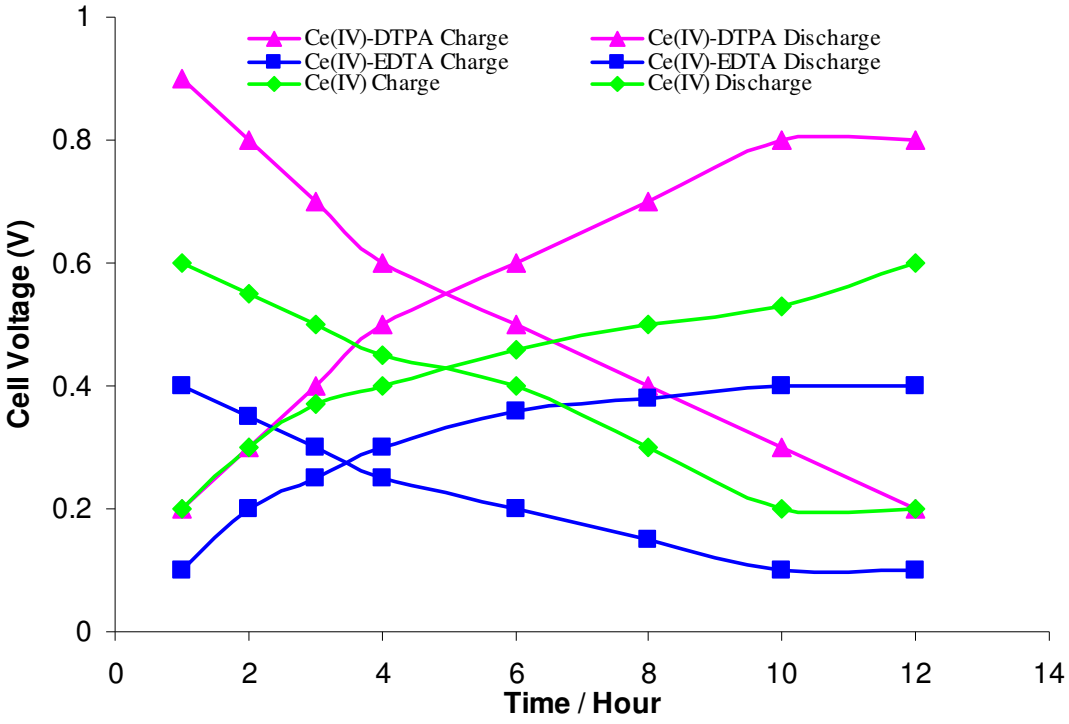

Figure 8.1(d): Charge/Discharge curves of the single cell with Ce(IV)–DTPA, Ce(IV)–EDTA and Ce(IV) as redox couples at a current density of 20 mA cm^{-2}.

Results of the cell voltage versus time for the charge/discharge cycles using various electrolytes Ce(IV), Ce(IV)–EDTA and Ce(IV)–DTPA are shown in **Figure 8.1(d).** The Ce(IV)–DTPA achieved the highest charge voltage (0.9 V) compared to Ce(IV) (0.6 V) and Ce(IV)–EDTA (0.4 V).The percentage efficiencies of the various electrolytes that were used were compared with that of the vanadium redox couple, which was previously reported [3]. From ***Table 8.1*** it is evident that the percentage energy efficiency for Ce(IV)-DTPA is the highest of all other electrolytes used. The Ce(IV)–DTPA system is comparable to the

acceptable vanadium redox couple [7] with the energy efficiency of 89% currently used in practical RFB systems, without the disadvantages associated with multiple high oxidation state species.

Table 8.1: Efficiencies of the redox flow battery electrolytes

Efficiencies (%)	**Vanadium [7]**	**Ce(IV)**	**Ce(IV)–EDTA**	**Ce(IV)–DTPA**
Coulombic	89 [a]	95	81	92
Voltage	91	63	45	93
Energy	81	59	36	85

[a] Current density of 40 mA/cm^2

8.4 Conclusion

The Ce(IV)–DTPA electrolytes had a higher open voltage circuit potential after charging compared to Ce(IV) and Ce(IV)–EDTA. A higher percentage of voltage efficiency and energy efficiency was obtained and found to be more favourable than the Ce(IV), Ce(IV)–EDTA and vanadium systems. A single cell charge/discharge cycle test with the Ce(IV)–DTPA redox couple demonstrates the promise for possible application in redox flow battery systems. This was a confirmation of the EIS results ***in Chapter 7 Section 7.3.10.*** Therefore Ce(IV)–DTPA was proven as a very good substitute as an electrolyte when compared with Ce(IV) and Ce(IV)–EDTA electrolytes and similar or slightly higher than those previous observed [7, 10].

8.5 References:

[1] Fang B, Iwasa S, Wei Y, Arai T, Kumagai M, Electrochim. Acta 47 (2002) 3971.

[2] Sum E, Skyllas-Kazacos M, J. Power Sources 15(1985) 179.

[3] Modiba P, Crouch A.M, J. Appl. Electrochem 38 (2008) 1293.

[4] Thaller LH. (1979) In: NASA TM-79143, National Aeronautics and Space Administration US Department of Energy.

[5] Abbaspour A, Mehrgardi MA Talanta 67 (2005) 579.

[6] Sum E, Skyllas-Kazacos M J. Power Sources 15 (1985) 179.

[7] Peng Q, Zhang H, Chen J, Wen Y, Luo Q, Liu Dongjiang Y, Yiu B, J. Power Sources 175 (2008) 613.

[8] Skyllas-Kazacos M, Grossmith F, J. Electrochem Soc 34 (1987) 2950

[9] Liu Y, Xia X, Liu H, J. Power Sources 130 (2004) 299.

[10] Ponce de Leon C, Frias-Ferrer A, Gonzalea-Garcia J, Szanto D.A, Walsh F.C, J. Power Sources 160 (2006) 716.

Chapter 9

Overall Conclusions, Recommendations, and Outputs

9.1 Conclusions

The electrochemical behaviour of vanadium, chromium, cerium, iron and manganese with various aminocarboxylates, (EDDS, NTA, EDTA, and DTPA) were investigated using CV and RDE. Suitable electrolytes for RFB systems were determined by studying the kinetics and thermodynamics of the electrolyte used in RFBs. Voltammograms of CV and RDE were used to determine the electrochemical behaviour of Ce(III)/(IV) couple using various electrodes, glassy carbon, gold and platinum electrodes. However, complex behavior was obtained at different electrodes, each electrode giving a slight different in CV and RDE voltammograms, while the platinium electrode was shown to be prefarable electrode with the best surface to study the complexes.

The results of this study, carried out to determine the most suitable electrolyte from various metals used with various ligands, have shown that the Ce-DTPA complex is the most suitable electrolyte to be used for RFB applications.

- Pt electrode the best surface to study the complexes.
- The first electrochemical study of Ce with aminocarboxylates using RDE and impedance etc.
- A comprehensive comparison of high oxidation state metal ions with aminocarboxylates using electrochemical techniques.
- An evaluation of the performance of the electrolytes as possible couples fo RFB applications.
- Kinetic and thermodynamic parameters for all the redox couples studied. Important for determining electron transfer rates and reversibility of redox couples.
- EIS Results also confirm fast kinetics and electron transfer. The first study of its kind.
- Ce(IV) DTPA found to be an electrolyte which fulfills many of the challenges associated with RFB, such as solubility, etc….. A relatively large open circuit potential = ~ 1.3 V. Reasonable cost = Ce(IV)–DTPA inexpensive. DTPA was a good complexing agent.

The most important purpose and aims of this project are discussed in ***Chapter one.*** This body of work has identified several important factors that affect the electrochemical performance of RFB systems, which are mentioned in ***Chapter two***. All the analytical techniques used in this study are briefly described in **C*hapter three.*** In **C*hapter four,*** three different electrodes (carbon, platinium and gold) were compared to determine the best electrode that can be suitable to study the cerium couple for a RFB system. And we observed that carbon and platinum were favoured when in use with the Ce(III)/(IV) couple. In the next chapter, **C*hapter five***, we evaluated cerium with two different ligands (EDTA and DTPA) for their electrochemical behaviour for RFB application using CV and RDE. The electrochemical kinetic parameters such as potential, limiting current, transfer coefficient, diffusion coefficients, and rate constants were detected from CV and RDE. The Ce(IV)–DTPA complex species have a higher electron transfer rate constant than other complex species used , indicating that the rate of electron transfer was fast. Therefore the results that were observed verify that DTPA was a suitable ligand when it complexes with cerium because of the quasi-reversible electrochemical behaviour, one electron transfer, mass transfer and fast electron transfer. The results from RDE confirmed that the parameters of measurement in CV are approved and can be used to determine the kinetic parameters of the redox couples.

In Chapter six the electrochemical impedance study of Ce (IV) with aminopolycarboxylate ligands (DTPA, EDTA, EDDS and NTA), were presented in CV. EIS verified that Ce(IV)-DTPA will be a suitable RFB electrolyte when compared to Ce(IV), Ce(IV)-EDTA, Ce(IV)-EDDS and Ce(IV)-NTA due to better electrochemical reversibility, lower resistance , higher potential, kinetics, diffusion control and mass transfer. In **C*hapter seven*** the electrochemical properties of metals (Cr, Fe, Mn, and V) using CV and EIS were evaluated for RFB applications. The Ce-DTPA still proved to be the most preferred and suitable electrolyte as compared to Mn-DTPA, Cr-DTPA, Fe-DTPA and V-DTPA, due to its better electrochemical reversibility, lower resistance and higher potential.

C*hapter eight* the charge/discharge characteristics and species formed for Ce(IV), Ce(IV)-EDTA and Ce-DTPA during the charge-discharge cycle performance are evaluated and the observed results where compared to those presently used in redox flow systems, which is the vanadium system. The Ce(IV)-DTPA electrolytes was found to have a higher open voltage circuit potential after charging compared to that of Ce(IV) and Ce(IV)-EDTA. A higher percentage of voltage efficiency and energy efficiency was also obtained and found to be more favourable than that of the Ce(IV), Ce(IV)-EDTA and Vanadium systems. A single cell

charge / discharge cycle test with the Ce(IV)-DTPA redox couple demonstrates the promise for possible application in a redox flow battery system.

Chapter nine is for overall conclusions and recommendations

The capillary electrophoresis was used to investigate the efficient separation of vanadium species in **C*hapter ten*** as addendum**.** The electrophoretic behaviour of vanadium species with four various complexing agents (EDTA, DTPA, EDDS and NTA) were examined. Cerium and other metal species (Mn, Cr & Fe) were also investigated even though their results were not clearly understandable. There are plenty of assumptions that need clarity. Further study on these metals and ligands is recommended using CE.

9.2 Recommendations and future work

In the view of the fact that there are several assumptions concerning CE results that need clarity. Further study on this metals and ligand is recommended.

9.3 Outputs

9.3.1 Papers Published

- Modiba P, Crouch A.M, J. Appl. Electrochem.38 (2008)1293.
- Modiba P, Crouch A.M, Proceedings of the 43rd Power Source Conference Philadelphia, New York, 7-10 July (2008).

9.3.2 Submitted Papers

- Modiba P, Matoetoe M, Crouch A.M, Electrochemical Impedance Study of Ce(IV) with Aminopolycarboxylate Ligands for Redox Flow Batteries Application, resubmitted to Electrochimica Acta (2009)
- Modiba P, Matoetoe M, Crouch A.M, Electrochemical Properties of Metals (Cr, Fe, Mn, and V) for Redox Flow Battery Applications, submitted to Electrochimica Acta (2009).

9.3.3 To be submitted

- Modiba P, Matoetoe M, Crouch A.M, J. Power Source (2010)

9.4 Conference contributions

9.4.1 Oral Presentations

- Modiba P, Crouch A.M, 10th International Symposium on Kinetics in Analytical Chemistry, Cape Town, South Africa. 02 - 04 December 2009.
- Modiba P, Crouch A.M, Proceedings of the 43rd Power Source Conference, Philadelphia, New York, 07 - 10 July 2008.
- Modiba P, Crouch A.M, 39th National Convention of the South African Chemical Institute (SACI), Stellenbosch, South Africa, 30 November - 05 December 2008.
- Modiba P, Crouch A.M, Student Symposium, Potchefsroom, South Africa. 07 December 2005.
- Modiba P, Crouch A.M, Student Symposium, Stellenbosch, South Africa, 06 December 2004.

9.4.2 Poster Presentations

- Modiba P, Crouch A.M, The South African Chemical Institute (SACI) Inorganic Chemistry Conference, Club Mykonos, Western Cape, South Africa, 8-12 July 2007
- Modiba P, Crouch A.M, 38th Convention of the South African Chemical Institute, (SACI) Conference, Durban, South Africa 3-8 December 2006.

Addendum Chapter 10

Study the speciation of Vanadium, Chromium, Iron, Manganese and Cerium using CE

10.1 Introduction

In this chapter, the focus was on understanding the oxidation state of vanadium, since it is a very complicated species, which has five different oxidation states. Capillary electrophoresis (CE) was used to investigate the efficient separation of vanadium species. The electrophoretic behaviour of vanadium species with four various complexing agents (EDTA, DTPA, EDDS and NTA) was examined. Factors that affect the migration behaviour of vanadium species, such as electrolyte pH and concentration, also EDTA, DTPA, EDDS and NTA concentration, applied voltage, and wavelength measurement, were studied in detail to improve the understanding of the five oxidation states of vanadium. Cerium and other metal ions (Mn,Cr & Fe) were also investigated even though their results were not clearly understandable, most of the results can be found in Appendix A, cerium results was expected to appear most favourable electrochemically than other metals, unfortunately the complexes are too labile at the higher pH.

10.2 Experimental details

10.2.1 Instrumentation

Capillary electrophoresis analyses were performed on a HP^{3D} CE Instrument (Agilent Technology, Waldbronn, Germany) system Hewlett Packard (More detailed info ***in Chapter 3 Section 3.5****)*

10.2.2 Materials and reagents

All reagents were of analytical reagent grade unless stated otherwise. Deionised water having resistivity of 18 MΩ.cm (Millipore). Ethylenediaminetetraacetic acid (EDTA), ethylenediamine disuccinate (EDDS), nitrilotriacetic acid (NTA) and diethylenetriamine pentaacetic acid (DTPA) were obtained from (Fluka- Riedel-de Haen) sulphuric acid, sodium

hydroxide (NaOH), hydrochloric acid (HCl), NH_4V0_3, cerium (IV) sulphate [$Ce(SO_4)_2$] vanadium vanadate (V_2SO_5), vanadium vanadyl ($VOSO_4$) were purchased from Sigma–Aldrich (Steinheim, Germany).

10.2.3 Preparation of buffer solution

The EOF mobilities at different pH were measured in the same capillary using six buffer solutions, which were made in the usual fashion: (i) 20 mM acetate buffer pH 4,)(ii) 20 mM phthalate buffer pH 5,(iii)-(vi) 20 mM phosphate buffer pH 6, 7, 8 and 9. 20 mM phosphate buffer (pH values of phosphate buffers were adjusted with 0.1 M phosphoric acid or 0.1 M NaOH). All buffer solutions were sonicated and filtered through 0.45 μm membrane syringe filter before analysis, to remove the sediment prior to CE analysis. All experiments were conducted at 25 ^{0}C.

10.2.4 Preparation of solutions and metal complexes

Fresh working single or various standards were prepared daily by appropriate dilution of the stock solutions. The solutions were prepared by diluting with deionized water with a resistivity of 18 mΩ. cm (Millipore system). Metal complexes were prepared by mixing metal solution with ligands and the electrolyte was prepared from 20mM sodium tetraborate buffer and 0.1 mM CTAB surfactant, 0.1 M NaOH and 0.1 M HCL was used to adjust the desired pH . Sample analyses were in the ratio of 1:1, 1:2, 1.3, 1.4 and 1:5 metal to Ligand (EDTA, DTPA, EDDS, and NTA) All solutions and electrolytes were sonicated and filtered through 0.45 μm membrane filter before analysis.

10.2.5 Capillary conditioning

Fused silica capillaries using various internal diameters, outer diameter 365 μm obtained from Poly Micro Technologies, Inc. (Phoenix, AZ). The required length of capillary (used 40-70 cm) was cut using a capillary cleaving tool to give a clean perpendicular cut without any uneven ends. The detection window was constructed by burning out about 2-3 mm of the outer polyimide coating. The window then was cleaned with acetone to remove coating residue or fingerprints.

When new bare fused silica capillaries were used for the first time, they were rinsed with 1 mol L^{-1} sodium hydroxide for 30 min and ultra pure water for 30 min and after these rinses.

Normal conditioning was done by rinsing with background standards electrolyte for 30 min followed by 0.1 M NaOH for 10 min, then with deionized water for another 10 min and equilibrated with the buffer solution for a further 10 min. Every day before and after runs, the capillary was conditioned by sequentially purging with 0.1 M NaOH for 5 min., 0.01 M NaOH for 5 min and ultra pure water for 10 min. During the sequence between the runs, the capillary was purged with buffer for 3 min. To assure that the capillary was in good condition throughout the sequence, the capillary was conditioned by washing it with 0.1 mol L^{-1} sodium hydroxide for 5 min, ultra pure water for 5 min and separation electrolyte for 5 min after every three samples. Between each injection, the capillary was filled with the buffer solution by flushing the entire capillary for 5 min at 50 mbar. The sample solution was introduced into the anodic end of the capillary by hydrostatic injection. A voltage of −25 kV was then applied for separation.

10.2.6 Procedure for Capillary Electrophoresis

The electrolyte required for CE was prepared by dissolution of an appropriate amount of NaH_2PO_4 in Deionised water, which contained appropriate amounts of tetradecyltrimethylammonium bromide (TTAB). All electrolytes were filtered through a Millipore 0.45 μm membrane filter and degassed in an ultrasonic bath prior to use. Milli-Q water was obtained from Milli-Q (Millipore, Bedford, MA, USA) equipment with a conductivity of 0.054 S/cm, and was used for preparing all solutions. Electrolyte pH was adjusted with 0.1 M NaOH or 0.1 M H_3PO_4 solution.

10.3 Results and Discussion

10.3.1 Speciation of Vanadium with (EDTA and DTPA)

During pre-column derivation, the complexing ligand will form a kinetically stable complex with each vanadium species and each metal complex will have a high absorptivity. The formation of kinetically stable complexes is important because anionic vanadium complexes may partially decompose in the capillary during separation.

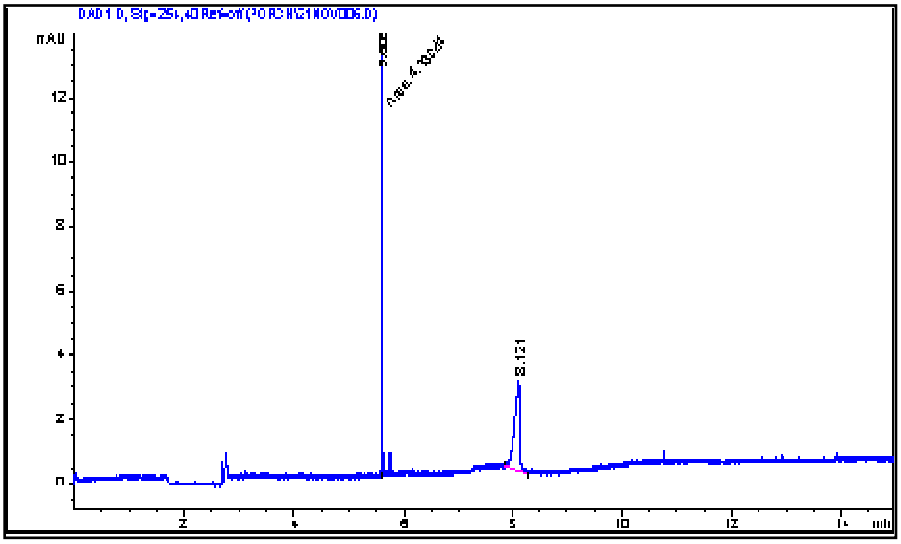

Figure 10.1*:* Typical electropherogram of V(IV) and V(V) with 10mM EDTA, 0.2mM of V(IV) and V(V)1st peak = marker, 2nd peak = V(V)–EDTA, 3rd peak = V(IV)–EDTA. Conditions: capillary, fused-silica capillary 60cm×50µm (effective length: 52.5cm); electrolyte, 25mM sodium phosphate, 0.50mM TTAB at pH 4.0 applied potential, −15kV; hydrostatic injection: 30s, UV detection at 200nm, capillary temperature of 25°C.

In all four ligands (EDTA, DTPA, EDDS and NTA) tested two single separate vanadium complexes were formed using EDTA and DTPA. The ligand EDTA complex with $[VO]^{2+}$ (V(IV) and $[VO_2]^{+}$ V(V) to form kinetically stable complexes is shown in ***Figure 10.3***. The V(V)-EDTA complex migrated faster than that of V(IV)-EDTA at pH 4, and also the peak height for V(V)-EDTA is higher than V(IV)-EDTA. The reason being that the formation of [VO2 (HEDTA]$^{2-}$ took place as descriped by Jone et al.[1]

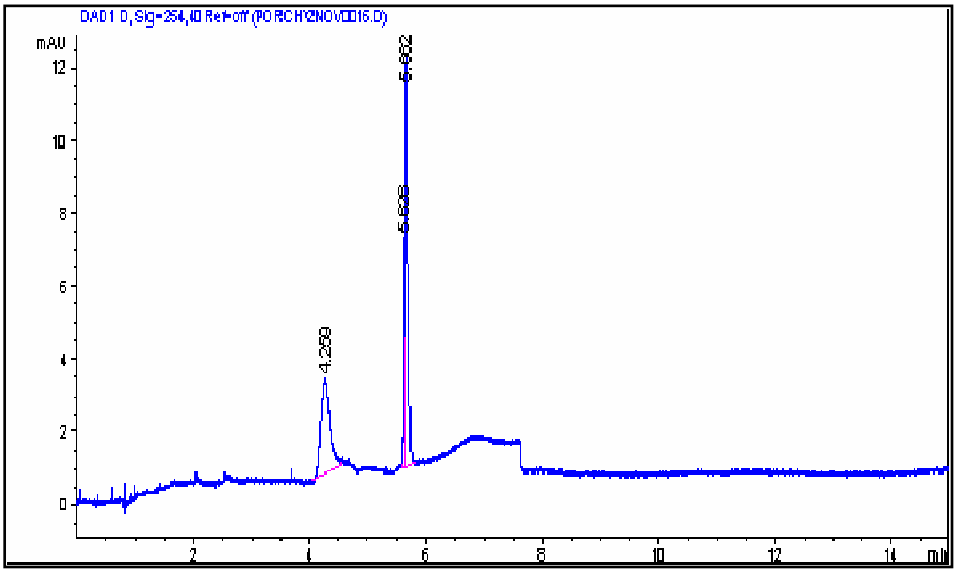

Figure 10.2*:* Typical electropherogram of V(IV) and V(V) with 10mM DTPA, 0.2mM of V(IV) and V(V)1st peak = V(V)–DT] V(IV)-DTPA ς = V(IV)–DTPA. (same conditions as in ***Figure 10.1***).

The V(V)-DTPA complex migrated faster than that of V(IV)-DTPA. But the peak height for V(V)-DTPA is lowe V(V)-DTPA)-DTPA as shown in ***Figure 10.3***, this might be the different charges on the complexes. The result for vanadate anion using EDDS, NTA were very broadened and had poorly shaped peaks, as can be seen in Appendix A, Using EDTA and DTPA, two single distinct vanadium complexes were formed as shown in ***Figure 10.1*** and ***Figure 10.3,*** specifically both ligands can complex with $[VO]^{2+}$ and $[VO_2]^{+}$ to form kinetically stable complexes. The complex was unstable in the electrophoretic system until EDTA and DTPA is added in the electrolyte. The V(IV)-complex peak appeared to be stable on the electropherogram if there was no EDTA in the electrolyte

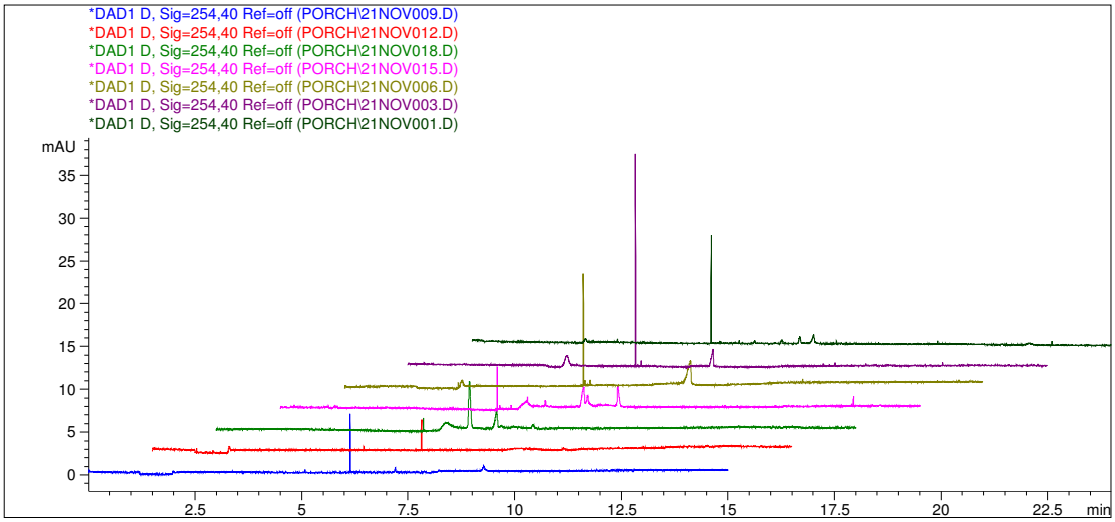

Figure 10.3*:* Electropherograms of V(IV) and V(V) with 10mM EDTA, 0.2mM of V(IV) and V(V) at various pH level from pH 2-8 , monitored at 200nm.

The effect of electrolyte pH was investigated, the electrolyte concentration was the same but various pH values of electrolyte were used from pH 2-8 level, the pH of the electrolyte controls the ionization and the electrophoretic mobility of the carrier ion, and the separation of lower mobility ions can be optimized by decreasing the pH. From the pH of 2-3 the peaks are not clearly detected, especially the second peak is not observed as shown if ***Figure 10.3***. Although from the pH of 4-7 both peaks are observed. Then at the pH 8 the second peak disappear totally, no observation for the second peak, the first peak correspond to V(V)-EDTA and the second V(IV)-EDTA. The increase in pH supplies more Y^{4-} for complexation and enhances the stability of $[V0^{2}Y]^{3-}$ and $[VOY]^{2-}$. On the other hand there is a high risk of the formation of precipitation at higher pH level. In general, migration at pH 4 gave the best sensitivity to detection and was chosen as the optimal electrolyte pH. Since both peaks are observed and are not far apart from each other, which simplify becouse the migration time is almost the same, even the high peaks are almost the same.

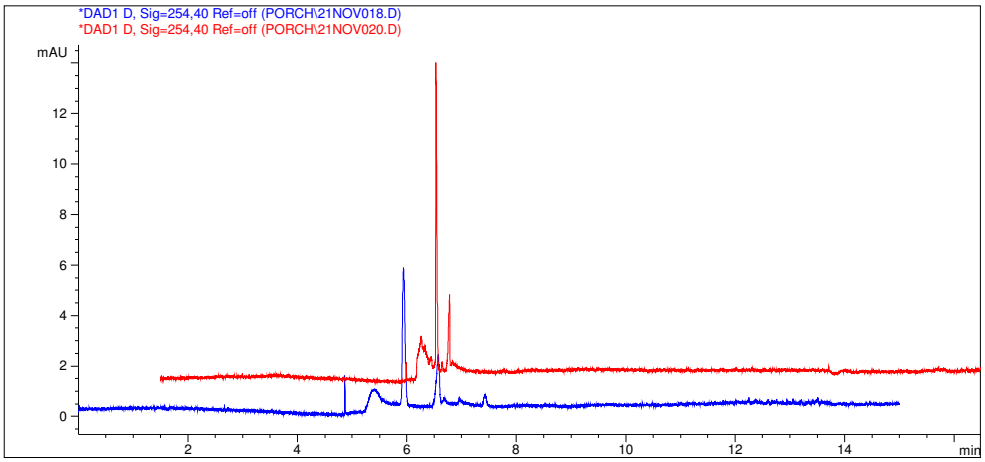

Figure 10.4*:* Electropherograms of V(IV) and V(V) with 10mM EDTA, 0.2mM and 0.5 mM concentration of V(IV) and V(V).

There effect of the electrolyte concentration also plays a major role in the speciation and separation of vanadium, the concentration of 0.2 and 0.5 mM for V(IV) and V(V) were investigated. In ***Figure 10.4*** when the concentration of 0.5 M was used, the first peak becomes broad and the peak hight decreases. Also the peak separation narrows. When the 0.2 mM was used the two peak of V(IV) and V(V) are observed more clearly and there is a small difference of migration between the two peak, the peak height improved and also another small peak is observed at the migration time of around 5.8 min. This could be the formation of another V(V)-EDTA complex. These electropherograms have the characteristics of almost stable base line and low noise levels are as shown in ***Figure. 10.4*** while with the increasing concentration of VO^{2+}, the peak height improved very much.

10.3.2 Separation of Vanadium with EDTA, EDDS, DTPA and NTA

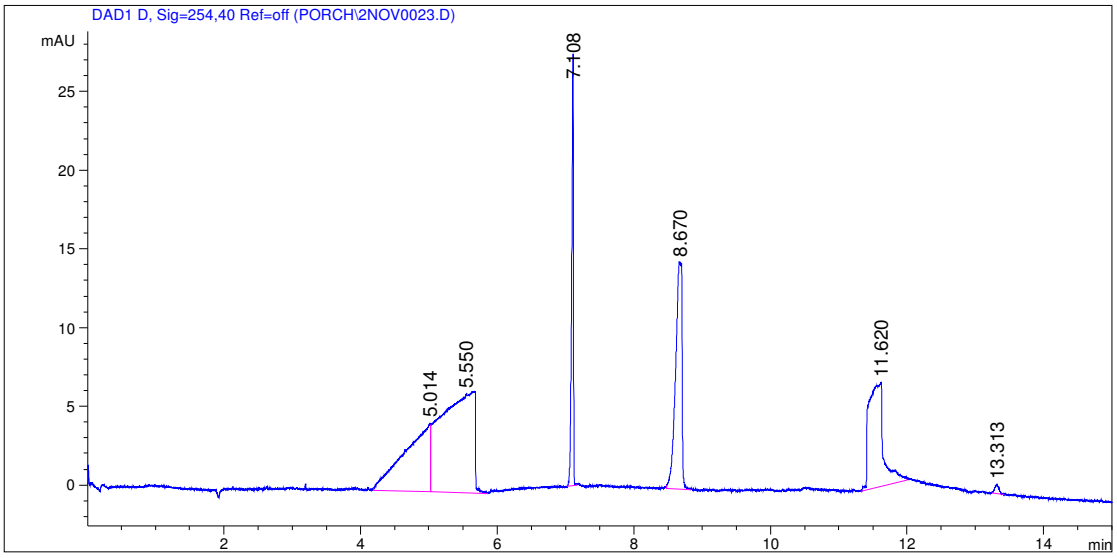

Figure 10.5*:* Typical electropherogram of vanadium with various ligands (EDTA, EDDS, DTPA and NTA) 1st peak = V(IV/V) -EDDS, 2nd peak = V(IV/V) –EDTA, 3rd peak = V(IV/V) -DTPA, 4th peak = V(IV/V) –NTA.

The choice of ligand to achieve high UV response and separation selectivity means that the complexing ligands should satisfy several requirements including: rapid complexation between metal ions and ligand, formation of a single distinct complex with V(IV) or V(V) under on-column conditions; and formation of a complex with large UV absorptivity. ***Figure 10.5*** illustrates the results obtained from different ligands in the supporting electrolyte for complexation and separation of V(IV) and V(V); the electrolyte contained 10 mmol ligand at pH 4.0. Two distinct peaks attributable to vanadium complexes were formed when EDTA and DTPA were used, and both resulted in good resolution. Higher detection sensitivity of V(IV) and V(V) was however, obtained.

Detection sensitivity for use of both NTA and EDDS was also much lower than that obtained by use of EDTA and DTPA. This indicated that NTA and EDDS were selective ligands for specific oxidation states and with lower UV absorptivity. Both can be attributed to the structure of the metal complex, which involves selective coordination. Although the use of NTA for Ce metal speciation has been reported previously [2], for reasons of speed of complexation, separation electivity, and detection sensitivity. EDTA was the most suitable

ligand for the complexation of V(IV) and V(V), because it best satisfied the requirements listed above, although the second best EDTA, EDDS and NTA are not good for the complexation of V(IV) and V(V). The addition of low concentrations of ligand to the background electrolyte can prevent the decomposition, but can also reduce the detection sensitivity due to the increase in the UV background. Hence, preliminary studies [3-5] of pre-capillary complexation, was investigated $[VO]^{2+}$ and $[VO_2]^{+}$. The vanadium complexes formed were separated by CE with an electrolyte containing 25mM phosphate, 0.5mM TTAB at pH 4 because this buffer system has been successfully used for the separation of many different anionic solutes [6-10].

10.3.3 Speciation of Cerium with EDTA, EDDS, DTPA .

The complexing ligand should therefore satisfy several requirements: It should form a single-state complex, with each vanadium oxidation state, the complex that formed should remain stable during electrophoresis, and the complex formed should have a large UV absorptivity that was previously investigated by [11] and [12]. Aminopolycarboxylic acids, such as EDTA, DTPA, EDDS, and NTA all form complexes with metal ions in solution and satisfy the three requirements described above and have all been used in developing separation methods. All cerium electropherograms have the characteristics of an unstable base line and too much interference, the results are shown in ***Appendix A1***. In view of the fact that most of them were not clearly observed and it was too complicated to be interpreted. And also other metals like (Mn, Cr, and Fe) were not clearly detected or separated as shown in ***Appendix A2-A7***, that could be the effect of electrolyte concentration, pH not suitable, effect of applied voltage to high or small , and ligand concentration to strong or low (and especially ligand exchange).

10.4 Conclusions

Four ligands tested, two single distinct vanadium complexes were formed only using EDTA, DTPA, EDDS, and NTA. The only ligands that complexes with $[VO]^{2+}$ and $[VO_2]^{+}$ to form kinetically stable complexes is EDTA and DTPA.

There are plenty of assumptions that need clarity. Further study on these metals and ligands is recommended.

10.5 References:

[1] Jones WR, Jandik P (1991) J Chromatogr. 546:445–458

[2] Liu WP, Lee HK (1999) J Chromatogr. 834:45–63

[3] Tuma P., Samcova E, Andelova K, J. Chromatogr. B 839 (2006) 12.

[4] Kirschner D.L, Jaramillo M, Green T.K, Anal. Chem. 79 (2007) 736.

[5] Li W, Fries D, Alli A, Malik A, Anal. Chem. 76 (2004) 218.

[6] Qu Q.S, Liu Y, Tang X.Q, Wang C.Y, Yang G.J, Hu X.Y, Yan C, Electrophoresis 27 (2006) 4500.

[7] Jimidar M, Massart DL (1994) Anal Chim Acta 294:165–176

[8] Chen ZL, Tang C, Yu JC J High Resol Chromatogr. 22 (1999)379.

[9] Liu B-F, Liu L-B, Cheng J-K J Chromatogr. A 848 (1999) 473

[10] Liu B-F, Liu L-B, Cheng J-K Anal Chim Acta 358: (1998) 157–162

[11] Liu B-F, Liu L-B, Cheng J-K Talanta 47 (1998) 291–299

[12] Macka M, Nesterenko P, Andersson P, Haddad PR J Chromatogr. A 803(1998) 279

[13] Vachirapatama N, Macka M, Paull B, Munker C, Haddad PR J Chromatogr. A 850 (1999)257

[14] Tsai S, Lee Y Analyst 116 (1991) 615

[15] http://www.makingcosmetics.com/products/51-antioxidants-EDTAethylenediaminetetra-acetic-acid-tetrasodium-salt.html.

Appendix A

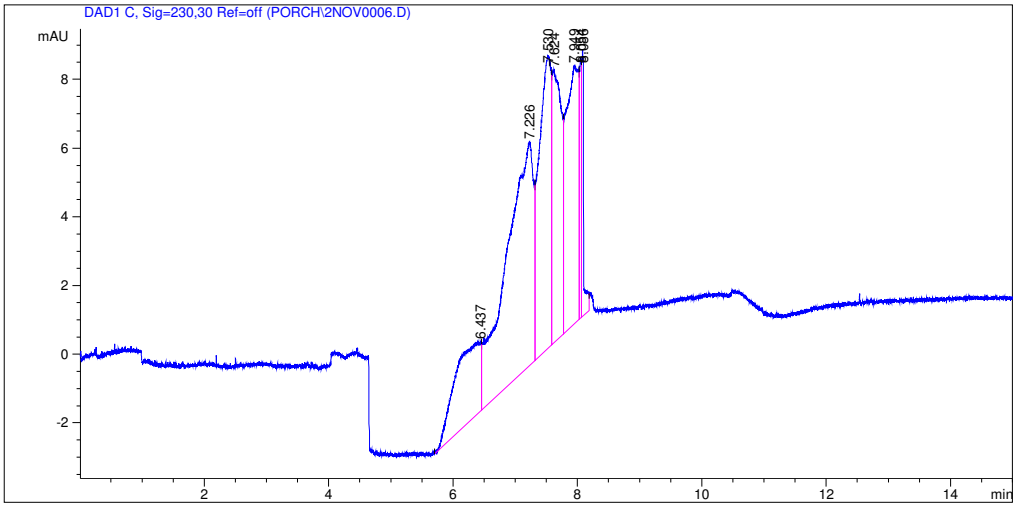

Figure A1: Typical electropherogram of 0.2mM Ce(IV) with 10mM EDTA, Conditions: capillary, fused-silica capillary 60cm×50µm (effective length: 52.5cm); electrolyte, 25mM sodium phosphate, 0.50mM TTAB at pH 4.0 applied potential, −25kV; hydrostatic injection: 30s, UV detection at 200nm, capillary temperature of 25°C.

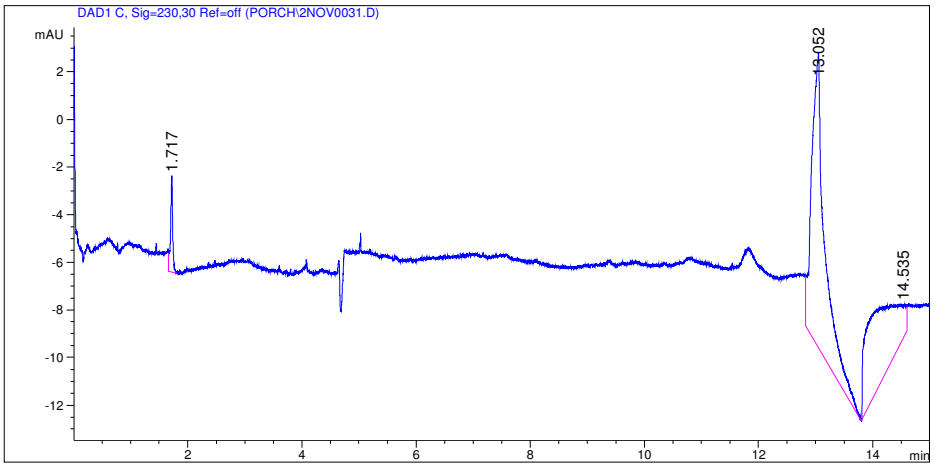

Figure A2*:* Typical electropherogram of 0.2mM Mn(II) with 10mM EDTA, Conditions: capillary, fused-silica capillary 60cm×50µm (effective length: 52.5cm); electrolyte, 25mM sodium phosphate, 0.50mM TTAB at pH 4.0 applied potential, −25kV; hydrostatic injection: 30s, UV detection at 200nm, capillary temperature of 25°C.

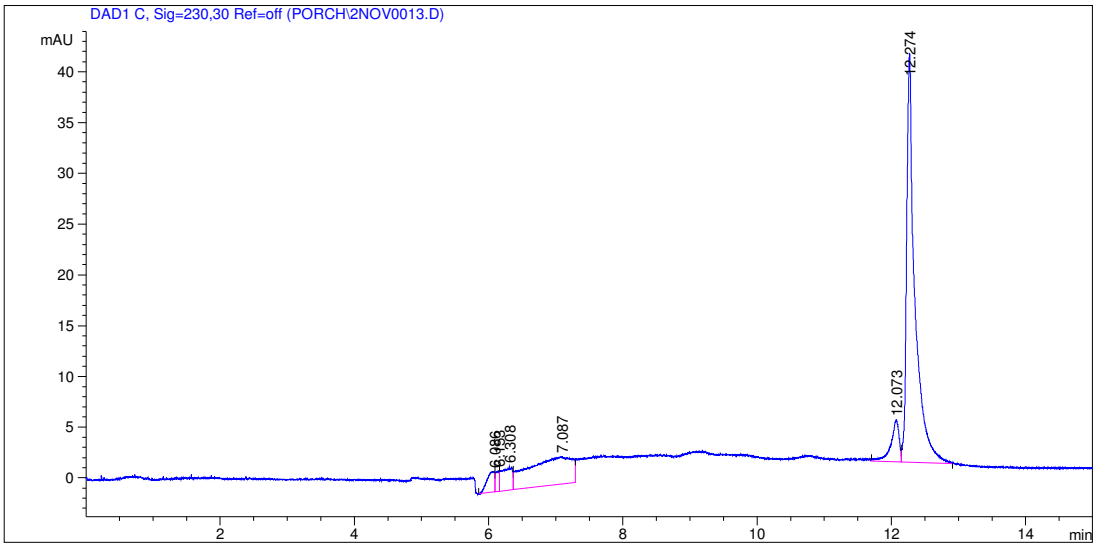

Figure A3: Typical electropherogram of 0.2mM V(IV) with 10mM EDTA, Conditions: capillary, fused-silica capillary 60cm×50µm (effective length: 52.5cm); electrolyte, 25mM sodium phosphate, 0.50mM TTAB at pH 4.0 applied potential, −25kV; hydrostatic injection: 30s, UV detection at 200nm, capillary temperature of 25°C.

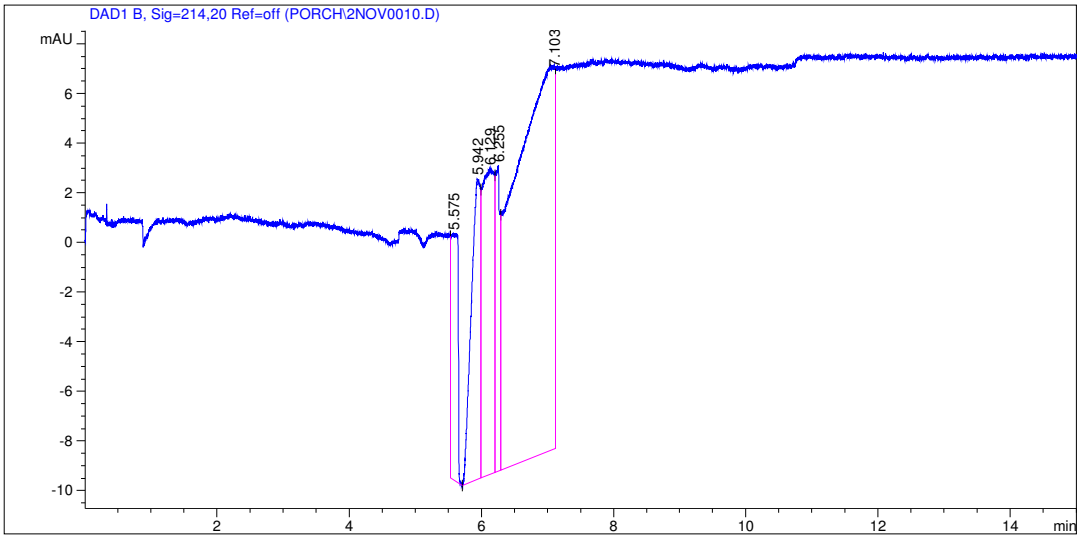

Figure A4: Typical electropherogram of 0.2mM Ce(IV) with 10mM DTPA, Conditions: capillary, fused-silica capillary 60cm×50µm (effective length: 52.5cm); electrolyte, 25mM sodium phosphate, 0.50mM TTAB at pH 4.0 applied potential, −25kV; hydrostatic injection: 30s, UV detection at 200nm, capillary temperature of 25°C.

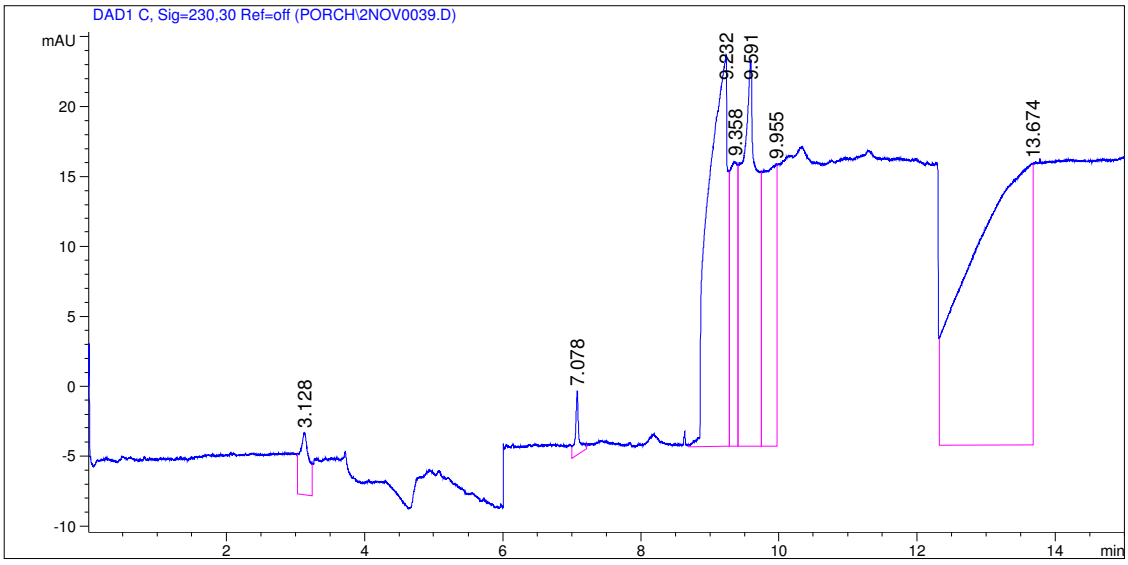

Figure A5: Typical electropherogram of 0.2mM Fe(III) with 10mM DTPA, Conditions: capillary, fused-silica capillary 60cm×50µm (effective length: 52.5cm); electrolyte, 25mM sodium phosphate, 0.50mM TTAB at pH 4.0 applied potential, −25kV; hydrostatic injection: 30s, UV detection at 200nm, capillary temperature of 25°C.

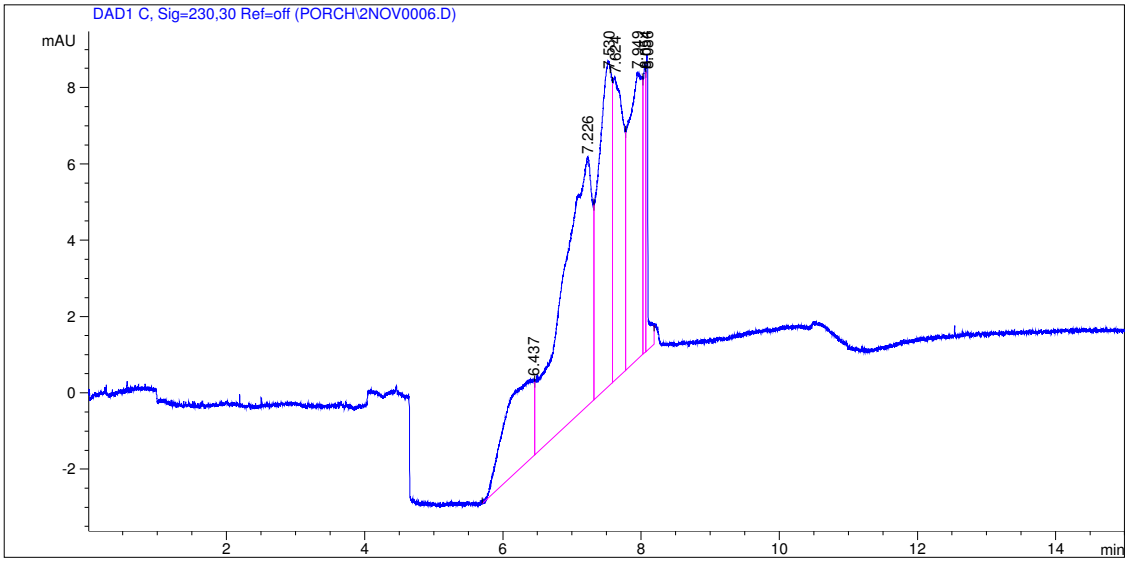

Figure A6: Typical electropherogram of 0.2mM Cr(III) with 10mM DTPA, Conditions: capillary, fused-silica capillary 60cm×50µm (effective length: 52.5cm); electrolyte, 25mM sodium phosphate, 0.50mM TTAB at pH 4.0 applied potential, −25kV; hydrostatic injection: 30s, UV detection at 200nm, capillary temperature of 25°C.

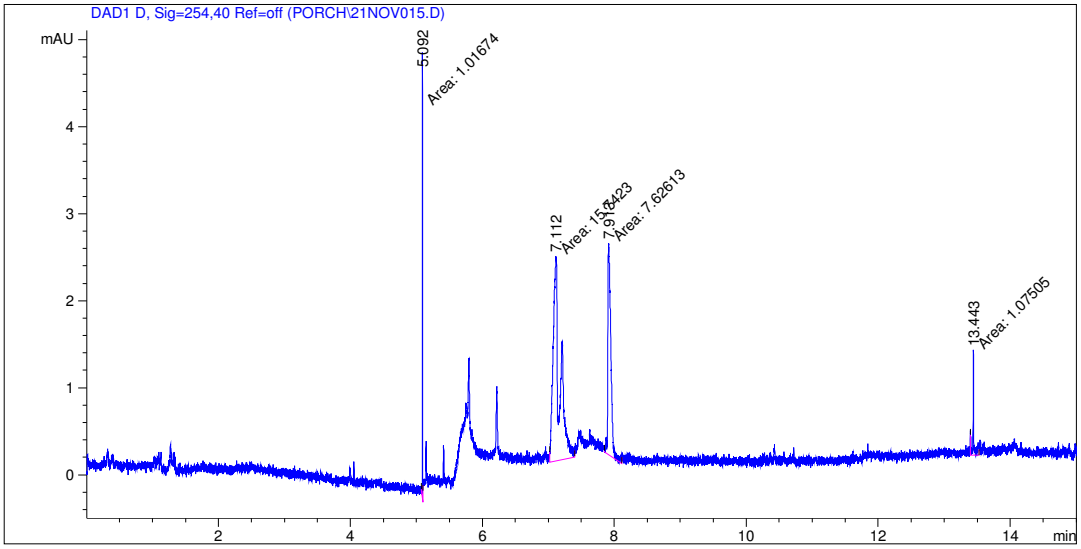

Figure A7 Typical electropherogram of 0.2mM V(IV) with 10mM DTPA, Conditions: capillary, fused-silica capillary 60cm×50µm (effective length: 52.5cm); electrolyte, 25mM sodium phosphate, 0.50mM TTAB at pH 4.0 applied potential, −25kV; hydrostatic injection: 30s, UV detection at 200nm, capillary temperature of 25°C.